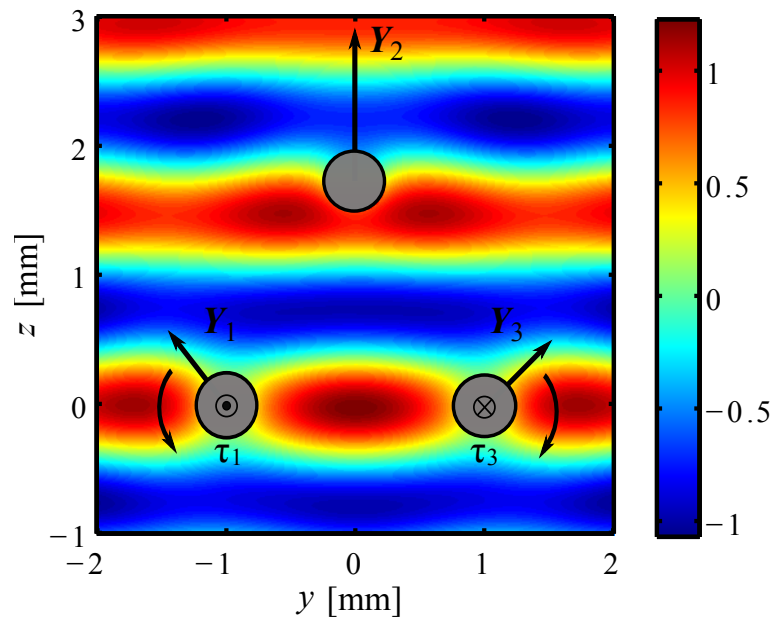




JOSÉ HENRIQUE ARAÚJO LOPES DE ANDRADE

Acoustic radiation force and torque on suspended objects in an inviscid fluid



JOSÉ HENRIQUE ARAÚJO LOPES DE ANDRADE

Acoustic radiation force and torque on suspended objects in an inviscid fluid

*Thesis presented at the Institute of Physics of the
Universidade Federal de Alagoas, as a requirement
needed to obtain the degree of doctor in physics.*

Supervisor: Prof. Dr. Glauber T. Silva

Maceió - 2014

Physics Institute - UFAL

Catálogo na fonte
Universidade Federal de Alagoas
Biblioteca Central
Divisão de Tratamento Técnico
Bibliotecária Responsável: Valter dos Santos Andrade

A553a	<p>Andrade, José Henrique Araújo Lopes</p> <p style="padding-left: 2em;">Acoustic radiation force and torque on suspended objects in an inviscid fluid / José Henrique Araújo Lopes de Andrade-2014. 90 f.: il.</p> <p style="padding-left: 2em;">Orientador: Glauber T. Silva.</p> <p style="padding-left: 2em;">Tese Tese (Doutorado em Física) Universidade Federal de Alagoas. Instituto de Física. Maceió, 2014.</p> <p style="padding-left: 2em;">Bibliografia: f. 87 – 90.</p> <p style="padding-left: 2em;">1. Torque de radiação. 2. Força de radiação. 3. Acústica - Espalhamento. 4. Espalhamento (Física). 5. Partículas. 6. Pinças acústicas. I. Título.</p> <p style="text-align: right;">CDU: 531.77-532.2</p>
-------	---



Universidade Federal de Alagoas
Instituto de Física

Programa de Pós Graduação em Física

BR 104 km 14. Campus A.C. Simões
 Cidade Universitária
 Tabuleiro dos Martins
 57072-970 Maceió - AL, Brasil
 FONE : (82) 3214-1423/FAX 3214-1645

PARECER DA BANCA EXAMINADORA DE DEFESA DE
TESE DE DOUTORADO

**“Acoustic radiation force and torque on suspended
 objects in an inviscid fluid”**

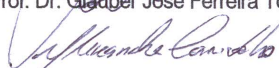
por

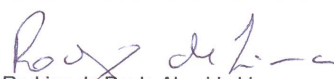
José Henrique Araújo Lopes de Andrade

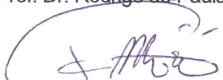
A Banca Examinadora composta pelos professores Glauber José Ferreira Tomaz da Silva (orientador), do Instituto de Física da Universidade Federal de Alagoas, Alexandre Manoel de Moraes Carvalho, do Instituto de Física da Universidade Federal de Alagoas, Rodrigo de Paula Almeida Lima, do Instituto de Física da Universidade Federal de Alagoas, Farid G. Mitri, da Chevron, Area 52 Technology e Mahdi Azarpeyvand, da University of Bristol, consideram o candidato aprovado com grau “B”.

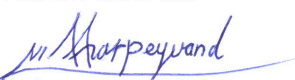
Maceió, 21 de agosto de 2014


 Prof. Dr. Glauber José Ferreira Tomaz da Silva


 Prof. Dr. Alexandre Manoel de Moraes Carvalho


 Prof. Dr. Rodrigo de Paula Almeida Lima


 Prof. Dr. Farid G. Mitri


 Prof. Dr. Mahdi Azarpeyvand

I dedicate this thesis to my mother Maria,
my grandparents Antônia and Severino,
and to Tamirys my great companion.

ACKNOWLEDGEMENTS

My continuing journey through work and education has been enriched by many people. Foremost is my wife, Tamirys, who has supported, encouraged, and shared my endeavors for the last years. I could not have found a better lifelong companion, friend, and partner.

Throughout my career as a physicist there has been a handful of individuals who have had a continuing and powerful influence on my path. First of all, I would like to give my heartfelt gratitude to my supervisor Professor. Glauber T. Silva for his invaluable guidance, support and encouragement throughout this entire research. His profound knowledge in scattering and acoustic radiation force and serious attitude towards academic research will benefit my whole life.

I would like to thank to all professors of the Institute of Physics by the knowledge transmitted during my academic life. In particular a big thank you to my friends Socorro, Wandearley and Baggio.

During the project I stayed for six months in England visiting the Mechanical Engineering at University of Bristol. I would like to thank to Glauber for encouraging me to come, and for Dr. Mahdi azarpeyvand, which help me a lot during this time there. His big knowledge in multiple scattering was very important for my learning. Thank you to the Dr. Bruce Drinkwater and all P.H.D students and post doctoral of the University of Bristol by the knowledge and time during this six months that i was there.

Thanks go to my mother and father in law, for all trips and good familiarity with you. It has been a pleasure to be part of your funny family.

Next, I would like to thank my 'Tucano Azul' friends, Gabé, Manusinha, Netão and Nane who provided many specially moments in group with trips, games and drinks. Each one of you is part of my family.

Lastly, I would like to thank my loving wife Tamirys, for all her love and patience during this period, making it a little easier to endure the hard times of the project. And thanks for my little pet Iali, for the funnies moments.

This work was supported by CAPES.

Abstract

Recent advances and interest in ultrasound particle manipulation calls for theoretical understanding of acoustic radiation force and torque exerted on a configuration of multiple particles. In this thesis we theoretically study the acoustic radiation force and torque exerted by an arbitrary acoustic beam on a cluster of spherical particles in an inviscid fluid. The method is based on the partial-wave expansion (PWE) and the translational addition theorem for spherical wave functions. The combination of (PWE) and addition theorem method enable us to solve the associated multiple scattering problem by numerically computing the (PWE) coefficients in a system of linear equations. On the other hand, when we consider the radiation force and torque exerted on a single sphere, the addition theorem has the advantage to solve this problem in a closed form. After obtaining the PWE coefficients, the acoustic radiation force and torque is computed through the farfield series solution. To illustrate the method, the acoustic radiation force and torque exerted on a single or multiple spheres are analyzed. In the case of a single sphere, the force is generated by a spherically focused ultrasound beam, whereas the torque is generated by a Bessel vortex beam. For the multiple spheres configuration, the radiation force is induced by a traveling and a standing plane wave. In a specific configuration of three olive oil droplets suspended in water, with radii of the order of the wavelength, we found that rescattering events produce an acoustic interaction force, which significantly changes the radiation force on each droplet depending on the inter-droplet distance. In addition, we have found for the first time that an acoustic interaction torque due to the nonsymmetric spatial distribution of the acoustic energy density to the droplets. Furthermore, our study does not have restrictions on the spheres size compared to the wavelength, nor on their composition material, which includes rigid, void, compressional liquid, elastic and viscoelastic solids, and layered material. Finally, this study has direct applications on methods for noncontact object handling by acoustic waves such as acoustic levitation, acoustical tweezers, and acoustophoresis in lab-on-a-chip devices.

Keywords: Acoustic Radiation Force. Acoustic Radiation Torque. Acoustophoresis.

Resumo

Recentes avanços e interesse em manipulação de partículas necessitam de uma maior compreensão teórica da força de radiação e torque acústico exercidos sobre uma configuração de múltiplas partículas. Nesta tese, nós estudamos teoricamente a força de radiação e torque acústico exercido por um feixe acústico arbitrário em um conjunto de partículas esféricas suspensas em um fluido não viscoso. O método baseia-se na expansão de ondas parciais (EOP) e no teorema translacional da adição para funções de onda esférica. A combinação do método de ondas parciais com o teorema da adição nos permitir resolver o problema de espalhamento múltiplo computando numericamente os coeficientes da expansão em um sistema de equações lineares. Por outro lado, quando consideramos a força e torque de radiação exercidos sobre uma única esfera, o teorema da adição tem a vantagem para resolver este problema exatamente. Após a obtenção dos coeficientes, a força e o torque de radiação são calculados usando um método em séries no campo distante. Para ilustrar o método, a força e o torque exercidos sobre uma ou multiplas esferas são analisados. Para o de uma única esfera, a força de radiação é gerada por um feixe de ultrassom focalizado. Para uma configuração de multiplas esferas, a força de radiação é induzida por ondas planas e estacionarias. Numa configuração específica de três gotas de azeite suspensas em água, com raios da ordem do comprimento de onda, verificou-se que as ondas reespalhadas produzem uma força de interação acústica, o que altera significativamente a força de radiação em cada gota em função da distância inter-gota. Além disso, verificou-se, pela primeira vez que um torque de interação acústico devido a uma distribuição espacial não simétrica da densidade de energia acústica para as gotas. Além disso, nosso estudo não tem restrições quanto ao tamanho esferas em comparação com o comprimento de onda, nem sobre a sua composição, que inclui rígida, líquida, elástica e sólidos viscoelásticos. Por fim, este estudo tem aplicações diretas sobre os métodos de manipulação de objetos sem contato por ondas acústicas, tais como a levitação acústica, pinças acústicas e acoustophoresis em dispositivos lab-on-a-chip

Palavras-chave: Força de radiação acústica, torque de radiação, espalhamento acústico, manipulação de partículas, pinças acústicas.

List of symbols

Symbol	Name	Units(I.S.)
ρ_0	ambient density	$\text{kg} \cdot \text{m}^{-3}$
ρ	density	$\text{kg} \cdot \text{m}^{-3}$
c_0	adiabatic speed of sound	m/s
c	speed of sound	m/s
a	particle radius	m
\mathbf{v}	particle velocity	m/s
p	acoustic pressure	Pa
\mathcal{L}	acoustic Lagrangian density	J/m^3
ϕ_{inc}	incident field	m^2/s
ϕ_{sca}	scattered field	m^2/s
ϕ_{tra}	transmitted field	m^2/s
ω	angular frequency	s^{-1}
λ	wavelength	m^{-1}
k	wavenumber	m^{-1}
a_{nm}	beam-shape coefficient	
s_{nm}	scattering coefficient	
t_{nm}	transmitted coefficient	
φ	azimuthal angle	
θ	radial angle	
j_n	spherical Bessel function of order n	
$h_n^{(1)}$	spherical Hankel function (1st) of order n	
$h_n^{(2)}$	spherical Hankel function (2nd) of order n	
Y_n^m	spherical harmonic	
P_n^m	associated Legendre polynomial of order n	
\mathbf{F}^{rad}	radiation force	N
\mathbf{N}^{rad}	radiation torque	Nm
τ_x, τ_y, τ_z	dimensionless radiation torque components	
∇	gradient vector operator	m^{-1}
$\nabla \cdot$	divergence scalar operator	m^{-1}
$\nabla \times$	curl vector operator	m^{-1}
∇^2	Laplacian scalar operator	m^{-2}
\mathbf{r}	position vector	m
(x, y, z)	cartesian coordinates	
(r, θ, ϕ)	spherical coordinates	
(e_i, e_j, e_k)	cartesian components unit	
\mathbf{n}	surface normal vector	
Re	real part	
Im	imaginary part	
$i = \sqrt{-1}$	imaginary unit	

List of Figures

2.1	Forces acting on fluid particles occupying volume $V'(t)$. Each point on the surface of which moves with the local fluid velocity $\mathbf{v}(\mathbf{r}_s, t)$	9
2.2	Spherical coordinates (r, θ, φ) : radial distance r , polar angle θ (theta), and azimuthal angle φ (phi) and $(\mathbf{e}_x, \mathbf{e}_y, \mathbf{e}_z)$ are the unit-vectors in Cartesian coordinate.	12
2.3	Coordinate system used in the single scattering problem	15
2.4	Multiple scattering from a cluster of scatterers	17
2.5	Geometric description of the multiple scattering by particles in a suspension. A source particle is located at r_q and its corresponding scattered wave is probed at r_p	19
2.6	Geometry of the problem of two rigid spheres scattering	23
2.7	Form function of two rigid spheres at an arbitrary (here $\alpha = \pi/4$ and $d/a = 4$) angular incidence. The truncation number is $M = 10$	24
2.8	Form function of two rigid spheres at an arbitrary (here $\alpha = \pi/4$ and $d/a = 10$) angular incidence. The truncation number is $M = 10$	24
2.9	Form function of two rigid spheres at an arbitrary (here $\alpha = \pi/4$ and $d/a = 10$) angular incidence. The truncation number is $M = 20$	25
3.1	Illustration of the interaction between an incident wave and a suspended object. Both pressure and momentum flux changes the object's linear momentum.	27
3.2	Coordinate system for the calculation of the acoustic radiation force on an arbitrary shape scatterer. The origin point O is at the center of the scatterer. 30	
3.3	Coordinate system for the calculation of the acoustic radiation torque on an arbitrary shape scatterer. The origin point O is at the center of the scatterer.	34
4.1	Sketch of the acoustic scattering by a sphere placed anywhere in the host medium. The systems O and O' correspond to the on- and off-focus scattering configurations.	39

4.2	Pressure amplitude generated by the spherically focused transducer with aperture 44 mm and F-number of 1.6, operating at 3.1 MHz. The pressure is evaluated along (a) the transverse and (b) the axial directions using the partial-wave expansion (PWE) method and the paraxial approximation. . .	41
4.3	Axial radiation force function Y_z for the silicone oil sphere due to the zero-order Bessel beam. The function Y_z is normalized to 1.3931. (a) The sphere is placed on the axis of the beam. (b) The islands of attractive force in the on-axis configuration.	42
4.4	Axial radiation force function Y_z for the silicone oil sphere due to the zero-order Bessel beam. The function Y_z is normalized to 1.3931. (a) The sphere location has a offset of $kx_0 = 1.6$ along the x -axis. (b) The islands of attractive force in the off-axial configuration.	44
4.5	Axial radiation force function Y_z for the silicon oil sphere due to the first-order Bessel beam. The function Y_z is normalized to 0.4201. (a) The sphere is placed on the beam's axis. (b) The islands of attractive radiation force in the on-axis configuration.	45
4.6	Axial radiation force function Y_z for the silicon oil sphere due to the first-order Bessel beam. The function Y_z is normalized to 0.4201. (a) The sphere location has a offset of $kx_0 = 1.6$ along the x -axis. (b) The islands of attractive radiation force in the off-axial configuration.	46
4.7	Transverse radiation force field $\mathbf{Y}_\perp = (Y_x, Y_y)$ caused by the zero-order Bessel beam with $\beta = 70^\circ$ for the silicone oil sphere with (a) $ka = 0.1$ and (b) $ka = 2$. The background images corresponds to the beam intensity. . .	47
4.8	Transverse radiation force field $\mathbf{Y}_\perp = (Y_x, Y_y)$ caused by the first-order Bessel beam with $\beta = 70^\circ$ upon the silicone oil sphere with (a) $ka = 0.1$ and (b) $ka = 3$. The background images correspond to the beam intensity.	48
4.9	Axial radiation force versus the droplet's position along z direction in the focal plane. The force is computed through the partial-wave expansion (PWE) and Gorkov's methods. The size factors of the sphere are (a) $ka = 0.1$ and (b) $ka = 0.5$	50
4.10	Transverse radiation force versus the droplet's position along x direction in the focal plane. The force is computed through the partial-wave expansion and Gorkov's methods. The size factors are (a) $ka = 0.1$ and (b) $ka = 0.5$.	51
4.11	Axial radiation force versus the droplet's position along z direction for the resonant scattering regime (a) $ka = 1$ and (b) $ka = 5$	52
4.12	Transverse radiation force on a silicone oil droplet (with and without attenuation) in the resonant scattering regime (a) $ka = 1$ and (b) $ka = 5$. . .	53
4.13	Vector field of the radiation force in the transducer focal plane produced on the silicone oil droplet in the resonant regime $ka = 1$. The vector field is plot on top of the axial radiation force.	53

- 5.1 A sketch of the interaction between a external incident wave of arbitrary wavefront (vertical bars) and three suspended objects of any geometrical shape. The total scattered wave is denoted by dotted arches. The surface of the objects are S_1 , S_2 , and S_3 , while a control surface is drawn with radius R_c and surface S_c 55
- 5.2 (Color online) Acoustic interaction force between two rigid Rayleigh particles ($ka_1 = ka_2 = 0.1$) induced by a plane wave propagating along $+z$ direction. The circles labeled as ‘1’ and ‘2’ denote, respectively, the particles located at $\mathbf{r}'_1 = -(d/2)\mathbf{e}_y$ and $\mathbf{r}'_2 = (d/2)\mathbf{e}_y$, where d is the inter-droplet distance. 60
- 5.3 (Color online) Cartesian components of the acoustic interaction force and torque between two olive oil droplets with size parameter $ka_1 = ka_2 = 1$ induced by a plane wave propagating along the $+z$ -direction. The circles labeled as ‘1’ and ‘2’ denote, respectively, the droplets located at $\mathbf{r}'_1 = -(d/2)\mathbf{e}_y$ and $\mathbf{r}'_2 = (d/2)\mathbf{e}_y$, where d is the inter-droplet distance. The dashed line in (b) denotes the acoustic radiation force caused by the external traveling plane wave. 61
- 5.4 (Color online) Cartesian components of the acoustic interaction force and torque between two olive oil droplets with size parameter $ka_1 = ka_2 = 1$ (Mie scatterers) induced by a plane wave propagating along the $+z$ -direction. The circles labeled as ‘1’ and ‘2’ denote, respectively, the droplets located at $\mathbf{r}'_1 = -(d\sqrt{2}/2)(\mathbf{e}_x + \mathbf{e}_y)$ and $\mathbf{r}'_2 = (d\sqrt{2}/2)(\mathbf{e}_x + \mathbf{e}_y)$, where d is the inter-droplet distance. The dashed line in (b) denotes the acoustic radiation force caused by the external traveling plane wave. 62
- 5.5 (Color online) Cartesian components of the acoustic interaction force and torque between three olive oil droplets with size parameter $ka_1 = ka_2 = ka_3 = 1$ induced by a plane wave propagating along the $+z$ -direction. The circles labeled as ‘1’, ‘2’, and ‘3’ denote, respectively, the droplets located at $\mathbf{r}'_1 = -(d/2)\mathbf{e}_y$, $\mathbf{r}'_2 = -(d\sqrt{3}/2)\mathbf{e}_z$, and $\mathbf{r}'_3 = (d/2)\mathbf{e}_y$, where d is the inter-droplet distance. The dashed line in (b) denotes the acoustic radiation force caused by the external traveling plane wave. 63
- 5.6 (Color online) Acoustic interaction forces and torques exerted on three olive oil droplets with size parameter $ka_1 = ka_2 = ka_3 = 1$ by a traveling plane wave along the $+z$ -direction. The droplets are located at $\mathbf{r}'_1 = -(d/2)\mathbf{e}_y$, $\mathbf{r}'_2 = -(d\sqrt{3}/2)\mathbf{e}_z$, and $\mathbf{r}'_3 = (d/2)\mathbf{e}_y$, with the inter-droplet distance being $d = 2$ mm. The dimensionless acoustic forces, which are depicted by the straight arrows, are $\mathbf{Y}_1^{(M)} = -0.06\mathbf{e}_y + 1.01\mathbf{e}_z$, $\mathbf{Y}_2^{(M)} = 1.28\mathbf{e}_z$, and $\mathbf{Y}_3^{(M)} = 0.06\mathbf{e}_y + 1.01\mathbf{e}_z$. The dimensionless interaction torques are represented by \odot (outward vector to the yz -plane) and \otimes (inward vector to the yz -plane) and they value $\tau_{1,x}^{(M)} = -\tau_{3,x}^{(M)} = 0.24$. The background is the amplitude of the external plus the scattered waves. 64

- 5.7 (Color online) The y -component of the acoustic interaction force exerted on two olive oil droplets with size parameter $ka_1 = ka_2 = 1$ induced by a standing plane wave along z -direction. The circles labeled as ‘1’ and ‘2’ denote, respectively, the droplets are located at $\mathbf{r}'_1 = -(d/2)\mathbf{e}_y$ and $\mathbf{r}'_2 = (d/2)\mathbf{e}_y$, where d is the inter-droplet distance. 65
- 5.8 (Color online) Cartesian components of the acoustic interaction force and torque exerted on two olive oil droplets with size parameter $ka_1 = ka_2 = 1$ induced by a standing plane wave along z -direction. The circles labeled as ‘1’ and ‘2’ denote, respectively, the droplets located at $\mathbf{r}'_1 = \mathbf{0}$ and $\mathbf{r}'_2 = (d\sqrt{2}/2)(\mathbf{e}_x + \mathbf{e}_y)$, where d is the inter-droplet distance. 66
- 5.9 (Color online) Cartesian components of the acoustic interaction force and torque between three olive oil droplets with size parameter $ka_1 = ka_2 = ka_3 = 1$ induced by a standing plane wave along z -direction. The circles labeled as ‘1’, ‘2’, and ‘3’ denote, respectively, the droplets located at $\mathbf{r}'_1 = -(d/2)\mathbf{e}_y$, $\mathbf{r}'_2 = -(d\sqrt{3}/2)\mathbf{e}_z$, and $\mathbf{r}'_3 = (d/2)\mathbf{e}_y$, where d is the inter-droplet distance. 67
- 5.10 (Color online) Acoustic interaction forces and torques exerted on three olive oil droplets with size parameter $ka_1 = ka_2 = ka_3 = 1$ by a standing plane wave along z -direction. The droplets are located at $\mathbf{r}'_1 = -(d/2)\mathbf{e}_y$, $\mathbf{r}'_2 = -(d\sqrt{3}/2)\mathbf{e}_z$, and $\mathbf{r}'_3 = (d/2)\mathbf{e}_y$, with the inter-droplet distance being $d = 2$ mm. The dimensionless acoustic forces, which are depicted by the straight arrows, are $\mathbf{Y}_1^{(M)} = -0.13\mathbf{e}_y - 0.3\mathbf{e}_z$, $\mathbf{Y}_2^{(M)} = 0.63\mathbf{e}_z$, and $\mathbf{Y}_3^{(M)} = 0.13\mathbf{e}_y - 0.3\mathbf{e}_z$. The dimensionless interaction torques are represented by \odot (outward vector to the yz -plane) and \otimes (inward vector to the yz -plane) and they value $\tau_{1,x}^{(M)} = -\tau_{3,x}^{(M)} = 0.003$. The background is the amplitude of the external plus the scattered waves. 68

Contents

Abstract	vi
Resumo	vii
List of symbols	viii
List of figures	ix
Contents	xiv
1 Introduction	1
1.1 Motivation	1
1.2 Literature Review	2
1.2.1 Acoustic radiation force	2
1.2.2 Acoustic radiation torque	3
1.2.3 Acoustic interaction force	4
1.3 Rationale	4
1.4 Contributions	4
1.5 Outline	5
2 Acoustic scattering in ideal fluids	6
2.1 Fluid conservation equations	6
2.1.1 Mass conservation equation	6
2.1.2 Momentum conservation equation	7
2.1.3 Energy conservation	8
2.2 Wave dynamics	10
2.2.1 Linear wave equation	11
2.2.2 Helmholtz equation	12
2.3 Solution of the Helmholtz equation	13
2.4 Scattering by a sphere	14
2.5 Multiple scattering theory	16
2.5.1 Acoustic scattering by two rigid spheres	22
3 Acoustic radiation force and torque	26
3.1 Acoustic radiation force	26
3.1.1 Inviscid approach	26

3.1.2	Time-average of products	27
3.1.3	Radiation stress tensor	27
3.1.4	Farfield method	31
3.2	Acoustic radiation torque	33
3.2.1	Angular momentum flux density	33
3.2.2	Farfield method	34
4	Acoustic radiation force exerted on a sphere by a focused and a Bessel beam	37
4.1	Methods to compute the beam shape coefficients	37
4.1.1	Discrete spherical harmonic transform (DSHT)	37
4.2	Spherically focused beam	39
4.3	Radiation force by a Bessel beam	41
4.4	Radiation force by a focused beam	49
4.4.1	Acoustic radiation force (Gorkov's method)	49
4.4.2	Results	49
5	Acoustic radiation force and torque exerted on a collection of objects	54
5.1	Acoustic radiation force on a many-body system	54
5.2	Acoustic radiation torque on a many-body system	57
5.3	Numerical results	58
5.3.1	Traveling plane wave	59
5.3.2	Standing plane wave	65
6	Conclusions	69
6.1	Summary	69
6.2	Conclusion	70
	Bibliography	71

Introduction

The interaction of a time-harmonic acoustic wave with a suspended object may give rise to two interesting nonlinear effects, namely the acoustic radiation force and torque. These phenomena are caused, respectively, by the linear and angular momentum flux transferring from the incident wave to the object. Ultrasonic manipulation allows the handling of a wide variety of particles such as synthesized, functionalized solid micro beads, droplets, bubbles and biological cells. Different manipulation strategies and techniques have been accomplished such as particle separation, focusing, concentration, removal, trapping, mixing and moving. These manipulation techniques are required for particle handling in lab-on-a-chip devices and micro-total analysis systems to realize different kinds of analysis steps. We present here a review of both phenomena generated from the interaction of an acoustic wave with a spherical target. In addition, the contributions of this work are also outlined.

1.1 Motivation

When an ultrasound field is imposed on a fluid containing a suspension of particles, the latter will be affected by the so-called acoustic radiation force and torque arising from the scattering of the acoustic waves on the particle. The particle motion resulting from the acoustic radiation force is denoted acoustophoresis, and plays a key role in on-chip microparticle handling. Many different biotechnical applications of acoustophoresis have subsequently emerged including cell trapping [1],[2] and [3], food analysis [4], cell sorting using surface acoustic waves [5],etc. Moreover, the ultrasound particle manipulation is a useful tool as it allows the positioning and rotating of objects and provides levitation to overcome surface forces.

In most of these applications, the systems are made for two or more particles or cells, and so, it's important to study of the behavior of the forces and torques in a configuration of multiple objects. The aim of this thesis is to present a study of the acoustic radiation forces and torques exerted by an arbitrary acoustic field on a collections of suspended objects in an inviscid fluid. This study may be a useful tool to development of news devices for acoustic particle manipulation.

1.2 Literature Review

1.2.1 Acoustic radiation force

The forces on particles in sound fields have been known for more than hundred years. In the middle of the 20th century the theoretical basis for the acoustophoresis has been developed. With the development of microfluidic systems and the concept of lab-on-a-chip technology acoustophoresis gained a strong interest in the last two decades. The acoustic radiation force arises when a wave is scattered by an object. The shape of the object and the material properties in comparison to the ones of the surrounding medium are important as well as the properties of the acoustic field such as pressure amplitude and frequency. The acoustic radiation force can be easily observed experimentally because it is a time averaged effect.

In this section we are present a review of some important publications for the thesis. The theory of the acoustic radiation force was first proposed by Lord Rayleigh [6]. Lord Rayleigh derived an equation for the acoustic radiation pressure on a perfectly reflecting solid wall. In a seminal work, King [7] obtained the acoustic radiation force exerted by a traveling and a standing plane wave on a rigid sphere of arbitrary radius suspended in an ideal fluid. He was the first to use the partial-wave expansion to solve radiation force problems. Although his approach can be applied to any axisymmetric acoustic field, King restricted himself to the two types of waves mentioned above. An extension of this studies considering an incident spherical wave was provided by Emblenton [8, 9]. He noticed that the particle could be attracted to or repulsed by the wave source depending on their relative distance. Subsequently, Yoshioka and Kawasima [10] extended King's theory and derived the acoustic radiation force acting on compressible spherical particles in an ideal fluid. They showed that when the particle is in a standing wave, it can move towards the pressure anti-node or node depending on the contrast of the compressibility and density between the particle and the medium. Westervelt [11] derived an expression for the radiation force on a scattering obstacle with arbitrary normal impedance for any scattering obstacle. Gorkov [12] proposed a radiation force model considering an incident beam of arbitrary shape, but his method is limited to compressional spheres smaller than the incident wavelength. Only the monopole and dipole in the scattered wave were included in this study. The force on a small rigid sphere in an axisymmetric wave was reported by Nyborg [13]. He expressed the radiation force as a function of spatial gradients of potential energy density and kinetic energy density, and suggested that only the field in the vicinity of the sphere needs to be axisymmetric. There is a series of works by Hasegawa et al. [14, 15] in which the acoustic radiation force on an elastic sphere is investigated. The common objective of these investigations is the improvement of the techniques of absolute acoustic intensity determination by the radiation force method. In particular, an expression is derived fo the force exerted by a plane traveling wave on an elastic sphere suspended in an ideal fluid [14].

Bearing in mind applications such as acoustic levitation in containerless processing and medical ultrasound equipment, Wu and Du [16] calculated the radiation force on

a small compressible sphere placed on the axis of a focused sound beam. Their study shows that the physical focal point of a focused beam is a stable point for small rigid spheres with and hence focused sound beams may be an alternative for levitating small high-density samples.

In most of the studies cited above, a plane wave was used due to its simplicity. Silva [17] obtained expression for the radiation force exerted by an acoustic beam with arbitrary wavefront. This expression is obtained as a function of the beam-shape and the scattering coefficients of an incident wave and the object, respectively. However, the possibility of generating negative radiation force using Bessel beams have also been studied. Marston [18] derived a expression for the radiation force on a sphere placed on the axis of an acoustic Bessel beam propagating in an inviscid fluid. Negative axial forces are found to be correlated with reduction of backscattering waves. Mitri [19] examined the negative axial radiation force on a fluid and elastic spheres illuminated by a high-order Bessel beam with particular emphasis on how the mechanical properties and resonances of spheres as well as the beam parameters affect the negative radiation force. Silva [20] analyzed the behavior of the acoustic radiation force generated by a Bessel beam on an absorbing sphere when this sphere lies outside the beam's axis.

1.2.2 Acoustic radiation torque

In combination with the translation of particles due to the acoustic radiation force, the rotational manipulation offers a new controllable degree of freedom for the movement of particles. One of the first observations concerning the acoustic radiation torque was reported by Rayleigh [21]. The Rayleigh torque is caused by the momentum of the radiation stress acting on an asymmetric object. M. Kotani [22] and King [23] computed the acoustic radiation torque upon a Rayleigh disk. Keller [24] extended their formulation for infinitely long thin strips and rigid disks of various shapes all used by Rayleigh's observations. In 1958, Maidanik [25] derived an expression to compute the radiation torque for an incident beam upon any arbitrarily shaped object.

The radiation torque produced by an arbitrary acoustic wave on a particle, which is much smaller than the incident wave, within a nonviscous fluid has been theoretically investigated [26]. Hefner et al. [27] showed that an axial acoustic radiation torque can be developed on an absorbing target by a paraxial vortex beam. Moreover, the axial radiation torque on an axysymmetric object suspended in an inviscid fluid was theoretically studied by Zhang et al [28]. The radiation torque is expressed as the integral of the time-averaged flux of angular momentum over a spherical surface far removed from the scattering object with its center at the centroid of the object. The axial radiation torque of a progressive, standing and quasi-standing Bessel beam on a spherical shell was studied by Mitri [29]. Mitri developed a closed formula for the radiation torque of an arbitrary acoustic beam upon an compressional spherical particle in a Rayleigh limit. The difference between Fan an Mitri's formulation is the fact that Mitri's formulation consider absorptive particles, thus, it takes into account angular momentum transfer between the incident wave field and the scatterer. Silva [30] derived a general formula for the Cartesian components of

the acoustic radiation torque produced by an arbitrary incident beam on an object of any geometrical shape in a nonviscous fluid.

1.2.3 Acoustic interaction force

The acoustic interaction force which arises in a system of two or more spheres has also been previously studied. Investigations on the interaction radiation force from many particles dates back to the nineteenth century with Bjerknes studies of the mutual force on a pair of bubbles [31] and the analysis performed by Konig on the interaction radiation force between two rigid spheres [32]. Subsequently, this force was investigated considering short-range interaction between particles of the types rigid-rigid [33, 34], bubble-bubble [35, 36], bubble-rigid [37], and bubble-droplet [38]; whereas long-range rigid-rigid [39] and bubble-bubble [40, 41] interactions have also been studied. The interaction radiation force between two droplets aligned relative to an incident plane wave with arbitrary inter-particle distance was also analyzed [42]. Moreover, bubble-bubble interaction at any separation distance has also been analyzed through a semi-numerical scheme based on the partial-wave expansion method and the translational addition theorem of spherical functions [41].

1.3 Rationale

An increasing interest on acoustic radiation force and torque has arisen after the concepts of acoustical tweezers and acoustophoretic devices on micro-sized particles. Despite, many works on radiation force and torque upon one single particle has been done in the last century. However, in an ideal sense the knowledge of the properties in a set of particles is necessary. Some works have been realized about the radiation force exerted by acoustic fields in a configuration of two particles [43], [39] and many particles system [44]. These works results presents the radiation force exerted on a system with no more than two particles. Furthermore, they we performed with some restrictions such as the particles are in the same direction of the acoustic fields. It is important to say that the acoustic radiation torque exerted by an arbitrary shaped wave in a cluster of particles has not been studied until now.

1.4 Contributions

Published articles

1. G. T. Silva, J. H. Lopes, F. G. Mitri, Off-axial acoustic radiation force of repulsor and tractor Bessel beams on a sphere, IEEE Transactions on Ultrasonics, Ferroelectrics, and Frequency Control 60, 1207-1212, 2013.

Articles submitted for publication

1. G. T. Silva, A. L. Baggio, J. H. Lopes, and F. G. Mitri, Exact computations of the acoustic radiation force on a sphere using the translational addition theorem, IEEE

Transactions on Ultrasonics, Ferroelectrics, and Frequency Control, 2014. Submitted.

Articles in preparation

1. J. H. Lopes, M. Azarpeyvand, and G. T. Silva, Acoustic radiation force and torque acting on multiple particles, IEEE Transactions on Ultrasonics, Ferroelectrics, and Frequency Control, 2014. To be submitted.

Conference proceedings

1. J. H. Lopes, Silva, G. T. Acoustic radiation force due to a spherical wave on a compressible sphere. 2013. (XXXVI Encontro Nacional de Física da Matéria Condensada).

2. J. H. Lopes, Silva, G. T. ; Lobo, T. P. ; Mitri, F. G. . Off-axial acoustic radiation force of pressor and tractor Bessel beams. 2012. (XXXII Encontro de Físicos do Norte e Nordeste).

1.5 Outline

In this thesis we begin by introducing the general scattering theory from a single a multiple particles in Chap. 2. We show how to describe the incident and scattering fields using the partial waves expansion method. Having introduced the basic foundation we proceed to a treatment of the acoustic radiation force and torque in Chap. 3. Chapter 4 presents the theoretical study of the acoustic radiation force exerted by a Bessel and focused beams on a compressible fluid sphere in an off-axis configuration. In Chap. 5 we computed the acoustic radiation force and torque exerted by an arbitrary incident wave on a cluster of spherical particles. The results are applied for a set of three olive-oil spheres in a plane and standing wave fields. Finally, a conclusion of this work is given in Chap. 7. Some suggestions for future work are also provided in this chapter.

2

Acoustic scattering in ideal fluids

In this chapter, we present the acoustic scattering theory for a single and a cluster of spheres suspended in an ideal fluid. In doing so, the fluid dynamics equations are derived as well the linear wave equation. Considering a single-frequency wave the corresponding wave equation, the so-called Helmholtz equation, follows immediately. The solution of the Helmholtz equation in spherical coordinates is presented in terms of the partial-wave expansion method for all waves involved in the scattering problems.

2.1 Fluid conservation equations

In fluid dynamics, we consider a fluid, i.e. a gas or a liquid, as a continuum medium. The fluid is described divided it into small elements which are fixed with respect to a coordinate system referred to as the laboratory coordinate system. An arbitrary fluid of volume fixed in space and located at \mathbf{r} is denoted by V . It is further assumed that the fluid parcel inside V has a very large number of atoms or molecules. Moreover, it is in local thermodynamic equilibrium. This hypothesis enables us to define quantities for the fluid element such as density, pressure, temperature, internal energy, and entropy. Another important quantity of the fluid element is its velocity, which will be defined in terms of the velocity of the center-of-mass that element.

2.1.1 Mass conservation equation

Consider a fixed volume V of a fluid element positioned at \mathbf{r} , which encloses N atoms or molecules at any time t . The density of V is given by

$$\rho(\mathbf{r}, t) = \frac{1}{V} \sum_{i=1}^N m_i, \quad (2.1)$$

where m_i is the mass of an atom or molecule and inside V . The velocity of the center-of-mass of the fluid element in V at the time t is defined as

$$\mathbf{v}(\mathbf{r}, t) = \frac{1}{\rho(\mathbf{r}, t)V} \sum_{i=1}^N m_i \mathbf{v}_i, \quad (2.2)$$

where v_i is the instantaneous velocity of the i th atom or molecule inside the volume V . This velocity is referred to as the fluid element velocity.

The net mass can only change by convection (transport) of density. The convection velocity of the density is $\mathbf{v}(\mathbf{r}, t)$. Hence, the net mass change of the volume V per unit time depends on the mass flow $\rho\mathbf{v}$ across the surface S of V , Fig.(2.1). Accordingly, the conservation of mass requires

$$\partial_t \int_V \rho d^3\mathbf{r} + \int_S \rho\mathbf{v} \cdot \mathbf{n} d^2\mathbf{r} = 0, \quad (2.3)$$

where $\partial_t = \partial/\partial t$, $d^3\mathbf{r}$ and $d^2\mathbf{r}$ are the volume and surface integral elements, \mathbf{n} is the unit-normal vector on S . Since the volume V is fixed, the operator ∂_t can be applied directly on the density function. On the other hand, the surface integral in Eq. (2.3) can be transformed to a volume integral using the Gauss divergence theorem,

$$\int_S \rho\mathbf{v} \cdot \mathbf{n} d^2\mathbf{r} = \int_V \nabla \cdot (\rho\mathbf{v}) d^3\mathbf{r}. \quad (2.4)$$

Combining Eqs. (2.3) and (2.4) and noticing that V is an arbitrary volume, we can write the mass conservation equation as

$$\partial_t \rho + \nabla \cdot \rho\mathbf{v} = 0. \quad (2.5)$$

2.1.2 Momentum conservation equation

The linear momentum inside the fixed volume V at any time t is $\rho\mathbf{v}$. Likewise the rate of change of density in the volume V , linear momentum may also change by convection. In this case, the momentum flux is defined as $\rho\mathbf{v}\mathbf{v}$. Note that the quantity $\mathbf{v}\mathbf{v}$, known as a dyad, is a second-rank tensor. From Newton's second-law the rate change of the linear momentum in V should be equal to the sum of the momentum flux, the pressure forces normal to the surface S , and any body force applied to the fluid, such as gravity. Moreover, an ideal fluid does support shear stress due to viscosity. Thus, the rate change of the linear momentum in the volume V is given by

$$\partial_t \int_V \rho\mathbf{v} d^3\mathbf{r} + \int_S p \mathbf{n} d^2\mathbf{r} + \int_S \rho\mathbf{v}\mathbf{v} \cdot \mathbf{n} d^2\mathbf{r} + \int_V \mathbf{f}^b d^3\mathbf{r} = \mathbf{0}, \quad (2.6)$$

where $p(\mathbf{r}, t)$ is the pressure at \mathbf{r} and \mathbf{f}^b is the body force density. The surface integrals in Eq. (2.6) can be transformed to volume integrals by means of the Gauss theorem for

tensors [45]. Therefore, we obtain

$$\partial_t \int_V \rho \mathbf{v} d^3\mathbf{r} + \int_V \nabla p \mathbf{n} d^3\mathbf{r} + \int_V \nabla \cdot (\rho \mathbf{v} \mathbf{v}) d^3\mathbf{r} + \int_V \mathbf{f}^b d^3\mathbf{r} = \mathbf{0}. \quad (2.7)$$

Since the volume V is arbitrary, we find the momentum conservation equation as

$$\partial_t(\rho \mathbf{v}) + \nabla p + \nabla \cdot (\rho \mathbf{v} \mathbf{v}) + \mathbf{f}^b = \mathbf{0}. \quad (2.8)$$

In most cases of study here, body forces are much smaller than other force contributions. Hence, we may set $\mathbf{f}^b = \mathbf{0}$ in Eq. (2.8). Furthermore, the gradient of the pressure can be expressed as second-rank tensor as $\nabla p = \nabla \cdot (p\mathbf{I})$, where \mathbf{I} is the unit tensor. Now, we can rewrite Eq. (2.8) as

$$\partial_t(\rho \mathbf{v}) + \nabla \cdot \mathbf{S} = \mathbf{0}, \quad (2.9)$$

where

$$\mathbf{S} = p\mathbf{I} + \rho \mathbf{v} \mathbf{v} \quad (2.10)$$

is the stress tensor.

It is useful to write Eq. (2.9) in a different format to use it in the derivation of the radiation force formula in Chap. 3. Consider the relation

$$\nabla \cdot \rho \mathbf{v} \mathbf{v} = (\nabla \cdot \rho \mathbf{v}) \mathbf{v} + \rho \mathbf{v} \cdot \nabla \mathbf{v}. \quad (2.11)$$

Using Eq. (2.5) into this equation we find

$$\nabla \cdot \rho \mathbf{v} \mathbf{v} = -(\partial_t \rho) \mathbf{v} + \rho \mathbf{v} \cdot \nabla \mathbf{v}. \quad (2.12)$$

Combining this equation with Eq. (2.9)

$$\begin{aligned} \partial_t(\rho \mathbf{v}) - (\partial_t \rho) \mathbf{v} + \rho \mathbf{v} \cdot \nabla \mathbf{v} + \nabla p &= 0, \\ \rho (\partial_t + \mathbf{v} \cdot \nabla) \mathbf{v} + \nabla p &= 0. \end{aligned} \quad (2.13)$$

The operator between the parenthesis is the material derivative

$$D_t \equiv (\partial_t + \mathbf{v} \cdot \nabla). \quad (2.14)$$

Therefore, we have

$$\rho D_t \mathbf{v} = -\nabla p. \quad (2.15)$$

This is another form to state the Newton's second-law.

2.1.3 Energy conservation

The energy processes in a fluid is governed by thermodynamic laws and convection. It is convenient to work with thermodynamic quantities per unit of mass. So, the internal energy per unit mass (specific energy) of a fixed volume V is denoted by ϵ , while its

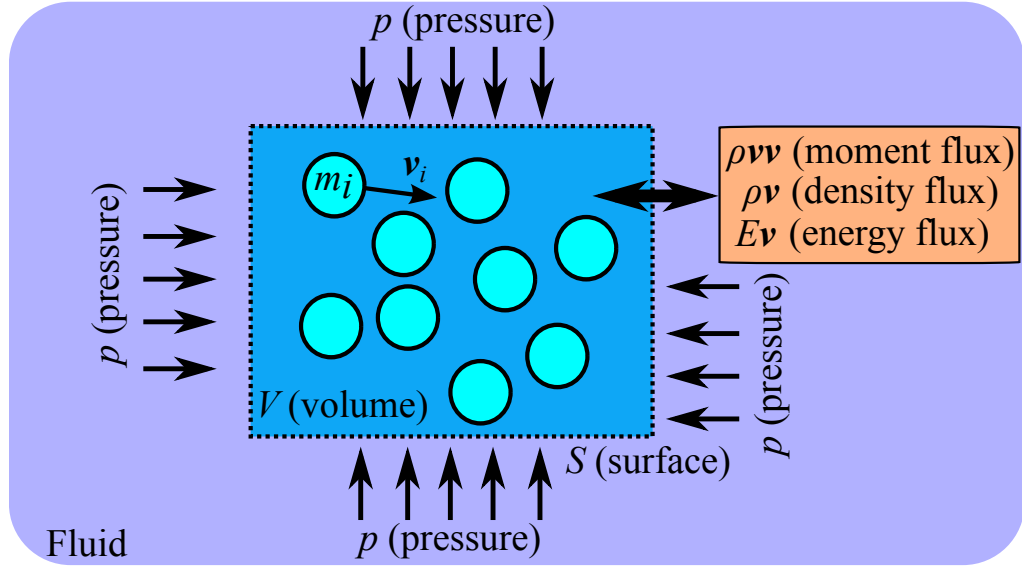


Figure 2.1: Forces acting on fluid particles occupying volume $V'(t)$. Each point on the surface of which moves with the local fluid velocity $\mathbf{v}(\mathbf{r}_s, t)$.

specific entropy is s . The first-law of thermodynamics states that

$$d\varepsilon = Tds - pd(\rho^{-1}) = Tds + \frac{p}{\rho^2}d\rho, \quad (2.16)$$

where T is the temperature at \mathbf{r} . It is assumed here that heat transport throughout the fluid is slow compared to acoustic propagation. Thus, we assume that the specific entropy is constant $s = s_0$ throughout the fluid. For further details see Ref. [46]. Therefore, the first-law of thermodynamics becomes $d\varepsilon = pp^{-2}d\rho$. Thus, both the specific internal energy and the pressure can be expressed as a function of density,

$$p = p(\rho), \quad (2.17)$$

$$\varepsilon = \varepsilon(\rho). \quad (2.18)$$

The energy density inside the volume V at the time t is the sum of the kinetic and the internal energy densities,

$$E(\mathbf{r}, t) = \frac{\rho v^2(\mathbf{r}, t)}{2} + \rho\varepsilon(\mathbf{r}, t). \quad (2.19)$$

In a similar way to the analysis performed for the linear momentum conservation equation in Sec. 2.1.2, the rate change of the energy density (power per volume) in the volume V is due to energy convection from the surroundings through the surface S of V and the rate change of the work done by pressure forces done on S . The energy density convection is given in terms of the energy flux $(\rho v^2/2 + \rho\varepsilon)\mathbf{v}$, while the power due to pressure is $p\mathbf{v}$ (see Fig. 2.1). Therefore, the energy density conservation can be written as

$$\partial_t \int_V \left(\frac{\rho v^2}{2} + \rho\varepsilon \right) d^3\mathbf{r} + \int_S \left(\frac{\rho v^2}{2} + \rho\varepsilon \right) \mathbf{v} \cdot \mathbf{n} d^2\mathbf{r} + \int_S p\mathbf{v} \cdot \mathbf{n} d^2\mathbf{r} = 0 \quad (2.20)$$

Using the Gauss divergence theorem and noticing that the volume V is arbitrary, we obtain the energy conservation equation, as

$$\partial_t \left(\frac{\rho v^2}{2} + \rho \varepsilon \right) + \nabla \cdot \left[\left(\frac{\rho v^2}{2} + \rho \varepsilon \right) \mathbf{v} + p \mathbf{v} \right] = 0. \quad (2.21)$$

2.2 Wave dynamics

The dynamics of wave propagation in an ideal fluids can be described the mass and momentum conservation equations and the pressure-density state relation. According to Eqs. (2.5), (2.9), and (2.17) we have

$$\partial_t \rho + \nabla \cdot \rho \mathbf{v} = 0, \quad (2.22)$$

$$\partial_t (\rho \mathbf{v}) + \nabla \cdot \mathbf{S} = \mathbf{0}, \quad (2.23)$$

$$p = p(\rho). \quad (2.24)$$

Let us further consider that the fluid is homogeneous. Thus, the ambient density ρ_0 and pressure p_0 are constants through the fluid. Moreover, we expand the excess of pressure $p - p_0$ in a Taylor series in terms of the fluctuation density $\rho - \rho_0$ to obtain

$$p - p_0 = \sum_{n=0}^{\infty} (\rho - \rho_0)^n (\partial_{\rho}^n p)_{\rho_0}, \quad (2.25)$$

where $\partial_{\rho} = \partial/\partial\rho$. The adiabatic speed of sound is defined as

$$c_0^2 = (\partial_{\rho} p)_{\rho_0}. \quad (2.26)$$

We see that the wave dynamics in an ideal fluid is described by a system of nonlinear partial differential equations in (2.22)-(2.24). For an specific problem, solutions of this nonlinear system should also satisfy the appropriate boundary conditions. However, exact solutions of these equations are usually not possible. Though, approximate solutions can be achieved using the method of successive approximation. In this method, the pressure, density, and fluid element velocity are expanded in powers of some small parameter $\epsilon < 1$ as follows

$$p - p_0 = \sum_{n=1}^{\infty} \epsilon^n p^{(n)}, \quad (2.27)$$

$$\rho - \rho_0 = \sum_{n=1}^{\infty} \epsilon^n \rho^{(n)}, \quad (2.28)$$

$$\mathbf{v} = \sum_{n=1}^{\infty} \epsilon^n \mathbf{v}^{(n)}. \quad (2.29)$$

The super-index denotes the expansion order. The derivation of the acoustic radiation force and torque formulas requires second-order fields. We will perform an analysis on

this problem in chapter 3. Nevertheless, for the related scattering problem, the linear approximation of the acoustic fields suffices.

The expansion parameter to be used here is the Mach number $\epsilon = v_0/c_0$, where v_0 is the maximum magnitude of the fluid element velocity and c_0 is the adiabatic speed of sound in the fluid. Therefore, our analysis is restricted to the very low speed regime, $\epsilon < 1$.

2.2.1 Linear wave equation

A small acoustic perturbation to which $\epsilon \ll 1$ can be described of linear approximation of the pressure, density and velocity fluid element fields,

$$p - p_0 = \epsilon p^{(1)}, \quad (2.30)$$

$$\rho - \rho_0 = \epsilon \rho^{(1)}, \quad (2.31)$$

$$\mathbf{v} = \epsilon \mathbf{v}^{(1)}, \quad (2.32)$$

Furthermore, in linear approximation the pressure-density from the expansion in Eq. (2.25) is

$$p^{(1)} = c_0^2 \rho^{(1)}. \quad (2.33)$$

Now, we substitute Eqs. (2.30), (2.31), and (2.32) into Eqs. (2.22) and (2.23). Keeping only ϵ -terms and dropping the super-index ⁽¹⁾ for the sake of simplicity, we obtain the linear fluid dynamics equations as

$$\frac{1}{c_0^2} \partial_t p + \rho_0 \nabla \cdot \mathbf{v} = 0, \quad (2.34)$$

$$\rho_0 \partial_t \mathbf{v} + \nabla p = \mathbf{0}. \quad (2.35)$$

Note that we have eliminated the density using the pressure-density relation in Eq. (2.33).

By taking the rotational $\nabla \times$ of Eq. (2.35) we find that fluid element velocity is irrotational,

$$\nabla \times \mathbf{v} = \mathbf{0}. \quad (2.36)$$

Therefore, we introduce a potential function $\phi(\mathbf{r}, t)$ for the fluid element velocity as follows

$$\mathbf{v} = -\nabla \phi. \quad (2.37)$$

From Eq. (2.35), the pressure is given in terms of the velocity potential by

$$p = \rho_0 \partial_t \phi. \quad (2.38)$$

Substituting the linear fluid element velocity and pressure in terms of the velocity potential into Eq. (2.34), we find the linear wave equation for the velocity potential,

$$\left(\nabla^2 - \frac{1}{c_0^2} \partial_t^2 \right) \phi(\mathbf{r}, t) = 0. \quad (2.39)$$

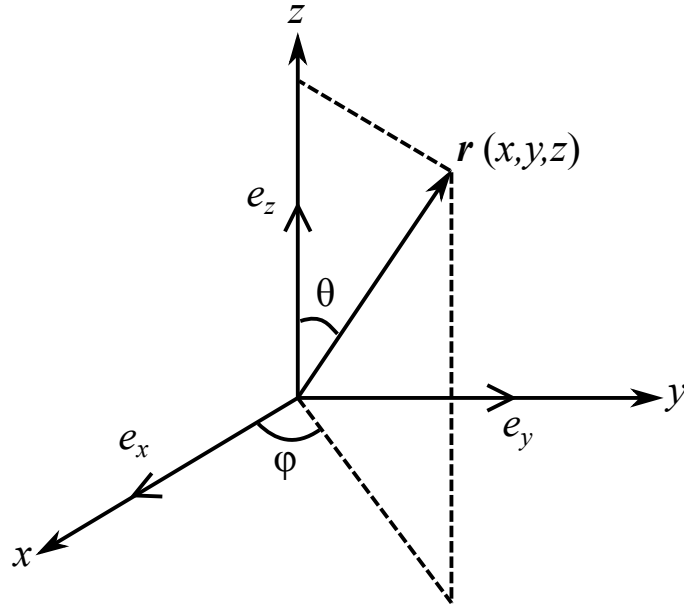


Figure 2.2: Spherical coordinates (r, θ, φ) : radial distance r , polar angle θ (theta), and azimuthal angle φ (phi) and $(\mathbf{e}_x, \mathbf{e}_y, \mathbf{e}_z)$ are the unit-vectors in Cartesian coordinate.

It is clear that both pressure and fluid element velocity also satisfy a linear wave equation.

2.2.2 Helmholtz equation

The radiation force and torque phenomena are related to a time-harmonic wave with angular frequency ω . Hence, the fluid element velocity is given by $\phi(\mathbf{r})e^{-i\omega t}$. Note that $\phi(\mathbf{r})$ is the complex spatial amplitude of the fluid element velocity. Substituting this expression into the linear wave equation in (2.39), we obtain the Helmholtz equation,

$$(\nabla^2 + k^2)\phi(\mathbf{r}) = 0. \quad (2.40)$$

This equation can be solved given the boundary conditions of an specific wave propagation problem, such as source distribution or inclusions (scatters) placed in the fluid.

In our study on acoustic scattering problems, we chose to solve the Helmholtz equation in spherical coordinate system (r, θ, φ) , where r is the radial distance, θ is the polar angle, and φ is azimuthal angle (see Fig. 2.2). The relations between Cartesian and spherical coordinates are

$$x = r \sin \theta \cos \varphi, \quad (2.41)$$

$$y = r \sin \theta \sin \varphi, \quad (2.42)$$

$$z = r \cos \theta. \quad (2.43)$$

It is useful to notice that the radial unit-vector is given by

$$\mathbf{e}_r = \sin \theta \cos \varphi \mathbf{e}_x + \sin \theta \sin \varphi \mathbf{e}_y + \cos \theta \mathbf{e}_z. \quad (2.44)$$

where e_i ($i = x, y, z$) are the unit-vectors in Cartesian coordinate.

2.3 Solution of the Helmholtz equation

In spherical coordinates, the Helmholtz equation takes the form

$$\frac{1}{r^2} \partial_r (r^2 \partial_r \phi) + \frac{1}{r^2 \sin \theta} \partial_\theta (\sin \theta \partial_\theta \phi) + \frac{1}{r^2 \sin^2 \theta} \partial_\varphi^2 \phi + k^2 \phi = 0. \quad (2.45)$$

The general solution of Helmholtz equation can be found in spherical coordinates using the method of separation of variables. In doing so, we write the fluid element velocity amplitude as

$$\phi(r, \theta, \varphi) = R(r)\Theta(\theta)\Phi(\varphi), \quad (2.46)$$

where $R(r)$, $\Theta(\theta)$, $\Phi(\varphi)$ are arbitrary radial, polar and azimuthal functions. Substituting Eq. (2.46) into Eq. (2.45), we have

$$\frac{1}{\Phi} d_\varphi^2 \Phi(\varphi) = -m^2, \quad (2.47)$$

$$\frac{1}{\sin \theta} d_\theta (\sin \theta d_\theta \Theta) - \frac{m^2}{\sin^2 \theta} \Theta + n(n+1)\Theta = 0, \quad (2.48)$$

$$\frac{1}{r^2} d_r (r^2 d_r R) + k^2 R - \frac{n(n+1)R}{r^2} = 0, \quad (2.49)$$

where m and n are integer constants to be determined. Note we are using the shorthand notation $d_r = d/dr$, $d_\theta = d/d\theta$ and $d_\varphi = d/d\varphi$.

We can solve Eq. (2.47) and obtain

$$\Phi(\varphi) = \Phi_1 e^{im\varphi} + \Phi_2 e^{-im\varphi}, \quad (2.50)$$

where Φ_1 and Φ_2 are constants and m must be an integer so that there is continuity and periodicity of $\Phi(\varphi)$.

To find the solution of Eq. (2.48), we introduce $\eta = \cos \theta$. Thus, Eq.(2.48) becomes

$$d_\theta [(1 - \eta^2) d_\theta \Theta] + \left[n(n+1) - \frac{m^2}{1 - \eta^2} \right] \Theta = 0. \quad (2.51)$$

The solution of Eq. (2.51) assumes the form

$$\Theta(\theta) = \Theta_1 P_n^m(\cos \theta), \quad (2.52)$$

where $P_n^m(\cos \theta)$ are the associated Legendre functions and Θ_1 is a constant. The angular functions Θ and Φ are conveniently combined into a single function called a spherical harmonic Y_n^m , which can be defined as

$$Y_n^m(\theta, \varphi) \equiv \sqrt{\frac{(2n+1)(n-m)!}{4\pi(n+m)!}} P_n^m(\cos \theta) e^{im\varphi}, \quad n \geq 0, -n \leq m \leq n. \quad (2.53)$$

The radial Eq. (2.49) is known as the spherical Bessel equation, which solution is given by

$$R(r) = R_1 j_n(kr) + R_2 y_n(kr), \quad (2.54)$$

where the j_n and y_n are the spherical Bessel and spherical Neumann functions of order n , respectively, and R_1 and R_2 are constants. Alternatively, this solution can be written as [47]

$$R(r) = R_3 h_n^{(1)}(kr) + R_4 h_n^{(2)}(kr), \quad (2.55)$$

The quantities $h_n^{(1)}$ and $h_n^{(2)}$ are the spherical Hankel functions of the first and second kind and order n , respectively, and R_3 and R_4 are constants.

Thus, the general solution of the Helmholtz equation can be given by

$$\phi(kr, \theta, \varphi) = \phi_0 \sum_{n,m} [a_{nm} j_n(kr) + b_{nm} y_n(kr)] Y_n^m(\theta, \varphi), \quad (2.56)$$

where ϕ_0 is the velocity potential magnitude and $\sum_{n,m} = \sum_{n=0}^{\infty} \sum_{m=-n}^n$. Alternatively, we can write

$$\phi(kr, \theta, \varphi) = \phi_0 \sum_{n,m} [s_{nm} h_n^{(1)}(kr) + c_{nm} h_n^{(2)}(kr)] Y_n^m(\theta, \varphi), \quad (2.57)$$

where a_{nm} , b_{nm} , s_{nm} and c_{nm} are coefficients to be determined from the boundary condition of a specific acoustic problem.

2.4 Scattering by a sphere

Given an ideal fluid medium of infinite extent, consider that a sphere of radius a is placed at the origin of the coordinate system (see Fig. 2.3). An incident wave will be scattered by the sphere. Hence, we can divide the scattering by the sphere into two parts, namely the interior and the exterior problems. For the interior problem, we are concerned to find the solution of a wave which propagates in a region which includes the origin of the coordinate system. Clearly, such a solution should be regular at the origin, i.e. it should remain finite inside the propagation region. The interior problem is related to the propagation of the incident and the transmitted waves to the sphere. Therefore, we can write the incident and the transmitted potential functions, respectively, as

$$\phi_{\text{in}}(kr, \theta, \varphi) = \phi_0 \sum_{n,m} a_{nm} J_n^m(kr, \theta, \varphi), \quad (2.58)$$

$$\phi_{\text{tr}}(kr, \theta, \varphi) = \phi_0 \sum_{n,m} t_n a_{nm} J_n^m(kr, \theta, \varphi), \quad (2.59)$$

where a_{nm} and $t_n a_{nm}$ are the beam-shape and the transmitting coefficients, with t_n is the scaled transmitting coefficient to be determined from the boundary conditions on the

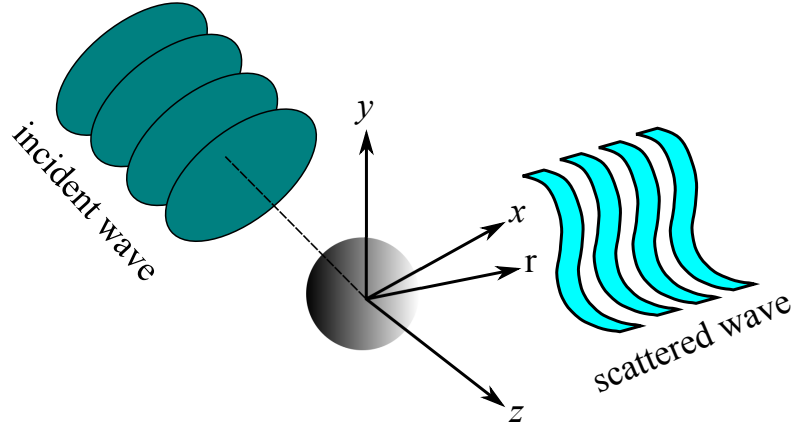


Figure 2.3: Coordinate system used in the single scattering problem

sphere surface. According to Eq. (2.56), the regular partial-wave function is defined as

$$J_n^m(kr, \theta, \varphi) \equiv j_n(kr)Y_n^m(\theta, \varphi). \quad (2.60)$$

The beam-shape coefficient can be determined in terms of the incident potential velocity evaluated on the surface of a control sphere of radius $R \gg a$. Thus, multiplying Eq. (2.58) by $Y_n^{m'*}(\theta, \varphi)$, performing the angular integral, and using the orthonormality relation of the spherical harmonics, we find

$$a_{nm} = \frac{1}{j_n(kR)} \int_0^\pi \int_0^{2\pi} \tilde{\phi}_{\text{in}}(kR, \theta, \varphi) Y_n^{m*}(\theta, \varphi) \sin\theta d\theta d\varphi,$$

where $\tilde{\phi}_{\text{in}} = \phi_{\text{in}}/\phi_0$ is the normalized incident potential.

The farfield approximation for the incident wave is obtained by substituting the asymptotic form of the spherical Bessel function

$$j_n(kr) \underset{kr \gg 1}{\sim} \frac{\sin(kr - n\pi/2)}{kr}. \quad (2.61)$$

into Eq. (2.58). Therefore,

$$\phi_{\text{in}}(kr, \theta, \varphi) \underset{kr \gg 1}{\sim} \phi_0 \frac{\sin(kr - n\pi/2)}{kr} \sum_{n,m} a_{nm} Y_n^m(\theta, \varphi), \quad (2.62)$$

On the other hand, the exterior problem excludes the region which includes the origin of the coordinate system. Thus, the exterior problem is connect to the scattered waves by the spherical scatterer. Moreover, the scattered wave amplitude ϕ_{sc} should satisfy the Sommerfeld radiation condition at infinity,

$$\lim_{r \rightarrow \infty} r (\partial_r - ik) \phi_{\text{sc}} = 0. \quad (2.63)$$

This condition imposes that the scattered wave should not be reflected back at infinity.

Therefore, the amplitude of the scattered wave is given by

$$\phi_{\text{sc}}(kr, \theta, \varphi) = \phi_0 \sum_{n,m} s_n a_{nm} H_n^m(kr, \theta, \varphi), \quad (2.64)$$

where $s_n a_{nm}$ is the scattering coefficient, with being s_n the scaled scattering coefficient. According to Eq. (2.57), the scattering partial-wave function is

$$H_n^m(kr, \theta, \varphi) \equiv h_n^{(1)}(kr) Y_n^m(\theta, \varphi). \quad (2.65)$$

The scattered wave in the farfield $kr \gg 1$ can be obtained by substituting the asymptotic relation

$$h_n^{(1)}(kr) \underset{kr \gg 1}{\sim} i^{-n-1} \frac{e^{ikr}}{kr}, \quad (2.66)$$

into the Eq. (2.64). Thus, we find

$$\phi_{\text{sc}}(kr, \theta, \varphi) \underset{kr \gg 1}{\sim} -\frac{i\phi_0 e^{ikr}}{kr} \sum_{n,m} i^{-n} s_n a_{nm} Y_n^m(\theta, \varphi). \quad (2.67)$$

Consider that the scatterer is a compressible fluid sphere with density ρ_1 and $1/(\rho_1 c_1^2)$ is called compressibility, where c_1 is speed of sound inside the sphere. In order to obtain a unique solution for the scattering by the sphere, both pressure and fluid-element velocity should be continuous on the sphere surface. Hence, we have

$$p_{\text{in}}(ka, \theta, \varphi) + p_{\text{sc}}(ka, \theta, \varphi) = p_{\text{tr}}(ka, \theta, \varphi), \quad (2.68)$$

$$\mathbf{v}_{\text{in}}(ka, \theta, \varphi) + \mathbf{v}_{\text{sc}}(ka, \theta, \varphi) = \mathbf{v}_{\text{tr}}(ka, \theta, \varphi), \quad (2.69)$$

where the sub-indexes ‘in’, ‘sc’ and ‘tr’ stand for the incident, the scattered, and the transmitted waves, respectively. Using Eqs. (2.58), (2.59) and (2.64) into Eqs. (2.68) and (2.69), with the aid of Eq. (2.38) and (2.37), we obtain the scaled scattering and the transmitted coefficients as

$$s_n = \frac{\gamma j_n'(ka) j_n(k_1 a) - j_n(ka) j_n'(k_1 a)}{\gamma h_n^{(1)'}(ka) j_n(k_1 a) - h_n^{(1)}(ka) j_n'(k_1 a)}, \quad (2.70)$$

$$t_{nm} = -\frac{a_{nm} j_n(ka) + s_n a_{nm} h_n^{(1)}(ka)}{j_n(k_1 a)}, \quad (2.71)$$

where the prime symbol means time derivation, $\gamma = k\rho_1/k_1\rho_0$ is the impedance index, and $k_1 = \omega/c_1$ is the wavenumber inside the sphere.

2.5 Multiple scattering theory

The intrinsically nonlinear nature of wave motion in fluids results in a great variety of nonlinear effects. One such effect is the time-averaged radiation interaction forces that are induced by an acoustic wave field between foreign inclusions (bubbles, drops,

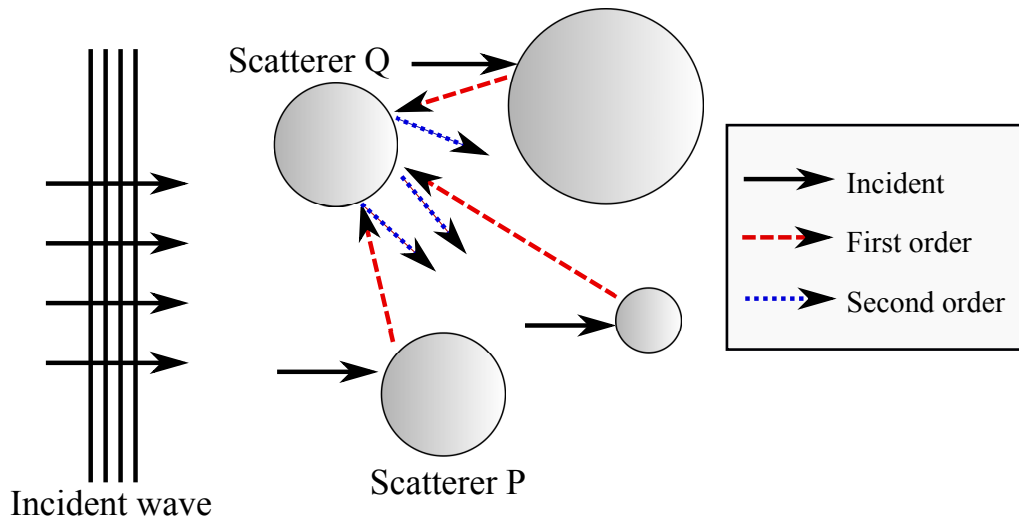


Figure 2.4: Multiple scattering from a cluster of scatterers

etc.) suspended in a fluid. Interest in this phenomenon is motivated by a number of important applications, such as acoustic cavitation, acoustic coagulation and precipitation of aerosols, biomedical ultrasonics, etc.

In this work, multiple scattering is referred to as the scattering process between multiple scatterers suspended in an infinite ideal fluid, for reviews see, [put some references here] It should be noticed that, in this case, rescattering events occur which means that a scattered wave by one particle is further scattered by other objects in the medium. It is useful to associate each rescattering events to an ordering scheme. The rescattering ordering scheme can be understood as follows. The first-order event is the scattering by the incident (external) wave to the suspended objects. The second-order event is the scattering by the objects of the first-order scattered wave. Higher-order events follows the same explanation. Figure 2.4 presents a pictorial view of the first- and the second-order scattering events.

Consider an inviscid fluid of infinite extent characterized by the ambient density ρ_0 and the speed of sound c_0 . We restrict our analysis to low-amplitude waves with the Mach number $\epsilon \ll 1$. Assume that an incident external wave interacts with a set of N fluid spheres ($N \geq 2$). One of the spheres is regarded as to the *probe*, with radius of has radius a_p , located at an arbitrary position \mathbf{r}'_p . The other spheres referred to as *sources* have radii a_q and are arbitrary placed at \mathbf{r}'_q for $q = 1, 2, \dots, N - 1$ (see Fig.(2.5)). The spheres in the medium are described by a density ρ_q and speed of sound c_q ($q = p, 1, 2, \dots, N - 1$). Due to the transferring of the linear and the angular momentum from the external wave, an external radiation force and torque may appear on the spheres. Moreover, re-scattering events may give rise to the acoustic interaction force and torque between the spheres. To calculate the acoustic interaction force and torque exerted on the *probe* sphere, we have to compute the effective incident wave on each sphere. In turn, this wave is generated due to multiple scattering events, which involves wave interaction with the other $N - 1$ source spheres.

The potential amplitude of the external incident wave can be expanded in the spherical

partial-wave series with respect to the coordinate system O_p , which is located at the center of the probe sphere. Hence, representing the observation vector \mathbf{r}_p in spherical coordinates $(r_p, \theta_p, \varphi_p)$, we express the external potential amplitude as

$$\phi_{p,\text{ex}}(\mathbf{r}_p) = \phi_0 \sum_{n,m} a_{p,nm} J_n^m(\mathbf{r}_p), \quad (2.72)$$

where $a_{p,nm}$ is the expansion coefficient referred to as the external beam-shape coefficient with respect to O_p . It is worthy to notice that the subindex (p) of the scattering ordering scheme should not be confused with that of the Mach number expansion of the acoustic fields given in Eqs. (2.27)-(2.29).

The beam-shape coefficient depends on the choice of the coordinate system. Thus, the coefficients $a_{q,nm}$ are related to system O_q . Furthermore, they can be obtained using the translational addition theorem for spherical functions, which provides a way to represent the partial-waves with respect to O_q in terms of those in the system O_p . Using the orthonormality property of the spherical harmonics in (2.72), we can obtain the beam-shape coefficient with respect to the system O_p as

$$a_{p,nm} = \frac{1}{j_n(kR_p)} \int_0^\pi \int_0^{2\pi} \tilde{\phi}_{p,\text{ex}}(kR_p, \theta_p, \varphi_p) Y_n^{m*}(\theta_p, \varphi_p) \sin\theta d\theta d\varphi,$$

where R_p is the radius of any spherical region centered at O_p which enclosed the particle at \mathbf{r}'_p , and $\tilde{\phi}_{p,\text{ex}} = \phi_{p,\text{ex}}/\phi_0$.

The external incident wave can be expanded in a partial-series from with respect to another system O_q as

$$\phi_{q,\text{ex}}(\mathbf{r}_q) = \phi_0 \sum_{\nu,\mu} a_{q,\nu\mu} J_\nu^\mu(\mathbf{r}_q). \quad (2.73)$$

The addition theorem of spherical functions provides a way to expand the partial-waves with respect to O_q in a series with respect to the system O_p . Accordingly, [48]

$$J_\nu^\mu(\mathbf{r}_q) = \sum_{\nu,\mu} S_{\nu\nu}^{m\mu,0}(\mathbf{r}'_{qp}) J_\nu^\mu(\mathbf{r}_p), \quad (2.74)$$

where $\mathbf{r}'_{qp} = \mathbf{r}'_q - \mathbf{r}'_p = \mathbf{r}_q - \mathbf{r}_p$ is the vector from O_q to O_p . The translational coefficient is given by

$$S_{\nu\nu}^{m\mu,0}(\mathbf{r}'_{qp}) = 4\pi i^{\nu-n} \sum_{\sigma=|n-\nu|}^{n+\nu} i^\sigma (-1)^m \mathcal{G}(n, m; \nu, \mu; \sigma) J_\sigma^{\mu-m}(kr_q, \theta_{qp}, \phi_{qp}), \quad (2.75)$$

where θ_{qp} and φ_{qp} are the polar and azimuthal angles of the vector \mathbf{r}'_{qp} , and $\mathcal{G}(n, m; \nu, \mu; \sigma)$ is the Gaunt coefficient given by [48]. This coefficient is zero if any of the following conditions happens $n + \nu + \sigma$ is odd, $\sigma > \nu + n$, or $\sigma < |n - \nu|$. Now, substituting (2.74)

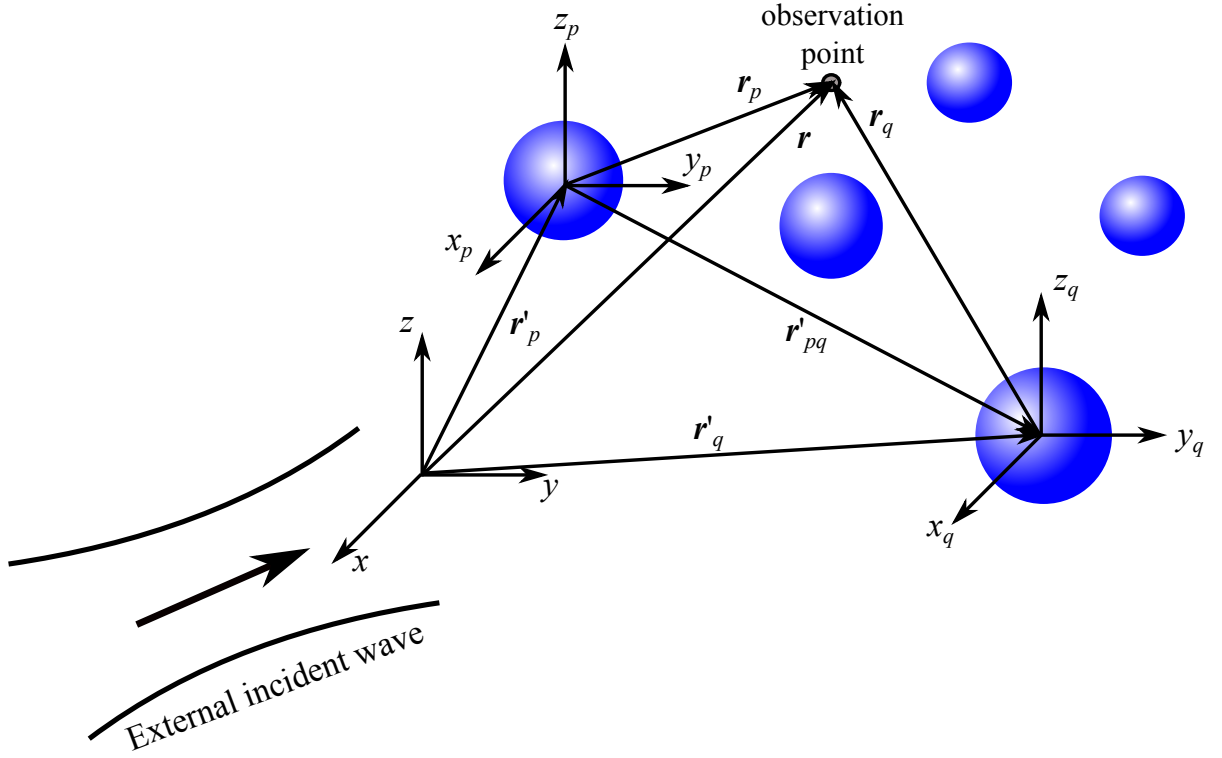


Figure 2.5: Geometric description of the multiple scattering by particles in a suspension. A source particle is located at \mathbf{r}_q and its corresponding scattered wave is probed at \mathbf{r}_p .

into (2.72) and using the result in (2.73), one obtains

$$a_{q,nm} = \sum_{\nu,\mu} a_{p,\nu\mu} S_{n\nu}^{m\mu,1}(\mathbf{r}'_{pq}), \quad (2.76)$$

with $\mathbf{r}'_{qp} = \mathbf{r}'_q - \mathbf{r}'_p = \mathbf{r}_q - \mathbf{r}_p$.

The amplitude of the scattered potential function of the probe sphere is given by

$$\phi_{p,sc}(\mathbf{r}_p) = \phi_0 \sum_{n,m} s_{p,nm} H_n^m(\mathbf{r}_p), \quad (2.77)$$

where $s_{p,nm}$ is the scattering coefficient with respect to O_p , which will be assessed using the boundary conditions on the sphere surface. Note that (2.77) satisfies the Sommerfeld radiation condition given in Eq. (2.63).

The external incident wave can penetrate into the probe sphere. The potential velocity inside each sphere can be expressed as

$$\phi_{p,tr}(k_p; \mathbf{r}_p) = \phi_0 \sum_{n,m} t_{p,nm} J_n^m(k_p; \mathbf{r}_p), \quad (2.78)$$

where $t_{p,nm}$ are the transmission coefficient to be determined using appropriate boundary conditions on the probe sphere surface, and $k_p = \omega/c_p$ is the internal wavenumber of the probe sphere.

Since we want to compute the radiation force and torque on the probe sphere, we need

to know the total scattered potentials resulting from all the other source spheres evaluated with respect to the system O_p . The amplitude of the scattered wave by a source sphere placed at \mathbf{r}'_q is given by

$$\phi_{qp,sc}(\mathbf{r}_p) = \phi_0 \sum_{n,m} s_{qp,nm} J_n^m(\mathbf{r}_p), \quad (2.79)$$

where $s_{qp,nm}$ are the source-probe scattering coefficients with respect to O_p .

To determine the source-probe scattering coefficients $s_{qp,nm}$, we use the translational addition theorem for spherical functions as explained for the beam-shape coefficient. Using the orthonormality property of the spherical harmonics in (2.84), the scattering coefficient with respect to the system O_p are found from

$$s_{qp,nm} = \frac{1}{h_n^{(1)}(kR_p)} \int_0^\pi \int_0^{2\pi} \tilde{\phi}_{qp,sc}(kR_p, \theta_p, \varphi_p) Y_n^{m*}(\theta_p, \varphi_p) \sin \theta d\theta d\varphi, \quad (2.80)$$

where R_p is the radius of any spherical region centered at O_p which enclosed the particle at \mathbf{r}'_p , and $\tilde{\phi}_{qp,sc} = \phi_{qp,sc}/\phi_0$. The scattered waves can be expanded in a partial-series with respect to another system O_q as

$$\phi_{qp,sc}(k; \mathbf{r}_q) = \phi_0 \sum_{\nu,\mu} s_{qp,\nu\mu} H_\nu^\mu(k; \mathbf{r}_q). \quad (2.81)$$

Similar to the regular partial-waves, we can use the addition theorem for the scattering partial-wave, given as follows [48]

$$H_\nu^\mu(\mathbf{r}_q) = \sum_{\nu,\mu} S_{n\nu}^{m\mu,1}(\mathbf{r}'_{qp}) J_\nu^\mu(\mathbf{r}_p), \quad (2.82)$$

where $\mathbf{r}'_{qp} = \mathbf{r}'_q - \mathbf{r}'_p = \mathbf{r}_q - \mathbf{r}_p$ is the vector from O_q to O_p , see Fig.(2.5) For this case, the translational coefficient is given by

$$S_{n\nu}^{m\mu,2}(\mathbf{r}'_{qp}) = 4\pi i^{\nu-n} \sum_{\sigma=|n-\nu|}^{n+\nu} i^\sigma (-1)^m \mathcal{G}(n, m; \nu, \mu; \sigma) H_\sigma^{\mu-m}(kr_q, \theta_{qp}, \phi_{qp}). \quad (2.83)$$

By substituting (2.82) into (2.84) and using the result in (2.80), one obtains

$$s_{qp,nm} = \sum_{\nu,\mu} s_{q,nm} S_{n\nu}^{m\mu,2}(\mathbf{r}'_{qp}), \quad (2.84)$$

where $s_{nm}^{(q)}$ are the scattering coefficient in (2.77) with $p = q$, and $S_{n\nu}^{m\mu,2}$ are given in (2.74).

Now, we can express the total potential velocity function outside the probe sphere as

$$\phi_p(\mathbf{r}_p) = \phi_{p,ex}(\mathbf{r}_p) + \phi_{p,sc}(\mathbf{r}_p) + \sum_{q=1}^N{}' \phi_{qp,sc}(\mathbf{r}_p), \quad (2.85)$$

where the primed summation symbol means $q \neq p$. The boundary conditions on the

surface of the probe sphere are the continuity of the pressure and the radial component of the fluid velocity. Therefore, from (2.85) we obtain for $r_p = a_p$,

$$\phi_{p,\text{ex}}(k_p a_p, \theta_p, \varphi_p) + \phi_{p,\text{sc}} + \sum_{q=1}^N \phi_{qp,\text{sc}}(k_p a_p, \theta_q, \varphi_q) = \phi_{p,\text{tr}}(k_p a_p, \theta_p, \varphi_p), \quad (2.86)$$

$$\begin{aligned} \partial_r \phi_{p,\text{ex}}(k_p a_p, \theta_p, \varphi_p) + \partial_r \phi_{p,\text{sc}}(k_p a_p, \theta_p, \varphi_p) + \sum_{q=1}^N \partial_r \phi_{qp,\text{sc}}(k_p a_p, \theta_q, \varphi_q) \\ = \partial_r \phi_{p,\text{tr}}(k_p a_p, \theta_p, \varphi_p). \end{aligned} \quad (2.87)$$

Likewise, they can be similarly applied to any other source spheres in the medium by setting $p = 1, 2, \dots, N - 1$. In doing so and using Eqs. (2.72), (2.77), (2.78), (2.79), and (2.84) into Eqs. (2.86) and (??), one finds that the scattering coefficients for all spheres suspended in the host fluid are given by

$$s_{q,nm} = s_{q,n} b_{q,nm}, \quad q = p, 1, 2, \dots, N - 1, \quad (2.88)$$

where $s_{q,n}$ are the scaled scattering coefficients to be given later, and $b_{q,nm}$ are the *effective* beam-shape coefficients that represent the compound wave formed by the superposition of the incident wave and all other scattered waves in the medium. Therefore, using (2.88) we find that effective beam-shape coefficients $b_{q,nm}$ ($q \leq N, n \geq 0, -n \leq m \leq n$) satisfying the of linear equations,

$$b_{q,nm} - \sum_{l=1}^N \sum_{\nu,\mu} s_{l,\nu} S_{n\nu}^{m\mu,2}(\mathbf{r}'_{lp}) b_{l,\nu\mu} = a_{q,nm} \quad (2.89)$$

where the primed sum means that $l \neq q$. The scaled scattering coefficients are expressed as

$$\begin{aligned} s_{q,n} = \det \begin{bmatrix} \gamma_q j_n(k a_q) & j_n(k_q a_q) \\ j'_n(k a_q) & j'_n(k_q a_q) \end{bmatrix} \\ \times \det \begin{bmatrix} -\gamma_q h_n(k a_q) & j_n(k_q a_q) \\ -h'_n(k a_q) & j'_n(k_q a_q) \end{bmatrix}^{-1}, \end{aligned} \quad (2.90)$$

where $\gamma_q = k_q \rho_0 / k \rho_q$ and $k_q = \omega / c_q$ is the wavenumber inside the sphere place at \mathbf{r}_q . An absorbing fluid sphere can be accounted for in the model by noticing that the wave propagation inside it has a complex wavenumber in the form [49]

$$k_q = \frac{\omega}{c_q} + i\alpha_q, \quad (2.91)$$

where $\alpha_q = \alpha_{0,q}(\omega/2\pi)^2$, with $\alpha_{0,q}$ being the sphere absorption coefficient.

The system of linear equations in (2.89) has an infinity number of unknown variables. Clearly, to solve (2.89) we need to impose a truncation order in the system. By assuming

that the truncation order in (2.89) is $n = M$, the number of linear equations and unknowns $b_{q,nm}$ becomes $N(M+1)^2$. After imposing the truncation, the system of linear equation is represented in the matrix format [43, 50] $\mathbf{Ax} = \mathbf{y}$ as, where \mathbf{A} is the coefficients matrix, \mathbf{x} and \mathbf{y} are the column vectors of the unknowns and the beam-shape coefficients $a_{q,nm}$. Hence, the solution of (2.89) can be expressed as $\mathbf{x} = \mathbf{A}^{-1}\mathbf{y}$, given that \mathbf{A} is nonsingular. Once the effective beam-shape coefficients $b_{q,nm}$ are determined, the acoustic radiation force and torque can be computed, as will be discussed in the next chapter. In calculating the unknown scattering coefficients, \mathbf{x} , special care must be taken in the above mentioned matrix system may become ill-conditioned at high frequencies or when the particles are very close to one another, producing numerical errors. This has been discussed in other articles on the use of addition theorem [43], [50],[51],[52].[53] and [54].

2.5.1 Acoustic scattering by two rigid spheres

Consider a traveling plane wave interacting with two rigid spheres as described in Fig. 2.6. The spheres are placed at \mathbf{r}'_1 and \mathbf{r}'_2 with respect to the system O . The wave propagation direction is determined by its wavevector

$$\mathbf{k} = k(\sin \alpha \cos \beta \mathbf{e}_x + \sin \alpha \sin \beta \mathbf{e}_y + \cos \alpha \mathbf{e}_z), \quad (2.92)$$

where α and β are, respectively, the polar and the azimuthal angles of the wavevector, and \mathbf{e}_i ($i = x, y, z$) are the unit-vectors in Cartesian coordinates. In the system O , the velocity potential amplitude of the traveling plane wave is given by [55]

$$\phi_{\text{ex}}(kr, \theta, \varphi) = \phi_0 e^{i\mathbf{k}\cdot\mathbf{r}} = \phi_0 \sum_{n,m} 4\pi i^n Y_n^{m*}(\alpha, \beta) j_n(kr) Y_n^m(\theta, \varphi). \quad (2.93)$$

From Eq. (2.58), we recognize the beam-shape coefficients as

$$a_{nm} = 4\pi i^n Y_n^{m*}(\alpha, \beta). \quad (2.94)$$

In the coordinate systems O_1 and O_2 defined by the spheres located at \mathbf{r}'_1 and \mathbf{r}'_2 , the external incident wave becomes

$$\phi_{s,\text{ex}} = \phi_0 e^{i\mathbf{k}\cdot(\mathbf{r}-\mathbf{r}'_s)}, \quad s = 1, 2. \quad (2.95)$$

Thus, the associated beam-shape coefficients are

$$a_{s,nm} = 4\pi i^n Y_n^{m*}(\alpha, \beta) e^{i\mathbf{k}\cdot\mathbf{r}'_s}, \quad s = 1, 2. \quad (2.96)$$

The scaled scattering coefficient for a rigid sphere is obtained from Eq. (2.90) by setting $\rho_1, c_1 \rightarrow \infty$. Thus, we have

$$s_{s,n} = -\frac{j'_n(ka_s)}{h_n^{(1)'}(ka_s)}, \quad s = 1, 2. \quad (2.97)$$

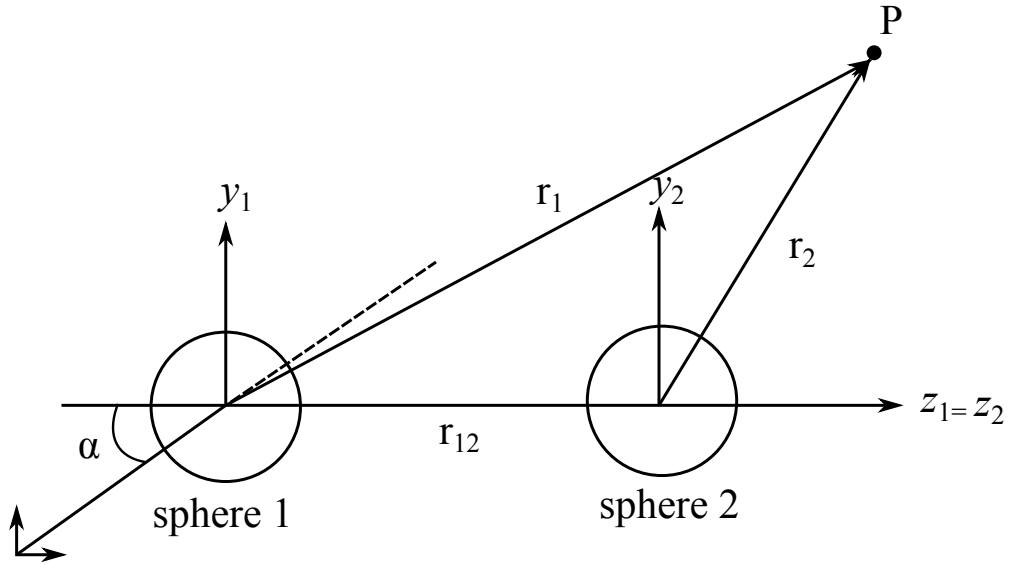


Figure 2.6: Geometry of the problem of two rigid spheres scattering

The total scattered field from both spheres from Eq.(2.64) can be write as,

$$\phi_{sc} = \phi_{1,sc} + \phi_{2,sc} \quad (2.98)$$

Using the asymptotic expansion in Eq.(2.66) we can express the farfield form function as

$$f_{\infty} \cong \frac{(2r)}{a} \frac{\phi_{sc}}{\phi_{s,ex}}. \quad (2.99)$$

The results were reproduced from the work published by [43]. Figs. (2.7), (2.8) and (2.9) shows the form function for an oblique incident plane wave ($\alpha = \pi/4$) on the two rigid spheres and plotted versus the size factor ka . The distance between the spheres are was chosen to be $d = 4a$, $d = 10a$ and $d = 20a$.

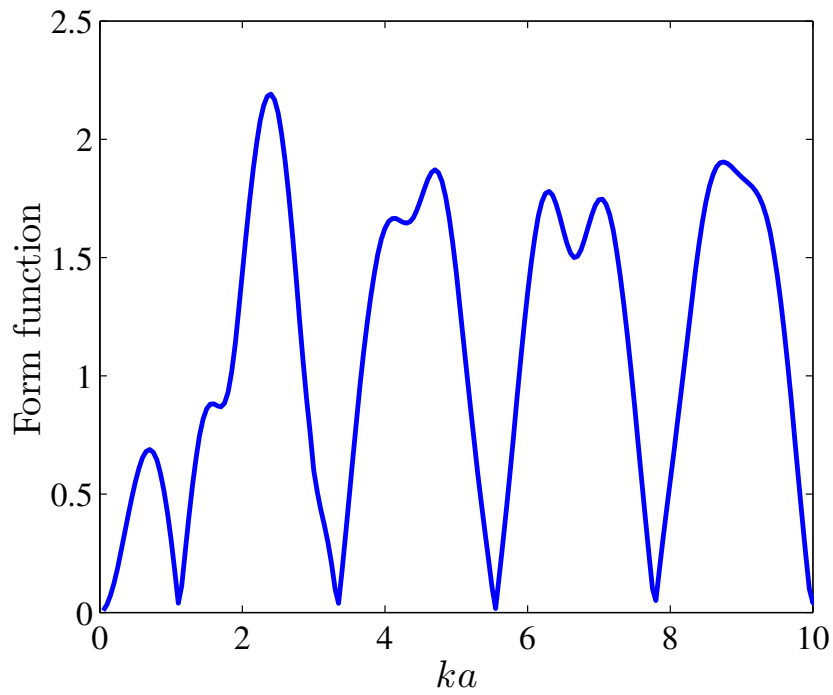


Figure 2.7: Form function of two rigid spheres at an arbitrary (here $\alpha = \pi/4$ and $d/a = 4$) angular incidence. The truncation number is $M = 10$

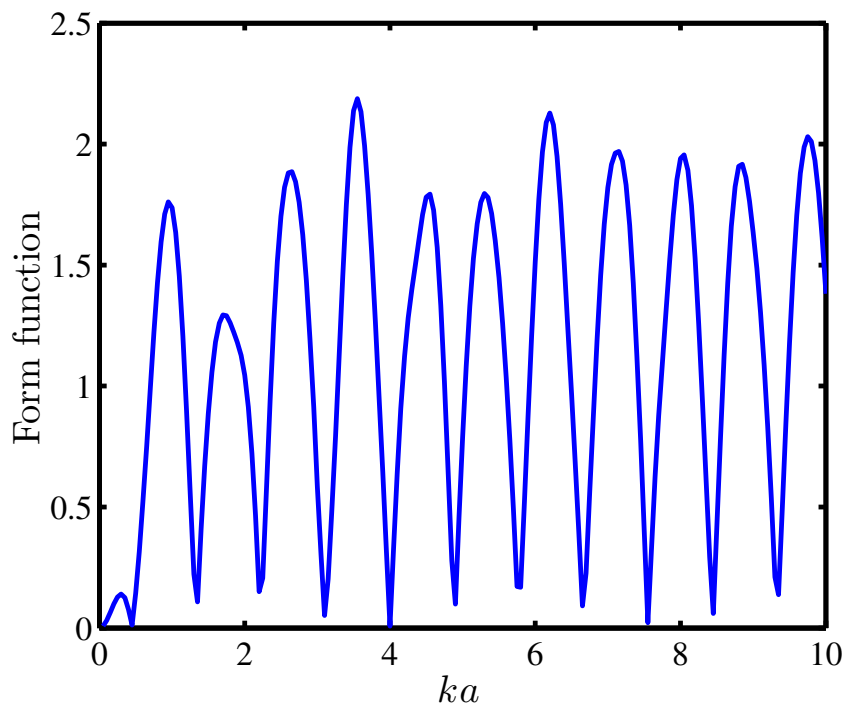


Figure 2.8: Form function of two rigid spheres at an arbitrary (here $\alpha = \pi/4$ and $d/a = 10$) angular incidence. The truncation number is $M = 10$

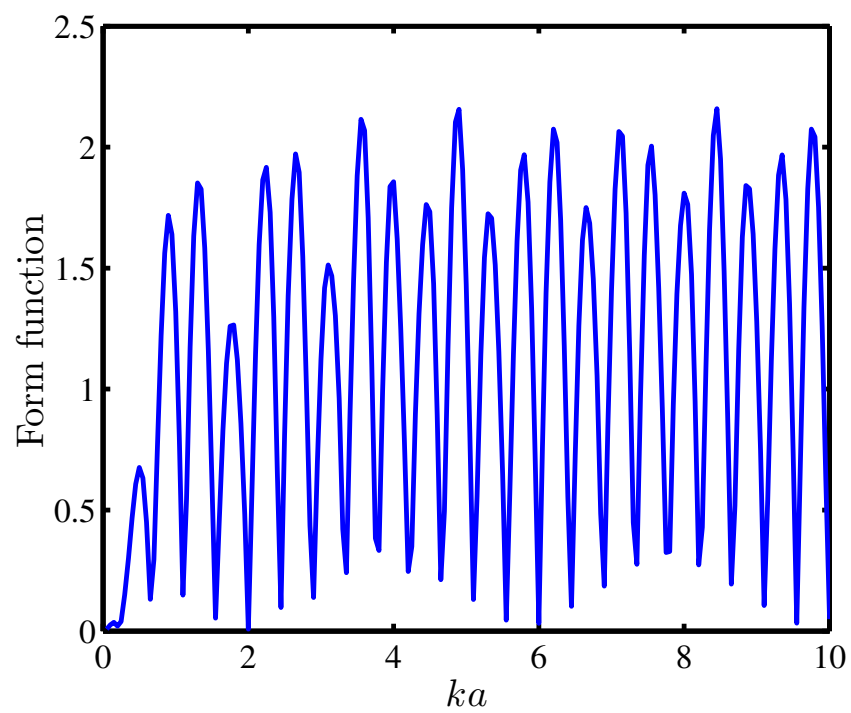


Figure 2.9: Form function of two rigid spheres at an arbitrary (here $\alpha = \pi/4$ and $d/a = 10$) angular incidence. The truncation number is $M = 20$

3

Acoustic radiation force and torque

We have seen in chapter 2 that an acoustic wave carries linear momentum. Hence, when an acoustic wave interacts with a suspended object, part of its linear momentum is transferred to the object. The time-averaged linear momentum flux and stresses acting on the object is called the acoustic radiation force. In a similar way, waves may possess angular momentum which can be transferred to a suspended object. The time-averaged angular momentum flux exerted on the object is referred to as the acoustic radiation torque. In this chapter, we will present the formulas for acoustic radiation force and torque exerted on an object with geometric form due to an arbitrary shaped wave. Examples of the radiation force and torque exerted on a compressible fluid sphere by, respectively, a plane wave and a Bessel vortex beam are presented.

3.1 Acoustic radiation force

3.1.1 Inviscid approach

Consider an acoustic beam of frequency ω interacts with an object with arbitrary geometry suspended in an ideal fluid. The object of characteristic dimension L and the wavelength is denoted by λ . It is important to mention that the fluid thermo-viscosity does not produce significant effects in the acoustic radiation force when the thermal boundary layer $\delta_t = \sqrt{2\kappa/\rho_0 c_p \omega}$ (κ is the thermal conductivity and c_p is the specific heat capacity at constant pressure) and the viscous boundary layer $\delta_v = \sqrt{2\nu/\omega}$ (ν is the kinematic viscosity) are much smaller than both the characteristic object size and wavelength λ [56]. In other words, we will consider the inviscid approach to the acoustic radiation force on an object given the condition

$$\delta_v, \delta_t \ll L, \lambda. \quad (3.1)$$

For example, consider a 1 MHz-wave with wavelength $\lambda = 1.5$ mm propagating in water. The physical properties of water are kinematic viscosity $\nu = 10^{-6}$ m²/s, thermal conductivity $\kappa = 0.6$ W/m · K, and specific heat capacity $c_p = 4180$ J/(kg · K). Hence, the wave produces a thermal $\delta_t = 1.5$ μ m and a viscous $\delta_v = 0.56$ μ m boundary layer on an object. Therefore, we can ignore the boundary layer effects on the acoustic radiation force for objects with characteristic size larger than, say 15 μ m.

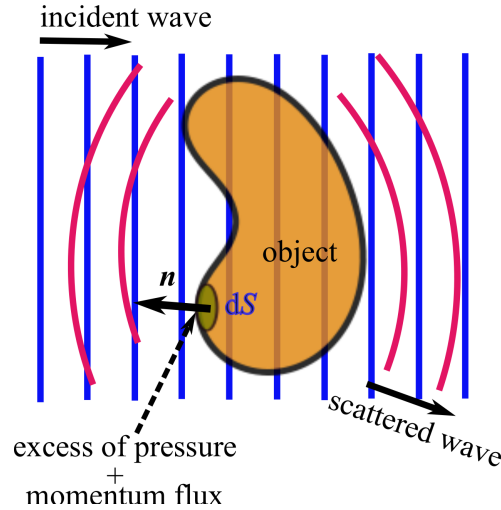


Figure 3.1: Illustration of the interaction between an incident wave and a suspended object. Both pressure and momentum flux changes the object's linear momentum.

3.1.2 Time-average of products

The acoustic radiation force and torque are by definition time-averaged quantities. It is, thus, useful to define some properties of the time-average of the products of sinusoidal functions. Acoustic quantities such as pressure, fluid velocity, energy density, and so on are real-valued quantities. Although, they are conveniently represented as complex functions. The time-average will thus be defined for real-valued functions.

Consider two harmonic and complex functions denoted by $f_1 = |F_1|e^{-i(\omega t + \alpha_1)}$ and $f_2 = |F_2|e^{-i(\omega t + \alpha_2)}$, where F_i and α_i ($i = 1, 2$) are the amplitude and phase functions, respectively. The time-average over a wave period $T = 2\pi/\omega$ is defined as

$$\overline{\text{Re}[f_1]\text{Re}[f_2]} = \frac{1}{T} \int_{t_0}^{T+t_0} |F_1||F_2| \cos(\omega t - \alpha_1) \cos(\omega t - \alpha_2) dt, \quad (3.2)$$

where t_0 is a constant given in units of time. By noticing that

$$\cos(\omega t - \alpha_1) \cos(\omega t - \alpha_2) = \frac{1}{2} [\cos(2\omega t + \alpha_1 + \alpha_2) + \cos(\alpha_2 - \alpha_1)] \quad (3.3)$$

we can rewrite Eq. (3.2) as

$$\overline{\text{Re}[f_1]\text{Re}[f_2]} = \frac{1}{2} |F_1||F_2| \cos(\alpha_2 - \alpha_1) = \frac{1}{2} \text{Re}[F_1^* F_2] = \frac{1}{2} \text{Re}[F_1 F_2^*], \quad (3.4)$$

where the symbol * means complex conjugation.

3.1.3 Radiation stress tensor

We want to know what is the time-average of all stress components caused by an acoustic wave on a suspended object. To do so, let us go back to Eq. (2.9), which is

repeated here for convenience

$$\partial_t(\rho\mathbf{v}) + \nabla \cdot \mathbf{S} = \mathbf{0}, \quad (3.5)$$

where

$$\mathbf{S} = p\mathbf{I} + \rho\mathbf{v}\mathbf{v} \quad (3.6)$$

is the stress tensor. By taking the time-averaged of Eq. (3.5) we get

$$\nabla \cdot \bar{\mathbf{S}} = \mathbf{0}, \quad (3.7)$$

where $\bar{\mathbf{S}}$ is called the radiation stress tensor. We see that the radiation stress is a zero divergent quantity.

Suppose now that the incident wave hits an object with fixed surface S as depicted in Fig. (3.1). The radiation force (averaged force) exerted by the wave is the result of all time-averaged stresses that act on the object. In other words,

$$\mathbf{F}^{\text{rad}} = \int_S \bar{\mathbf{S}} \cdot \mathbf{n} d^2\mathbf{r}, \quad (3.8)$$

In linear-approximation of the acoustics fields in Eqs. (2.27)-(2.29), the radiation stress tensor is $\bar{\mathbf{S}}^{(1)} = \overline{p^{(1)}}\mathbf{I}$. Considering only time-harmonic waves we have $\overline{p^{(1)}} = 0$ then $\bar{\mathbf{S}}^{(1)} = 0$. Therefore, the acoustic radiation force is at least a second-order effect. Taking this approximation in the acoustic fields in Eqs. (2.27)-(2.29), we find the radiation stress tensor as

$$\bar{\mathbf{S}}^{(2)} = \overline{p^{(2)}}\mathbf{I} + \rho_0 \overline{\mathbf{v}^{(1)}\mathbf{v}^{(1)}}. \quad (3.9)$$

It should be noticed from Eq. (3.7) that the second-order stress tensor is also divergenceless,

$$\nabla \cdot \bar{\mathbf{S}}^{(2)} = \mathbf{0}, \quad (3.10)$$

We need to express the second-order pressure $p^{(2)}$ in terms of first-order acoustic fields. To do so, we write Eq. (2.13) in terms of the potential velocity $\mathbf{v} = -\nabla\phi$,

$$\rho(-\partial_t\nabla\phi + \nabla\phi \cdot \nabla\nabla\phi) + \nabla p = 0. \quad (3.11)$$

But, we have that

$$|\nabla\phi|^2 = \nabla(\nabla\phi \cdot \nabla\phi) = 2\nabla\phi \cdot \nabla\nabla\phi. \quad (3.12)$$

Hence,

$$\nabla \left(-\partial_t\phi + \frac{1}{2}|\nabla\phi|^2 \right) = -\frac{\nabla p}{\rho}. \quad (3.13)$$

We can eliminate the quantity $\rho^{-1}\nabla p$ in terms of the specific enthalpy as follows. Consider that the enthalpy is a function of the specific entropy s and the pressure p . Thus, we have the differential relation

$$dh = Tds + \frac{dp}{\rho}. \quad (3.14)$$

Given that the wave propagation is considered an adiabatic process, $ds = 0$, then

$$dh = \frac{dp}{\rho}, \quad \nabla h \cdot d\mathbf{r} + \partial_t h dt = \nabla p \cdot d\mathbf{r} + \partial_t p dt. \quad (3.15)$$

Therefore,

$$\frac{\nabla p}{\rho} = \nabla h. \quad (3.16)$$

From Eq. (3.13) we have

$$h(\mathbf{r}, t) = \partial_t \phi(\mathbf{r}, t) - \frac{1}{2} |\nabla \phi(\mathbf{r}, t)|^2 + C(t), \quad (3.17)$$

where C is an arbitrary function of time. In linear approximation,

$$h^{(1)} = \partial_t \phi^{(1)} + C^{(1)} = \frac{p^{(1)}}{\rho_0} + C^{(1)}. \quad (3.18)$$

In the absence of acoustic waves $h^{(1)} = 0$, $p^{(1)} = 0$, thus $C^{(1)} = 0$.

Now let us expand the excess of pressure $p - p_0$ in a Taylor series in terms of h ,

$$p - p_0 = (\partial_h p)_{s_0} h + \frac{1}{2} (\partial_h^2 p)_{s_0} h^2 + O(h^3). \quad (3.19)$$

From Eq. (3.14) we have $(\partial_p h)_s = \rho^{-1}$, hence $(\partial_h p)_s = \rho$. Furthermore, $(\partial_h^2 p)_s = (\partial_h \rho)_s = (\partial_p \rho)_s (\partial_h p)_s = \rho/c^2$, where $c^2 = (\partial_p p)_s$. Thus, considering these quantities evaluated for the ambient specific entropy s_0 , we have $(\partial_h p)_{s_0} = \rho_0$ and $(\partial_h^2 p)_{s_0} = \rho_0/c_0^2$. With these results Eq. (3.19) can be rewritten as

$$p - p_0 = \rho_0 h + \frac{\rho_0}{2c_0^2} h^2 + O(h^3). \quad (3.20)$$

Using Eq. (3.17) we get

$$p - p_0 = \rho_0 \left(\partial_t \phi - \frac{1}{2} |\nabla \phi|^2 + C \right) + \frac{\rho_0}{2c_0^2} \left(\partial_t \phi - \frac{1}{2} |\nabla \phi|^2 + C \right)^2 + O(h^3) \quad (3.21)$$

In second-order approximation, we find

$$p^{(2)} = \rho_0 \partial_t \phi^{(2)} + \rho_0 C^{(2)} - \frac{\rho_0}{2} |\nabla \phi^{(1)}|^2 + \frac{\rho_0}{2c_0^2} (\partial_t \phi^{(1)})^2. \quad (3.22)$$

By taking the time-average of this equation and express it in terms of pressure and fluid velocity, we have

$$\overline{p^{(2)}} = \rho_0 \overline{C^{(2)}} - \frac{\rho_0 \overline{v^{(1)2}}}{2} + \frac{\overline{p^{(1)2}}}{2\rho_0 c_0^2}, \quad (3.23)$$

where $v^{(1)2} = \mathbf{v}^{(1)} \cdot \mathbf{v}^{(1)}$. Moreover, the quantity $\overline{C^{(2)}}$ is constant in both time and space, and does not contribute to the acoustic radiation force since its integration over a closed surface is zero. Thus, we discard $\overline{C^{(2)}}$ in Eq. (3.23). Additionally, the last two terms

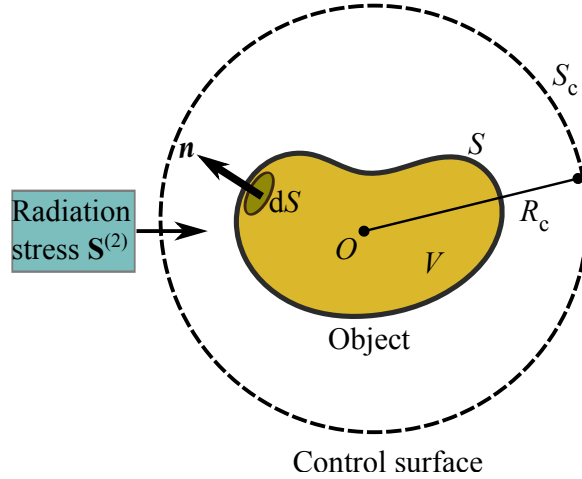


Figure 3.2: Coordinate system for the calculation of the acoustic radiation force on an arbitrary shape scatterer. The origin point O is at the center of the scatterer.

in the right-hand side of Eq. (3.23) are the second-order Lagrangian density averaged in time,

$$\overline{\mathcal{L}^{(2)}} = \frac{\overline{\rho_0 v^{(1)2}}}{2} - \frac{\overline{p^{(1)2}}}{2\rho_0 c_0^2}. \quad (3.24)$$

The first and the second terms on the right-hand side of this equation are the kinetic and potential energy densities.

Now, substituting Eq. (3.23) into Eq. (3.9) yields

$$\overline{\mathbf{S}^{(2)}} = - \left(\frac{\overline{\rho_0 v^{(1)2}}}{2} - \frac{\overline{p^{(1)2}}}{2\rho_0 c_0^2} \right) \mathbf{I} + \rho_0 \overline{\mathbf{v}^{(1)} \mathbf{v}^{(1)}}. \quad (3.25)$$

So, $\overline{\mathbf{S}^{(2)}}$ can be used in Eq. (3.25) into Eq. (3.8), to obtain the acoustic radiation force to the second-order approximation as

$$\mathbf{F}^{\text{rad}} = \int_S \left[\left(\frac{\overline{p^{(1)2}}}{2\rho_0 c_0^2} - \frac{\overline{\rho_0 v^{(1)2}}}{2} \right) \mathbf{I} + \rho_0 \overline{\mathbf{v}^{(1)} \mathbf{v}^{(1)}} \right] \cdot \mathbf{n} d^2 \mathbf{r}. \quad (3.26)$$

Therefore, to calculate the acoustic radiation force on an object we have to know what is the total pressure and fluid velocity acting on the the object surface. In turn, the total pressure depends on the incident and the scattered waves by the object. Hence, we have to solve the acoustic scattering problem by the object in order to compute the radiation force exerted by the incident wave. Equation (3.26) is referred to as *the nearfield formula* for the acoustic radiation force due to the fact that the incident and the scattered acoustic fields should be calculated on the surface of (“near to”) the object.

3.1.4 Farfield method

We can go beyond Eq. (3.26) and derive a farfield radiation force formula with the acoustic fields evaluated many wavelength away from the objects, $kr \gg 1$. In the farfield region, the acoustic fields are represented by much simpler radial functions compared to those in the nearfield; see Eqs. (2.62) and (2.67).

Assume that a control spherical surface S_c with radius R is centered at the origin of the coordinate system as depicted in Fig. (3.2). Now we integrate Eq. (3.10) with the second-order radiation stress $\mathbf{S}^{(2)}$ over the volume V of the control spherical surface and use the divergence theorem as follows

$$\int_V \nabla \cdot \overline{\mathbf{S}^{(2)}} d^3\mathbf{r} = \int_S \overline{\mathbf{S}^{(2)}} \cdot \mathbf{n} d^2\mathbf{r} + \int_{S_c} \overline{\mathbf{S}^{(2)}} \cdot \mathbf{n} d^2\mathbf{r} = 0. \quad (3.27)$$

Thus, from Eq. (3.26) we find that the acoustic radiation force is given by

$$\mathbf{F}^{\text{rad}} = - \int_{S_c} \mathbf{S}^{(2)} \cdot \mathbf{n} d^2\mathbf{r}. \quad (3.28)$$

By taking the farfield limit we have

$$\mathbf{F}^{\text{rad}} = - \frac{1}{k^2} \lim_{kR \rightarrow \infty} (kR)^2 \int_{4\pi} \left[\left(\frac{\overline{p^{(1)2}}}{2\rho_0 c_0^2} - \frac{\rho_0 \overline{v^{(1)2}}}{2} \right) \mathbf{I} + \rho_0 \overline{\mathbf{v}^{(1)} \mathbf{v}^{(1)}} \right] \cdot \mathbf{e}_r d\Omega, \quad (3.29)$$

where $d\Omega = \sin\theta d\theta d\varphi$ is the differential solid angle and the integration domain 4π means that we integrate over the entire solid angle of a sphere.

Now, we turn to compute the acoustic radiation force in Eq. (3.29). We know that in linear approximation the total pressure and fluid velocity in the medium is given by the superposition of the incident and the scattered fields. Hence,

$$p^{(1)} = (p_{\text{in}} + p_{\text{sc}}) e^{-i\omega t}, \quad (3.30)$$

$$\mathbf{v}^{(1)} = (\mathbf{v}_{\text{in}} + \mathbf{v}_{\text{sc}}) e^{-i\omega t}. \quad (3.31)$$

Substituting these equations into Eq. (3.29) and using time-averaging formula in Eq. (3.4), yields

$$\begin{aligned} \mathbf{F}^{\text{rad}} = & - \frac{1}{k^2} \lim_{kR \rightarrow \infty} (kR)^2 \int_{4\pi} \text{Re} \left[\frac{1}{4\rho_0 c_0^2} (|p_{\text{in}}|^2 + 2p_{\text{in}} p_{\text{sc}}^* + |p_{\text{sc}}|^2) \right. \\ & \left. - \frac{\rho_0}{4} (|\mathbf{v}_{\text{in}}|^2 + 2\mathbf{v}_{\text{in}} \cdot \mathbf{v}_{\text{sc}}^* + |\mathbf{v}_{\text{sc}}|^2) + \rho_0 (v_{\text{in},r} \mathbf{v}_{\text{in}}^* + v_{\text{in},r} \mathbf{v}_{\text{sc}}^* + v_{\text{sc},r} \mathbf{v}_{\text{in}}^* + v_{\text{sc},r} \mathbf{v}_{\text{sc}}^*) \right] d\Omega, \end{aligned} \quad (3.32)$$

where $v_{\text{in},r} = \mathbf{v}_{\text{in}} \cdot \mathbf{e}_r$ and $v_{\text{sc},r} = \mathbf{v}_{\text{sc}} \cdot \mathbf{e}_r$. In the absence of an object there is no radiation force in the fluid. Hence, the radiation force component due to the incident fields only

should be zero. Therefore, Eq. (3.32) becomes

$$\begin{aligned} \mathbf{F}^{\text{rad}} = & -\frac{1}{k^2} \lim_{kR \rightarrow \infty} (kR)^2 \int_{4\pi} \left[\frac{1}{4\rho_0 c_0^2} (2p_{\text{in}} p_{\text{sc}}^* + |p_{\text{sc}}|^2) - \frac{\rho_0}{4} (2\mathbf{v}_{\text{in}} \cdot \mathbf{v}_{\text{sc}}^* + |\mathbf{v}_{\text{sc}}|^2) \right. \\ & \left. + \rho_0 (v_{\text{in},r} \mathbf{v}_{\text{in}}^* + v_{\text{in},r} \mathbf{v}_{\text{sc}}^* + v_{\text{sc},r} \mathbf{v}_{\text{in}}^* + v_{\text{sc},r} \mathbf{v}_{\text{sc}}^*) \right] d\Omega. \end{aligned} \quad (3.33)$$

The incident and scattered pressure and fluid velocity fields can be obtained from the relations in (3.13) and (2.37). Accordingly,

$$p_{\text{in}} = -i\omega\phi_{\text{in}}, \quad \mathbf{v}_{\text{in}} = -\nabla\phi_{\text{in}}, \quad (3.34)$$

$$p_{\text{sc}} = -i\omega\phi_{\text{sc}}, \quad \mathbf{v}_{\text{sc}} = -\nabla\phi_{\text{sc}}. \quad (3.35)$$

Using these relations into Eq. (3.33) yields

$$\mathbf{F}^{\text{rad}} = -\frac{1}{k^2} \lim_{kR \rightarrow \infty} (kR)^2 \int_{4\pi} \text{Re} \left[\left(\phi_{\text{in}} - \frac{i}{k} \partial_r \phi_{\text{in}} \right) \phi_{\text{sc}}^* + |\phi_{\text{sc}}|^2 \right] \mathbf{e}_r d\Omega. \quad (3.36)$$

It is useful to express the acoustic radiation force in terms of the characteristic energy density $E_0 = \rho_0 k^2 \phi_0 / 2$ and the cross-section area A of the object. Thus, substituting the asymptotic form of the velocity potentials given in Eqs. (2.62) and (2.67) into this equation and using $\mathbf{e}_r = \sin\theta \cos\varphi \mathbf{e}_x + \sin\theta \sin\varphi \mathbf{e}_y + \cos\theta \mathbf{e}_z$, results

$$\mathbf{F}^{\text{rad}} = AE_0 (Y_x \mathbf{e}_x + Y_y \mathbf{e}_y + Y_z \mathbf{e}_z), \quad (3.37)$$

where Y_x , Y_y , and Y_z are the Cartesian components of the dimensionless radiation force. They are given by

$$\begin{aligned} Y_x + iY_y &= \frac{i}{2k^2 A} \sum_{n,m} \sqrt{\frac{(n+m+1)(n+m+2)}{(2n+1)(2n+3)}} \\ &\times (S_n a_{nm} a_{n+1,m+1}^* + S_n^* a_{n,-m}^* a_{n+1,-m-1}), \end{aligned} \quad (3.38)$$

$$\begin{aligned} Y_z &= \frac{1}{k^2 A} \text{Im} \sum_{n,m} \sqrt{\frac{(n-m+1)(n+m+1)}{(2n+1)(2n+3)}} \\ &\times S_n a_{nm} a_{n+1,m}^*, \end{aligned} \quad (3.39)$$

where ‘Im’ denotes the imaginary part of and

$$S_n = s_n + s_{n+1}^* + 2s_n s_{n+1}^*. \quad (3.40)$$

Note that Y_x , Y_y , and Y_z are real-valued quantities.

The acoustic radiation force exerted on an object with any geometry by a wave of arbitrary wavefront depends on the scaled scattering coefficient s_n of the object and the beam-shape coefficient. Thus, the radiation force depend on the acoustic properties of

the object as given in s_n and on the wave spatial characteristics described in a_{nm} .

The farfield radiation force formulas given in Eqs. (3.39) and (3.40) were first obtained in Ref. [17]. These formulas go beyond classical results of the radiation force exerted by a traveling plane and a spherical wave on a sphere. In fact, using the farfield radiation force formulas we can recover classical results of the radiation force exerted on a sphere by a traveling plane [14] and a spherical wave [15] both obtained with the nearfield method based on Eq. (3.26).

3.2 Acoustic radiation torque

When an acoustic wave encounters a suspended object of volume V and surface S , the momentum flux with respect to a point inside the object, i.e. the angular momentum flux, can be transferred to the object. This process gives rise to the acoustic radiation torque phenomenon. As a consequence the object may be set to spin around one or more rotation axes.

Here, we consider the acoustic radiation torque exerted by a wave with arbitrary wavefront on an absorbing object suspended in an ideal fluid.

3.2.1 Angular momentum flux density

Similar to the acoustic radiation force, the acoustic radiation torque is a time-averaged quantity. It is also a second-order effect on the amplitude of the acoustic fields.

Consider the time-averaged angular momentum flux with respect to the coordinate system be defined, in second-order approximation, as

$$\overline{\mathbf{M}^{(2)}} = \mathbf{r} \times \overline{\mathbf{S}^{(2)}}. \quad (3.41)$$

Here, this quantity is referred as to the angular momentum tensor. By definition, the acoustic radiation force exerted on an object of arbitrary geometric form with surface S is given by

$$\mathbf{N}^{\text{rad}} = \int_S \left[\mathbf{r} \times \overline{\mathbf{S}^{(2)}} \right] \cdot \mathbf{n} d^2\mathbf{r}. \quad (3.42)$$

It follows from Eq. (3.10) that the angular momentum tensor is a zero divergent quantity,

$$\nabla \cdot \overline{\mathbf{M}^{(2)}} = \mathbf{r} \times \left[\nabla \cdot \overline{\mathbf{S}^{(2)}} \right] = \mathbf{0}. \quad (3.43)$$

This will enable us to use farfield expansions of the acoustic fields to compute the acoustic radiation torque.

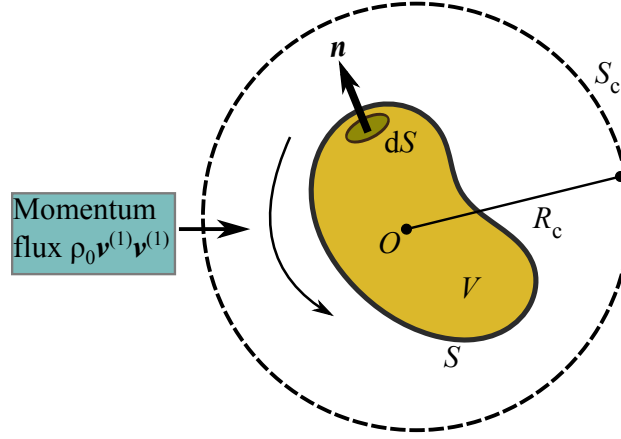


Figure 3.3: Coordinate system for the calculation of the acoustic radiation torque on an arbitrary shape scatterer. The origin point O is at the center of the scatterer.

3.2.2 Farfield method

Consider a farfield spherical surface of radius R enclosing the object target to which a radiation force is exerted, Fig(3.3). Using the divergent theorem in Eq. (3.42), we obtain

$$\mathbf{N}^{\text{rad}} = \int_S [\mathbf{r} \times \overline{\mathbf{S}^{(2)}}] \cdot \mathbf{n} d^2\mathbf{r} = - \int_{S_c} [\mathbf{r} \times \overline{\mathbf{S}^{(2)}}] \cdot \mathbf{n} d^2\mathbf{r}. \quad (3.44)$$

Substituting Eq. (3.25) results

$$\begin{aligned} \mathbf{N}^{\text{rad}} &= \int_{S_c} \mathbf{r} \times \left[\left(\frac{\rho_0 \overline{v^{(1)2}}}{2} - \frac{\overline{p^{(1)2}}}{2\rho_0 c_0^2} \right) \mathbf{I} - \rho_0 \overline{\mathbf{v}^{(1)} \mathbf{v}^{(1)}} \right] \cdot \mathbf{n} d^2\mathbf{r}, \\ &= -\rho_0 \int_{S_c} [\mathbf{r} \times \overline{\mathbf{v}^{(1)} \mathbf{v}^{(1)}}] \cdot \mathbf{n} d^2\mathbf{r}, \\ &= -\rho_0 \int_{S_c} [\overline{\mathbf{r} \times \mathbf{v}^{(1)}}] [\overline{\mathbf{v}^{(1)} \cdot \mathbf{n}}] d^2\mathbf{r}. \end{aligned} \quad (3.45)$$

If the object is rigid, the fluid velocity is zero on the object surface is zero,

$$\overline{\mathbf{v}^{(1)}}|_{\mathbf{r} \in S} = \mathbf{0}. \quad (3.46)$$

Hence, the radiation torque is zero. We can write the radiation torque in Eq. (3.45) using Eq. (3.31) as follows

$$\begin{aligned} \mathbf{N}^{\text{rad}} &= -\frac{\rho_0}{2k^2} \lim_{kR \rightarrow \infty} (kR)^2 \\ &\quad \times \int_{4\pi} \text{Re} [\mathbf{r} \times (\mathbf{v}_{\text{in}} v_{\text{in},r}^* + \mathbf{v}_{\text{in}} v_{\text{sc},r}^* + \mathbf{v}_{\text{sc}} v_{\text{in},r}^* + \mathbf{v}_{\text{sc}} v_{\text{sc},r}^*)] d\Omega, \end{aligned} \quad (3.47)$$

where $v_{\text{sc},r} = \mathbf{v}_{\text{sc}} \cdot \mathbf{e}_r$. The contribution of the incident fluid velocity to the acoustic radiation torque vanishes because it is related to the medium without the target object.

It is useful to define the angular momentum operator as

$$\hat{\mathbf{L}} \equiv -i(\mathbf{r} \times \nabla). \quad (3.48)$$

In terms of the incident ϕ_{in} and the scattered ϕ_{sc} velocity potentials and the angular momentum operator $\hat{\mathbf{L}}$, Eq. (3.47) becomes

$$\begin{aligned} \mathbf{N}^{\text{rad}} &= -\frac{\rho_0}{2k^2} \lim_{kR \rightarrow \infty} (kR)^2 \\ &\times \int_{4\pi} \text{Re} \left[i(\partial_r \phi_{\text{sc}}^*)(\hat{\mathbf{L}}\phi_{\text{in}}) + i(\partial_r \phi_{\text{in}}^*)(\hat{\mathbf{L}}\phi_{\text{sc}}) + i(\partial_r \phi_{\text{sc}}^*)(\hat{\mathbf{L}}\phi_{\text{sc}}) \right] d\Omega. \end{aligned} \quad (3.49)$$

The linear momentum operator is given in spherical coordinates by

$$\hat{\mathbf{L}} = -iR(\mathbf{e}_r \times \nabla) = -iR \left(\mathbf{e}_\varphi \partial_\theta - \frac{\mathbf{e}_\theta}{\sin \theta} \partial_\varphi \right). \quad (3.50)$$

This operator depends only on the polar and azimuthal angles.

We can write the acoustic radiation torque in terms of a dimensionless torque $\boldsymbol{\tau}$ as

$$\mathbf{N}^{\text{rad}} = VE_0 \boldsymbol{\tau}, \quad (3.51)$$

where

$$\boldsymbol{\tau} = -\frac{1}{k^3 V} \text{Re} \sum_{n,m} \sum_{n',m'} i^{n-n'} (1+s_n^*) a_{nm}^* a_{n'm'} \int_{4\pi} Y_n^{m*} \hat{\mathbf{L}} Y_{n'}^{m'*} d\Omega. \quad (3.52)$$

To obtain the Cartesian components of the acoustic radiation torque, we decompose the angular momentum into the Cartesian operator components \hat{L}_i ($i = x, y, z$) as

$$\hat{\mathbf{L}} = \hat{L}_x \mathbf{e}_x + \hat{L}_y \mathbf{e}_y + \hat{L}_z \mathbf{e}_z. \quad (3.53)$$

It is convenient to write the operators \hat{L}_x and \hat{L}_y in terms of the ladder operators \hat{L}_+ and \hat{L}_- ,

$$\hat{L}_x = \frac{1}{2} (\hat{L}_+ + i\hat{L}_-), \quad (3.54)$$

$$\hat{L}_y = \frac{1}{2} (\hat{L}_+ - i\hat{L}_-). \quad (3.55)$$

The ladder operators are given by [57]

$$\hat{L}_\pm = \pm e^{i\varphi} (\partial_\theta \pm i \cot \theta \partial_\varphi). \quad (3.56)$$

One can show that when the ladder operators and the z -component of the angular momentum operator acts on a spherical harmonics function, we have

$$\hat{L}_\pm Y_n^m = c_{n,\pm m} Y_n^{m\pm 1}, \quad (3.57)$$

$$\hat{L}_z Y_n^m = m Y_n^m, \quad (3.58)$$

where $c_{n,\pm m} = \sqrt{(n \mp m)(n \pm m + 1)}$. Using these equations into Eq. (5.15) we obtain the Cartesian components of the dimensionless radiation torque as

$$\begin{aligned} \tau_x + i\tau_y = & -\frac{1}{2k^3V} \sum_{n,m} \sqrt{(n-m)(n+m+1)} [(1+s_n)s_n^* a_{nm} a_{n,m+1}^* \\ & + (1+s_n^*)s_n a_{n,-m}^* a_{n,-m-1}], \end{aligned} \quad (3.59)$$

$$\tau_z = -\frac{1}{k^3V} \sum_{n,m} m \operatorname{Re}[(1+s_n)s_n^*] |a_{nm}|^2. \quad (3.60)$$

The acoustic radiation torque formulas given in Eqs. (5.16) and (5.17) are valid for an acoustic beam with arbitrary wavefront and for any object target. To numerically evaluate the acoustic radiation torque, it is necessary to calculate the beam-shape a_{nm} and the scaled scattering s_n of the object. The latter coefficients are related to the boundary conditions for the acoustic fields on the object's surface. Furthermore, the obtained results can be applied to different types of objects such as rigid, void, compressible fluid, elastic and viscoelastic solids, layered materials.

4

Acoustic radiation force exerted on a sphere by a focused and a Bessel beam

We will present here some results about the studies from the acoustic radiation force exerted by a Bessel and a focused beam in an off-axis configuration. The main results of this chapter has been submitted for publication.

4.1 Methods to compute the beam shape coefficients

4.1.1 Discrete spherical harmonic transform (DSHT)

Representing an acoustic beam using the partial wave expansion is an useful method to solve scattering [58], [59] and radiation force problems [14], [60] for spherical targets. Most applications of the partial-wave expansion (PWE) method to these problems are restricted to axisymmetric beams with respect to the propagation axis of the coordinate system, which is set at the sphere center. In multiple scattering problems, the beam symmetry is broken due to the lack of a preferred reference frame for the boundary condition description.

Besides scattering involving non-axisymmetric beams are generally solved with the aid of numerical methods. In general, numerical simulations of acoustic waves spanning over many wavelengths demands large computational resources. Methods such as finite-differences [61] and finite-elements [62] demand several sampling points per wavelength. They also develop numerical dissipation and dispersion, which scale with the propagation distance. Moreover, these methods require a careful truncation of the simulation domain. On the other hand, the PWE can represent an arbitrary acoustic beam in an infinity domain using the spherical wave functions. The method is semi-analytical, thus it expected to be more accurate without numerical dissipation and dispersion.

Furthermore, the PWE does not need a computational mesh, only the boundary of the propagation domain is discretized. Thus, it is suitable to describe acoustic beams spanning over a large number of wavelengths without the need of large-scale computation. To illustrate the PWE method, consider a fixed reference frame described by the spherical coordinates (r, θ, φ) . The velocity potential of a regular acoustic beam of frequency ω in

a medium with speed of sound c_0 can be expressed as Eq.(2.58).

Assume that the wave propagation takes place within a region defined by a virtual sphere of radius R centered at the origin of the coordinate system. Using the orthogonality properties of spherical harmonics, we write the beam shape coefficient as [47]

$$a_{nm} = \frac{1}{j_n(kR)} \int_0^{2\pi} \int_0^\pi \tilde{\phi}_{\text{in}}(kR, \theta, \varphi) Y_n^{m*} \sin \theta d\theta d\varphi, \quad (4.1)$$

where $n \geq 0$, $|m| \leq n$ and $d\Omega$ is the differential solid angle. The beam-shape coefficients correspond to the spherical harmonics transform (SHT) of the velocity potential. The region size factor kR is associated to the bandwidth of the velocity potential function. Thus, the number of these coefficients needed to reconstruct the beam depends on kR .

Despite the PWE method be an old subject discussed in several textbooks, e.g. [63], only recently it was applied to the scattering of acoustic beams with arbitrary wavefront [64]. In these studies, the computation of low-order beam-shape coefficients sufficed to determine the scattered pressure by spheres whose radius is compatible to the incident wavelength. The scattering by larger spheres demands the computation of higher-order a_{nm} . Here, the a_{nm} are computed using the discrete SHT, which is based on Gaussian quadrature and FFT algorithm [55].

For an arbitrary shaped beam, Eq.(4.1) can be computed through the discrete SHT. Here we present the discrete SHT described in Ref. [55]. Consider that the velocity potential amplitude ϕ is sampled over the virtual sphere surface at the points $\varphi_l = 2\pi l/M$ and $\theta_s = \arccos(t_s)$ with t_s ($s = 1, 2, \dots, N$) being the roots of the Legendre polynomial of N th-order. The sampling numbers M and N can be chosen independently. The discrete version of Eq. (4.1) is

$$a_{n,m} = d_{n,m} + ie_{n,m}, \quad (4.2)$$

where

$$\begin{aligned} \begin{bmatrix} d_{n,m} \\ e_{n,m} \end{bmatrix} &= \frac{1}{M} \sqrt{\frac{\pi(2n+1)(n-m)!}{j_n^2(kR)(n+m)!}} \sum_{s=1}^N w_s P_n^m(t_s) \sum_{l=0}^{M-1} \begin{bmatrix} \text{Re} \\ \text{Im} \end{bmatrix} \\ &\times \tilde{\phi}(kR, \theta_s, \varphi_l) e^{-i\pi ml/N}, \end{aligned} \quad (4.3)$$

where $0 \leq m \leq n < N$ and

$$w_s = \frac{2(1-t_s^2)}{[NP_{N-1}(t_s)]^2}, \quad (4.4)$$

is the weight coefficient in the Gauss-Legendre quadrature method. The second summation in Eq. (4.3) can be evaluated through the FFT algorithm.

4.2 Spherically focused beam

A spherically focused transducer with diameter $2b$ and curvature radius z_0 is used to produce a focused beam (see 4.1). The origin of the coordinate system O is set at the transducer's focus. When the center of the sphere coincides with O , the scattering of the incident beam is referred to as the on-focus scattering configuration [65].

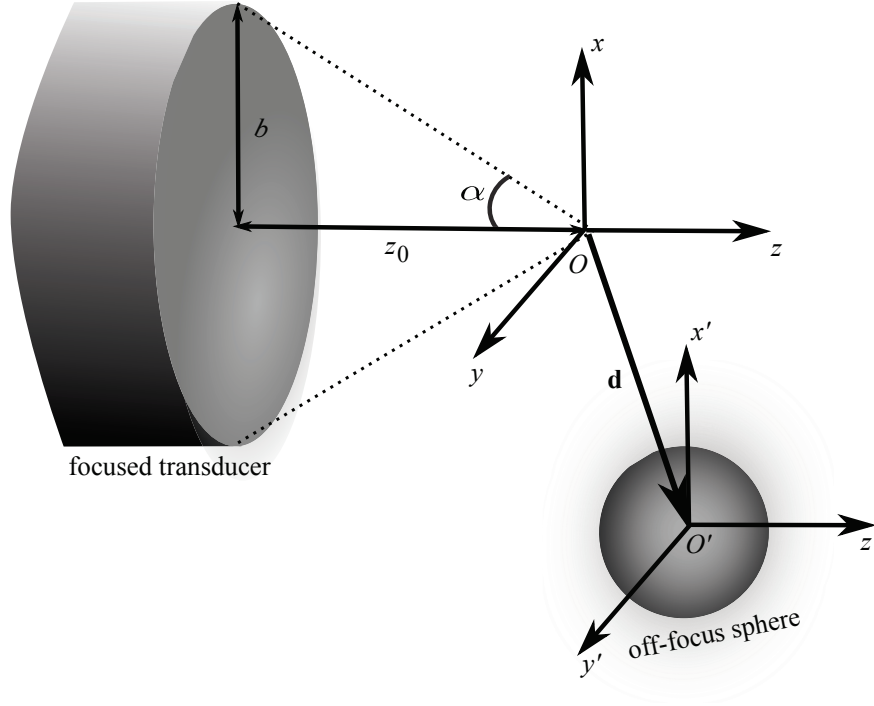


Figure 4.1: Sketch of the acoustic scattering by a sphere placed anywhere in the host medium. The systems O and O' correspond to the on- and off-focus scattering configurations.

In the on-focus scattering formalism, the normalized amplitude of the velocity potential beam can be described in spherical coordinates $\mathbf{r} = r\mathbf{e}_r(\theta, \varphi)$, where \mathbf{e}_r is the radial unit-vector, θ and φ are the polar and the azimuthal angles, respectively. The velocity potential generated by a transducer is given in terms of the Rayleigh integral by [46]

$$\phi_{\text{in}}(\mathbf{r}) = \frac{v_0}{2\pi} \int_S \frac{e^{ik|\mathbf{r}-\mathbf{r}'|}}{|\mathbf{r}-\mathbf{r}'|} dS', \quad (4.5)$$

where S is the surface of the transducer's active element and v_0 is the uniform velocity distribution on S . Physically, the Rayleigh integral expresses the Huygens' principle in which the pressure at a position \mathbf{r} is the sum of wavelets generated on the surface S .

To derive the on-focus beam shape coefficients, the origin of the coordinate system is centered at the transducer focal point. By assuming that $r \ll z_0$, with $|\mathbf{r}'| = z_0$, the following expansion is used [55]

$$\frac{e^{ik|\mathbf{r}-\mathbf{r}'|}}{|\mathbf{r}-\mathbf{r}'|} = 4\pi \frac{e^{ikz_0}}{z_0} \sum_{n,m} (-i)^n j_n(kr) Y_n^m(\theta', \varphi') Y_n^{m*}(\theta, \varphi) \quad (4.6)$$

into (4.5). Thus, integrating in the angular variables (θ', φ') yields

$$\phi_{\text{in}} = v_0 z_0 e^{ikz_0} \sum_{n=0}^{\infty} i^n \sqrt{\frac{4\pi}{2n+1}} [P_{n+1}(\cos \alpha) - P_{n-1}(\cos \alpha)] j_n(kr) Y_n^0(\theta, \varphi), \quad (4.7)$$

where $\alpha = \sin^{-1}(b/r_0)$ is the half-spread angle of the transducer and P_n is the Legendre polynomial of order n . The on-focus BSCs are found by comparing Eqs.(2.58) and (4.7). Accordingly,

$$a_n^m = -i^{n+1} k z_0 e^{ikz_0} \sqrt{\frac{4\pi}{2n+1}} [P_{n+1}(\cos \alpha) - P_{n-1}(\cos \alpha)] \delta_{m,0}.$$

The partial-wave expansion of the focused beam can be compared to results based on the paraxial approximation in (4.5). In adopting this approximation, it is assumed that $b^2 \ll z_0^2$. Let the radial distance in cylindrical coordinates be given by $\varrho = \sqrt{x^2 + y^2}$. The pressure produced by the transducer in the focal plane is given by [66]

$$\phi_{\text{in}}(\varrho, 0) = -\frac{v_0}{k} \left(\frac{b}{\varrho}\right) \exp \left[ik \left(\frac{\varrho^2}{z_0} + z_0 \right) \right] J_1(k\varrho \sin \alpha), \quad (4.8)$$

where J_1 is the first-order Bessel function. Along the transducer's axis, we have

$$\phi_{\text{in}}(0, z) = -\frac{v_0}{k} \frac{z_0}{z - z_0} \left\{ 1 - \exp \left[\frac{ikb^2}{2} \left(\frac{1}{z} - \frac{1}{z_0} \right) \right] \right\}. \quad (4.9)$$

These equations will be compared to the result obtained by the partial-wave expansion given in (4.7).

The truncation error in computing the translational BSCs in (2.89) is given by

$$N = \nu + kd + 1.8(\log \epsilon^{-1})^{2/3} (kd)^{1/3}. \quad (4.10)$$

The error considered in the translational BSC computations is $\epsilon = 10^{-6}$. The truncation order L of the radiation force series in (5.11) is established by the scattering coefficient ratio $|s_L^m/s_0^0| < 10^{-7}$.

In Fig. (4.2), the velocity potential (normalized to ϕ_0) produced by the focused transducer is shown along both x and z directions. The pressure is computed using the partial-wave expansion method and the paraxial approximation based on (4.8). Good agreement is found between the methods in the transverse direction and in the vicinity of the focal region. Though moving away from the focal region, the partial-wave expansion method deviates from the paraxial approximation result. This happens because the partial-wave expansion is valid in the vicinity of the focal region, i.e. $r \ll z_0$.

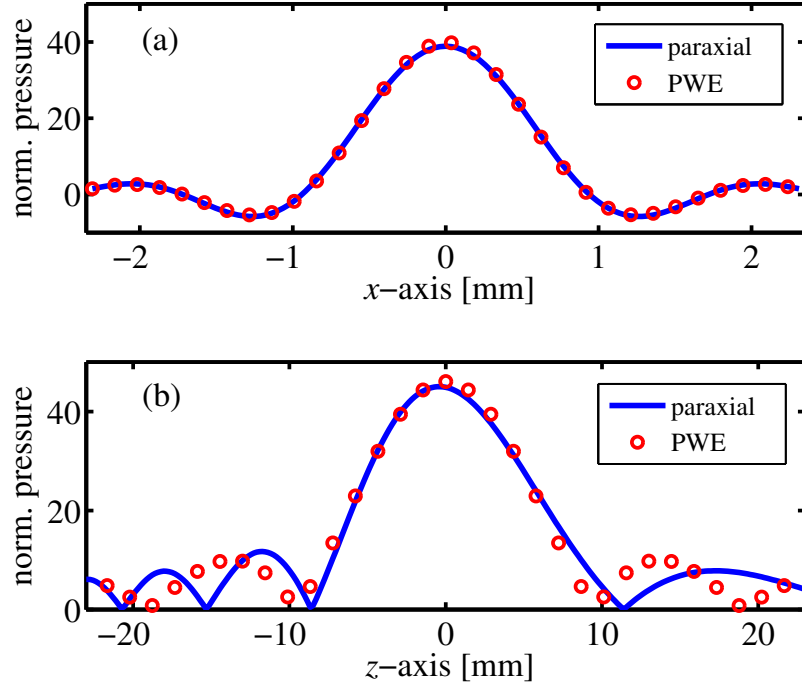


Figure 4.2: Pressure amplitude generated by the spherically focused transducer with aperture 44 mm and F-number of 1.6, operating at 3.1 MHz. The pressure is evaluated along (a) the transverse and (b) the axial directions using the partial-wave expansion (PWE) method and the paraxial approximation.

4.3 Radiation force by a Bessel beam

Acoustic Bessel beams form a class of important limited-diffraction waves. They represent exact solutions of Helmholtz equation in cylindrical coordinate (ρ, φ, z) . The amplitude of the potential velocity of a m th-order Bessel beam is given by [67]

$$\phi_{\text{in}}(\rho, \varphi, z) = \phi_0 e^{ik_z z} J_m(\kappa \rho) e^{im\varphi}, \quad (4.11)$$

J_m is the m -th-order Bessel function, m is also known as the topological charge of the beam whose sign defines the handedness of the wavefront rotation and its magnitude determines the pitch of the helix. k_z and κ are the axial and radial wave numbers, respectively. This number are related through the dispersion relation $\kappa^2 + k_z^2 = k^2$, where $k = \omega/c_0$. An exact expression of a Bessel beam in the spherical basis centered on the sphere can be expressed as [68]

$$a_{nm} = i^{n-m} (2n+1) \frac{(n-m)!}{(n+m)!} P_n^m(\cos \beta), \quad (4.12)$$

where the half-cone angle $\beta = \arcsin(\kappa/k)$ is formed by the wave vector k relative to the beam axis. In the limit when $\beta = 0$ the beam is a plane progressive wave.

The radiation force caused by a zero- and a first-order Bessel beams ($m = 1$) on a sphere suspended in water ($\rho_0 = 1000 \text{ kg/m}^3$ and $c_0 = 1500 \text{ m/s}$) is analyzed here.

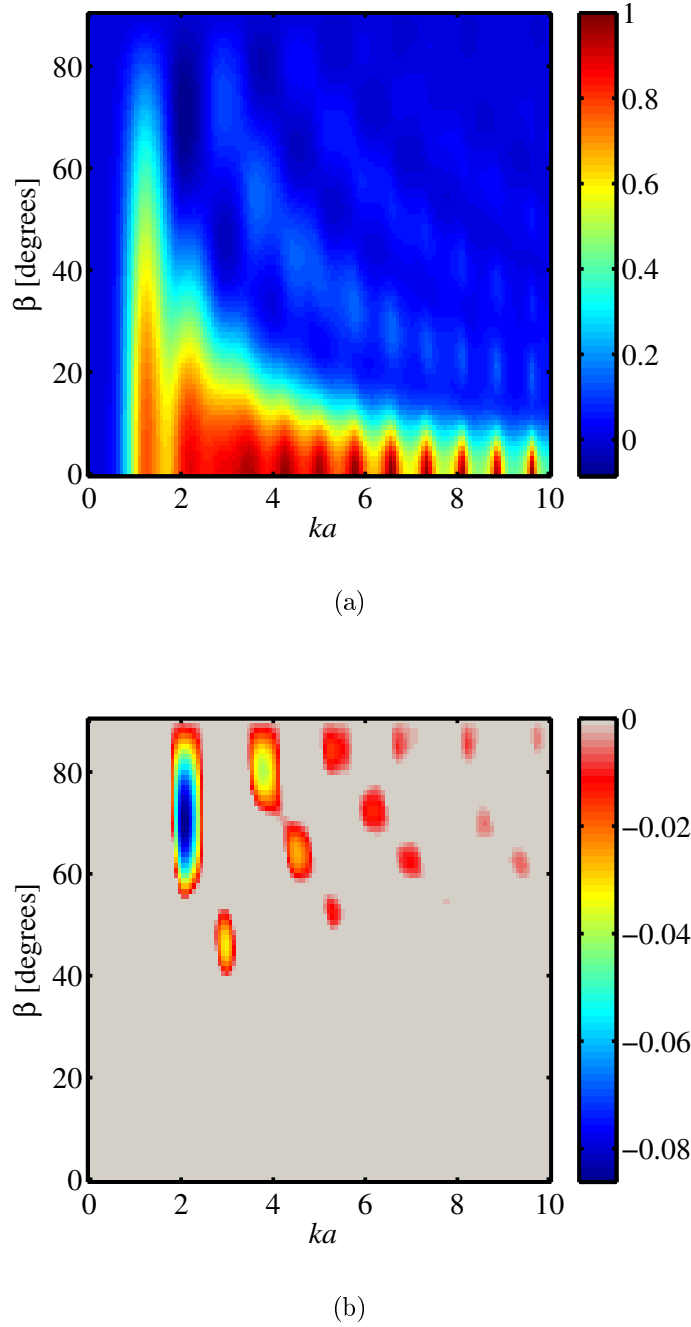


Figure 4.3: Axial radiation force function Y_z for the silicone oil sphere due to the zero-order Bessel beam. The function Y_z is normalized to 1.3931. (a) The sphere is placed on the axis of the beam. (b) The islands of attractive force in the on-axis configuration.

The sphere is made of silicone oil [69] ($\rho_1 = 970 \text{ kg/m}^3$, $c_1 = 1004 \text{ m/s}$, and $\alpha = 2 \times 10^{-10} f^{1.7} \text{ Np} \cdot \text{Hz}^{-1.7}/\text{m}$, with f being the frequency). The silicone oil was chosen because it may form drops into water without mixing. The frequency of the incident beams is fixed to 1 MHz. Acoustic Bessel beams are known to produce an axial radiation force on a sphere centered on the beam axis (on-axial configuration) that exhibits both

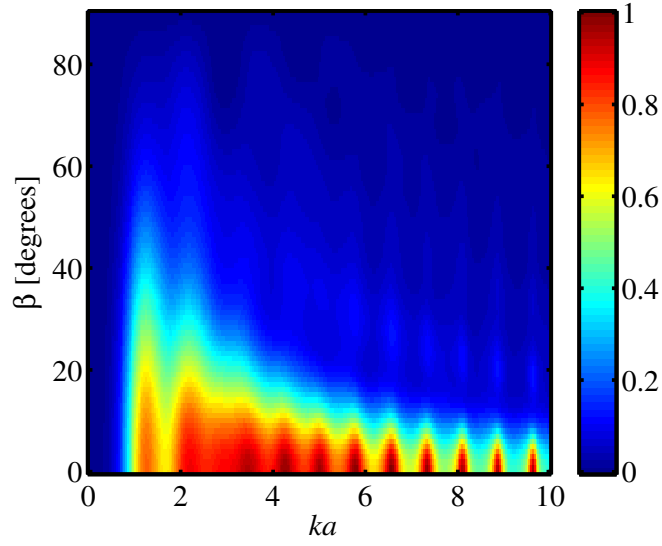
repulsor and tractor behaviors. The repulsor and the tractor forces are oriented along the beams direction of propagation and opposite to it, respectively. The behavior of the acoustic radiation force generated by Bessel beams when the sphere lies outside the beams axis (off-axial configuration) is unknown. Using the radiation force formulas given in terms of the partial wave expansion coefficients for the incident and scattered waves, both axial and transverse components of the force exerted on a silicone-oil sphere are obtained for a zero- and a first-order Bessel vortex beam.

To compute the radiation force, we have to obtain the beam-shape a_{nm} and then the scattering coefficients s_{nm} . To compute the beam-shape coefficient we use the DSHT algorithm with $M = 2^{12}$ and $N = 256$. In this case, the mean absolute error between the pressure amplitude of the Bessel beams using the beam-shape coefficients is about 10^{-9} . Furthermore, the infinite series in (3.39) and (3.40) should be truncated at $n = L$. The truncation order L should be the smallest integer for what the scattering coefficient ratio $|s_L^m/s_0^0| \ll 1$. This is required to ensure proper convergence of the radiation force series. In the performed computations, the truncation order is such that the scattering coefficient ratio is as small as 10^{-9} .

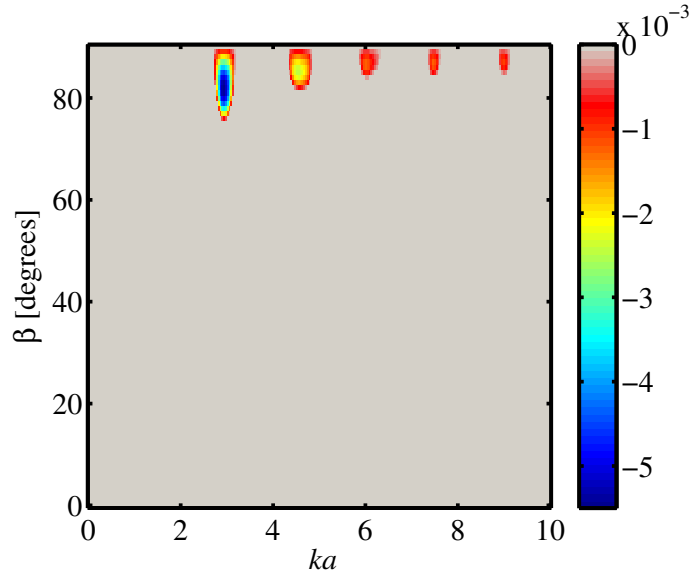
To analyze the behavior of the axial radiation force, 2D plots of the radiation force Y_z are computed in the range $0^\circ \leq \beta \leq 90^\circ$ and $0 \leq ka \leq 10$. As an initial test, we have recovered previous results based on the analytical calculation of the axial radiation force upon an hexane sphere in the on-axis configuration [19]. Furthermore, we have numerically validated the radiation force functions given in (3.39) and (3.40) by considering a first-order Bessel beam propagating along each Cartesian axis. The computed radiation forces were compared to the axial radiation force expression given in Ref. [19]. For the sake of brevity, these results will not be shown here.

The 2D plots of the axial radiation force function Y_z produced by the zero-order Bessel beam are depicted in Fig. 4.3. The radiation force function is normalized to 1.3931. The on-axis configuration is shown in Figs. 4.3(a) and 4.3(b). In this configuration, islands of negative radiation force (tractor beam) are clearly spotted. The largest magnitude of the negative axial force lies in the region around $ka = 2$ and $60^\circ < \beta < 80^\circ$. In this region, the attractive force magnitude corresponds to approximately 10% of the maximum value of the repulsive axial force at $ka = 2$. With an offset of $kx_0 = 1.6$ along the x -axis Fig.(4.4), the islands of attractive force shift toward higher ka values. Moreover, the strength of the negative force drops one order of magnitude.

Results of the axial radiation force function due to the first-order Bessel vortex beam as a function of β and ka are shown in Figs.(4.5) and (4.6). The radiation force function is normalized to 0.4201. In the on-axis configuration Figs. 4.5(a) and 4.5(b), islands of attractive radiation force arise. The largest magnitude of the negative force takes place within the region $65^\circ < \beta < 80^\circ$ and $ka = 3$. The attractive force here is about 20% lower than that due to the zero-order Bessel beam. At $ka = 3$, the attractive force is about 25% of the repulsive force. When an offset of $kx_0 = 1.6$ is applied to beam along the x -axis, Figs.4.6(a) and 4.6(b), the islands of attractive force move toward higher ka values. Furthermore, with this offset the attractive force islands shrink and their strength drop by one order of magnitude.



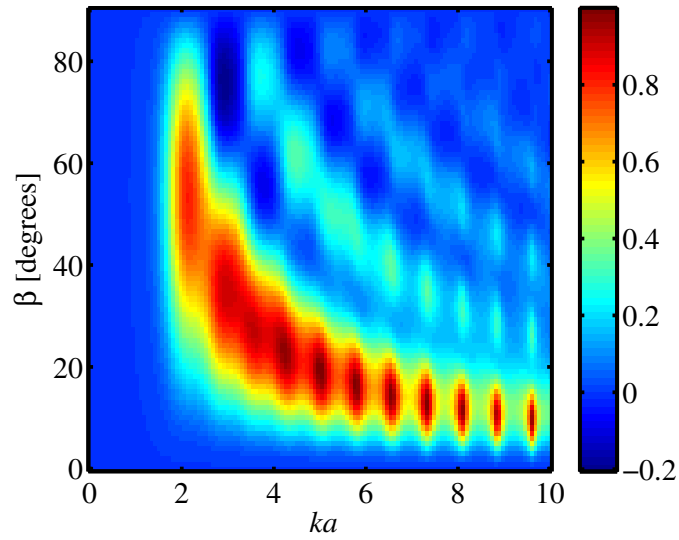
(a)



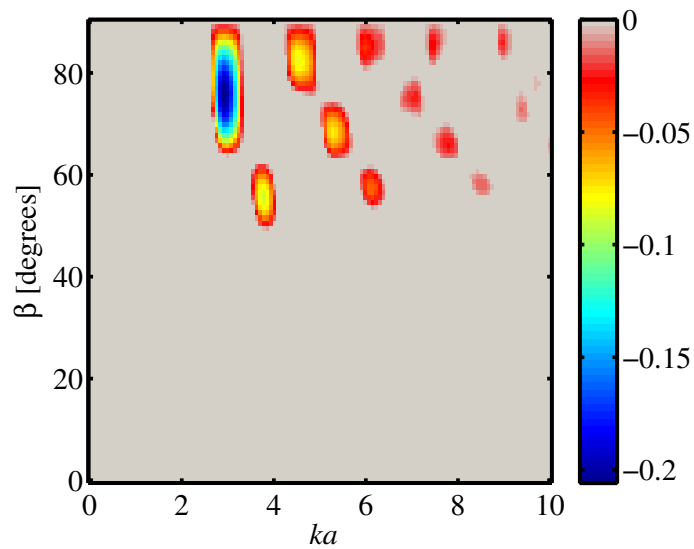
(b)

Figure 4.4: Axial radiation force function Y_z for the silicone oil sphere due to the zero-order Bessel beam. The function Y_z is normalized to 1.3931. (a) The sphere location has a offset of $kx_0 = 1.6$ along the x -axis. (b) The islands of attractive force in the off-axial configuration.

The transverse radiation force field $\mathbf{Y}_\perp = (Y_x, Y_y)$ caused by the zero-order Bessel beam with $\beta = 70^\circ$ for the silicone sphere is illustrated in Fig. (4.7). The transverse force fields are computed by varying the relative position between the sphere and the beam (offset) within $-4 \leq kx_0, ky_0 \leq 4$. Furthermore, the corresponding vector fields are plotted on



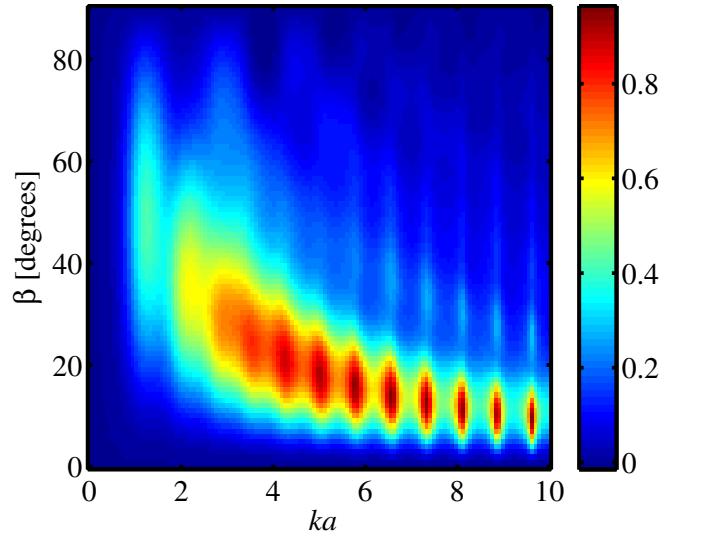
(a)



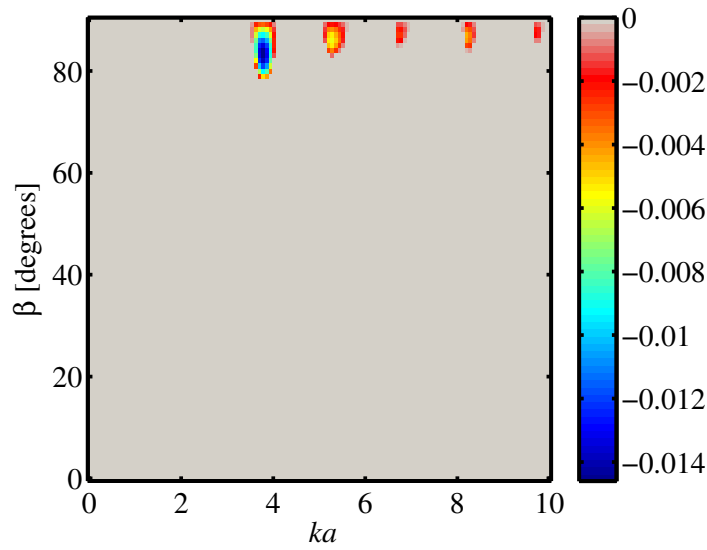
(b)

Figure 4.5: Axial radiation force function Y_z for the silicon oil sphere due to the first-order Bessel beam. The function Y_z is normalized to 0.4201. (a) The sphere is placed on the beam's axis. (b) The islands of attractive radiation force in the on-axis configuration.

top of the time-averaged energy flux (intensity) of the incident beam normalized to the unit. Two different sphere's size factors are considered, which correspond to a repulsive ($ka = 0.1$) and an attractive ($ka = 2$) axial radiation force, Fig. (4.3). In both cases, the central spot of the beam is a region of unstable equilibrium for the sphere. The lines of force diverge from the beam axis.



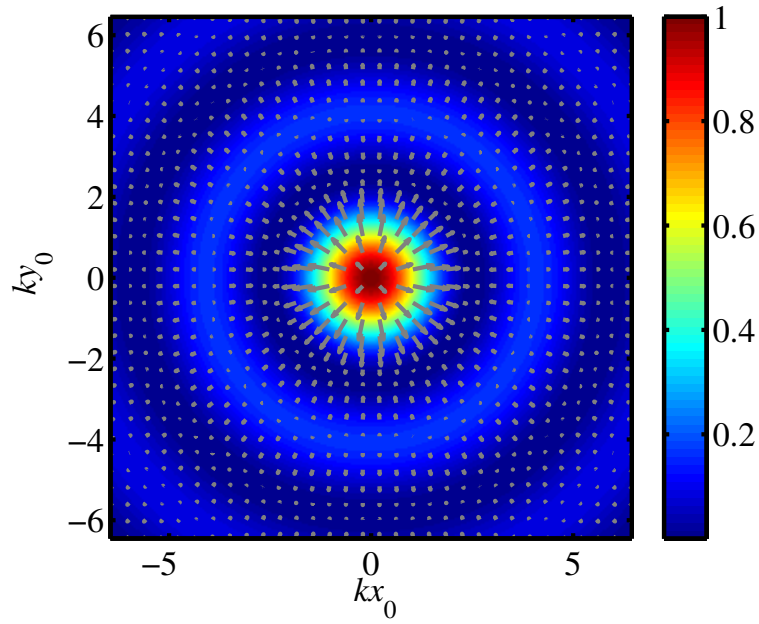
(a)



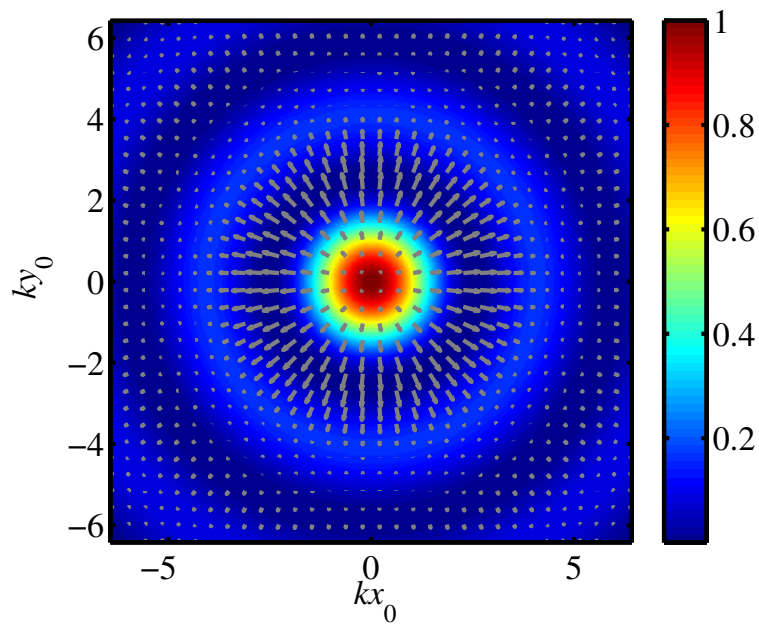
(b)

Figure 4.6: Axial radiation force function Y_z for the silicon oil sphere due to the first-order Bessel beam. The function Y_z is normalized to 0.4201. (a) The sphere location has a offset of $kx_0 = 1.6$ along the x -axis. (b) The islands of attractive radiation force in the off-axial configuration.

In Fig. (4.8), the transverse radiation force field due to the first-order Bessel beam with $\beta = 70^\circ$ for the silicone sphere is depicted. The force fields are computed similarly to those in Fig. (4.7). To analyze the repulsor and the tractor beam two size factors are chosen, namely $ka = 0.1$ and $ka = 3$. For $ka = 0.1$ the beam central spot is a region of



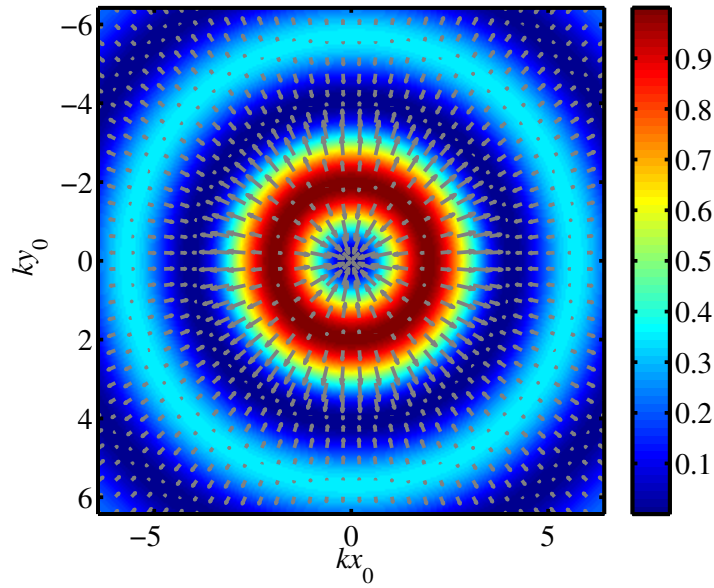
(a)



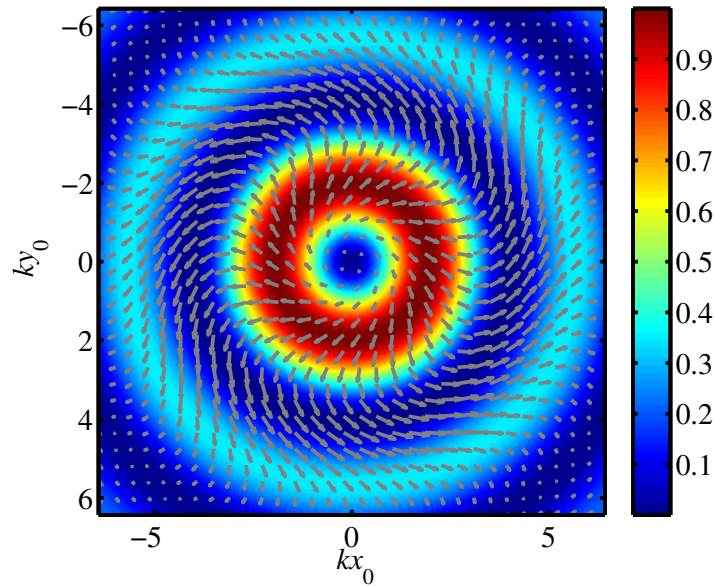
(b)

Figure 4.7: Transverse radiation force field $\mathbf{Y}_\perp = (Y_x, Y_y)$ caused by the zero-order Bessel beam with $\beta = 70^\circ$ for the silicone oil sphere with (a) $ka = 0.1$ and (b) $ka = 2$. The background images corresponds to the beam intensity.

stable equilibrium for the sphere. The sphere is pushed by the repulsor beam along the



(a)



(b)

Figure 4.8: Transverse radiation force field $\mathbf{Y}_\perp = (Y_x, Y_y)$ caused by the first-order Bessel beam with $\beta = 70^\circ$ upon the silicone oil sphere with (a) $ka = 0.1$ and (b) $ka = 3$. The background images correspond to the beam intensity.

z -axis. The transverse force points inwardly toward the beam axis. Thus, the sphere can be trapped in the beam's axis. As the sphere is moved radially away from the beam's axis, the transverse radiation force reverses its direction. It flips from inward to outward

direction as the spheres varies from the first maximum to the first minimum of the beam's intensity. Moreover, the transverse radiation force points inwardly in the region from the first minimum to the second maximum beam's intensity. In this region, the sphere might be trapped. The transverse radiation force field changes considerably when $ka = 3$. It points outwardly following the clockwise direction as the sphere moves radially away from the beam's axis. Moreover, inside the beam's central spot, the sphere is pulled back along the z -axis by the tractor beam. Moving the sphere radially from the first maximum to the first minimum, the transverse radiation force points outwardly along the counterclockwise direction. Thus, the transverse radiation force reverses its direction by moving the sphere radially. The change of direction of the radiation force is somehow unexpected because the direction of this force is supposed to be caused by the orbital angular momentum carried by the first-order Bessel beam. However, this phenomenon has been already observed in radiation force generated by optical Bessel beams [70].

4.4 Radiation force by a focused beam

4.4.1 Acoustic radiation force (Gorkov's method)

In 1954, Gorkov [12], elegantly derives a general radiation force expression for small particles obeying the same restrictions in an inviscid fluid as in the previous sections. We shall not consider the details in the derivation but merely state the result, which holds for any field except purely or approximately plane traveling waves [12].

The first-order pressure and velocity of the incoming acoustic field at the position where the particle is located are sufficient for the calculation. This fact yields a very useful and simple equation which helps to understand the characteristic and in fluency parameters of the acoustic radiation force. The theory is valid for a compressible spherical particle suspended in an infinite, inviscid fluid and exposed to an arbitrary pressure field. Additionally the following condition has to be fulfilled: $ka \ll 1$, where a is the particle radius and k the wavenumber of the acoustic field. The acoustic radiation force \mathbf{F}^{rad} can be expressed as the gradient of the force potential field U^{rad}

$$\mathbf{F}^{\text{rad}} = -\nabla U^{\text{rad}}, \quad (4.13)$$

where

$$U^{\text{rad}} = \frac{4}{3}\pi a^3 \left[f_1 \frac{1}{2} \kappa_0 \overline{p_1^2} - f_2 \frac{3}{4} \rho_0 \overline{v_1^2} \right], \quad (4.14)$$

with $f_1 = 1 - \kappa/\kappa_0$ and $f_2 = 2(\rho - \rho_0)/(2\rho + \rho_0)$, where ρ_0 and κ_0 denote the density and the compressibility of the fluid, respectively, and ρ and κ the density and compressibility of the particle, respectively.

4.4.2 Results

Consider an acoustic beam that is generated in water for which $c_0 = 1500$ m/s and $\rho_0 = 1000$ kg/m³. The focused transducer has a radius $b = 22$ mm, a F-number of 1.6, and

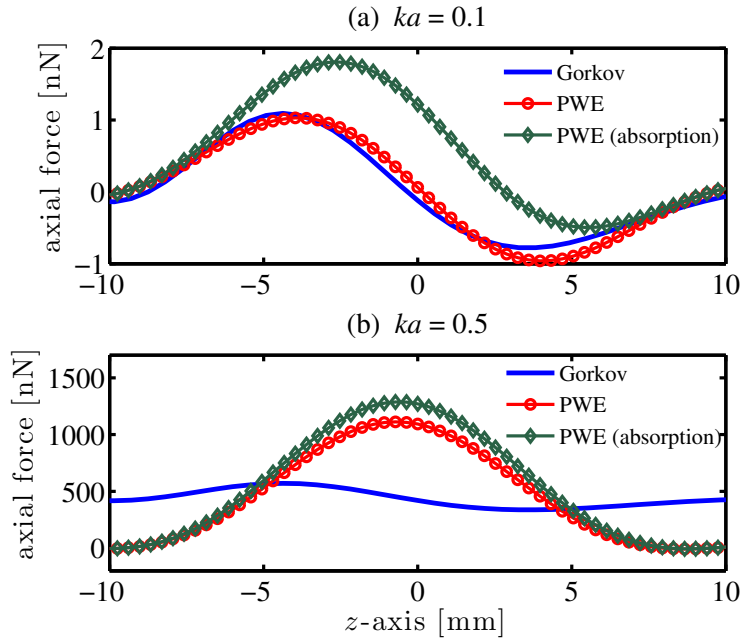


Figure 4.9: Axial radiation force versus the droplet’s position along z direction in the focal plane. The force is computed through the partial-wave expansion (PWE) and Gorkov’s methods. The size factors of the sphere are (a) $ka = 0.1$ and (b) $ka = 0.5$.

operates at 3.1 MHz. Note that $(b/z_0)^2 = 0.1$, which ensures the paraxial approximation for the incident beam. The magnitude of the pressure generated by the transducer is $p_0 = \rho_0 c_0 v_0 = 10^5$ Pa. A droplet made out of silicone-oil ($c_1 = 974$ m/s, $\rho_1 = 1004$ kg/m³, and $\alpha_0 = 21$ Np/m at 3.1 MHz) is used as the target object.

Figure (4.9) exhibits the axial radiation force versus the droplet’s position along the transducer’s axis (z direction). The droplet’s size factors are $ka = 0.1$ (Rayleigh regime) and $ka = 0.5$ (resonant regime). The solid line represents the radiation force computed with Gorkov’s method. Good agreement between the methods is found when no ultrasound absorption is considered in the droplet. However, when ultrasound absorption is taking into account, a significant deviation between these methods is observed. This result is expected since the acoustic radiation force caused by a plane traveling wave on a sphere depends on the sum of the scattered and absorbed power [11]. The Gorkov’s theory does not take into account absorption inside the particle. Therefore, if absorption is considered, the radiation force will be larger than in the case where absorption is neglected [71, 72]. The droplet with $ka = 0.1$ is axially trapped along the transducer axis at $z = 2.5$ σ mm (with absorption). Note that a nonabsorptive droplet would be trapped at $z = 0$. Gorkov’s method no longer describes the behavior of the radiation force generated by the focused transducer when $ka = 0.5$. Furthermore, it is not possible to axially trap the droplet with the analyzed transducer at this size factor. This can be understood as follows. The radiation force exerted on a small particle by the spherically focused beam is formed by two contributions [12]: “the scattering force” caused mostly by the traveling wave part of the beam, while “the gradient force” is due to the spatial variation of the potential and kinetic energy densities of the beam. As the size factor increases, so does

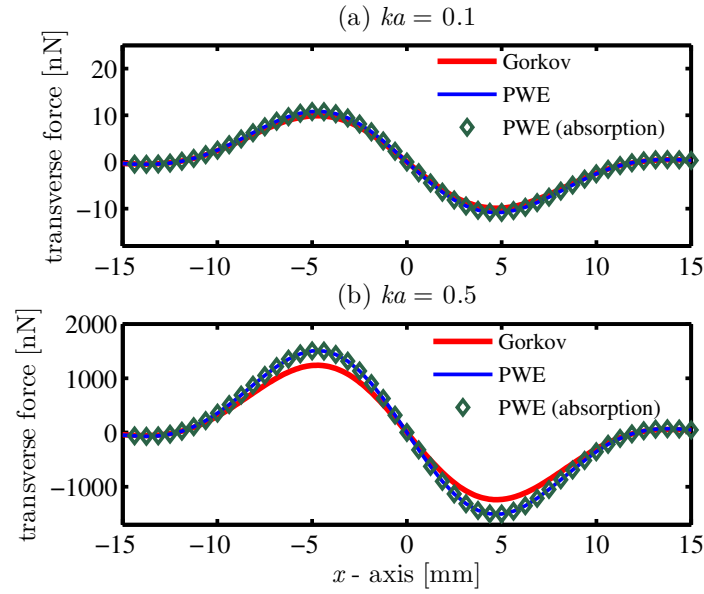


Figure 4.10: Transverse radiation force versus the droplet's position along x direction in the focal plane. The force is computed through the partial-wave expansion and Gorkov's methods. The size factors are (a) $ka = 0.1$ and (b) $ka = 0.5$.

the scattering force. When this force overcomes the gradient force, the axial trapping is no longer possible. This might be prevented using tightly focused beams [73].

The transverse radiation force versus the droplet's position along x direction in the focal plane is shown in Fig.(4.10). Excellent agreement is found between the partial-wave expansion and Gorkov's methods when $ka = 0.1$. Some deviation between the methods arises when $ka = 0.5$. Note that the results with and without absorption are very alike. The transverse trapping happens for both $ka = 0.1$ and 0.5 , because no scattering radiation force is present in the transverse direction. Only the gradient radiation force appears in this direction. Based on Figs. (4.9) and (4.10), we conclude that the focused transducer forms a 3D acoustical tweezer for silicone-oil droplets in the Rayleigh scattering regime.

The axial radiation force versus the droplet's position along z direction for the resonant scattering regime ($ka = 1$ and 5) is shown in Fig. 4.11. In this case, the scattering force totally overcomes the gradient force. Thereby, no trapping is possible in the axial direction with the analyzed transducer. The axial radiation force pushes the droplet to the forward scattering direction.

In Fig.(4.12), the transverse radiation force versus the droplet's position along x direction is displayed for the resonant scattering regime ($ka = 1$ and 5). It is clearly shown that the transverse trapping is still possible in this scattering regime. This happens because the incident beam is tightly focused in the transverse direction. Moreover, the transverse radiation force remains practically the same regardless of ultrasound absorption within the droplet.

The vector field of the transverse radiation force on the silicone-oil droplet placed in the transducer focal plane is displayed in Fig. (4.13). The background map represents

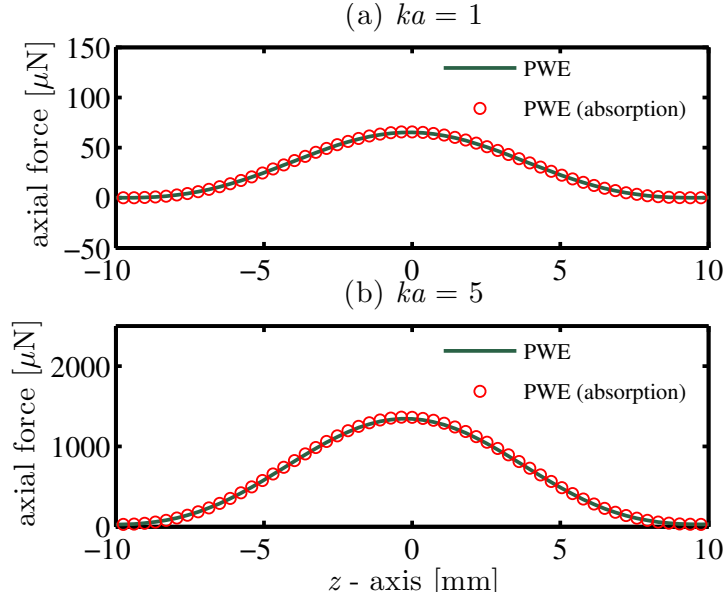


Figure 4.11: Axial radiation force versus the droplet's position along z direction for the resonant scattering regime (a) $ka = 1$ and (b) $ka = 5$.

the axial radiation force exerted on the droplet. If the droplet lies in the circular region with radius of 0.5 mm around the focus point, it will be attracted and trapped along the transducer's axis. The droplet is transversely trapped by a force of about $10\mu N$, see Fig.(4.10), but it will be further pushed axially by a force of $60\mu N$. Therefore, the focused transducer operates as a 2D acoustical tweezer for droplets in the resonant scattering regime ($ka = 1$).

Then, the radiation force produced by a zero- and a first-order Bessel beam upon a silicone-oil sphere in both on- and off-axial configurations has been studied. The analysis was based on the 3D radiation force expressions given in terms of the beam-shape and the scattering coefficients. The beam-shape coefficients were numerically computed through the DSHT algorithm, while the scattering coefficients were obtained by applying the acoustic boundary conditions across the sphere's surface. With appropriate selection of the sphere size factor ka and the beam half-cone angle β , the axial radiation force exerted on the sphere might be repulsive (repulsor beam) or attractive (tractor beam). As the sphere departs radially from the beam's axis, the attractive axial radiation force becomes weaker. In addition, the transverse radiation force field was computed showing that the silicone sphere can be trapped by using the first-order Bessel beam. These results represent an important step toward the design of a new generation of acoustical tweezers operating with Bessel beams for potential applications in bioengineering, biophysics, and other related fields.

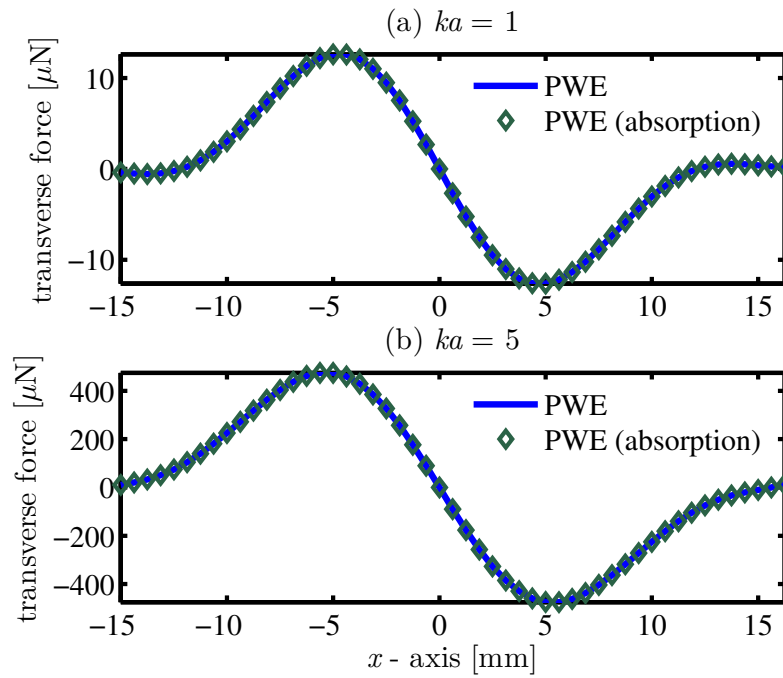


Figure 4.12: Transverse radiation force on a silicone oil droplet (with and without attenuation) in the resonant scattering regime (a) $ka = 1$ and (b) $ka = 5$.

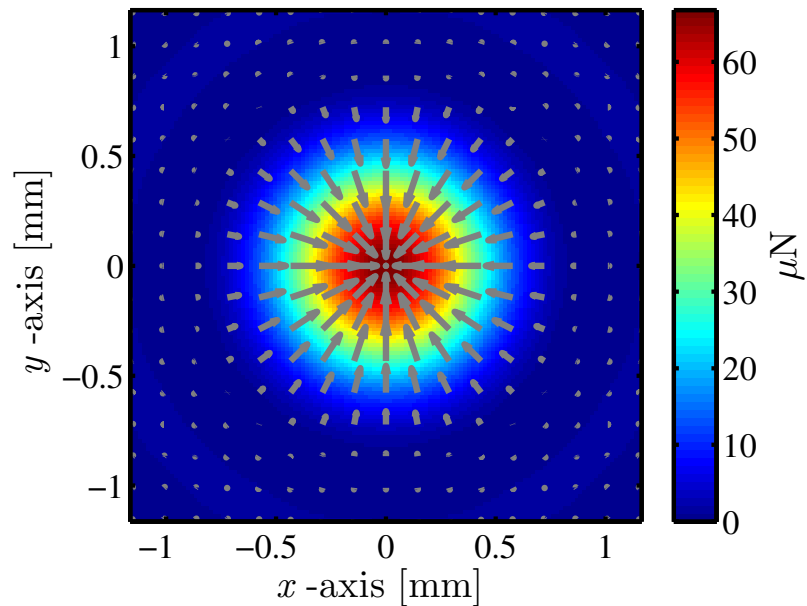


Figure 4.13: Vector field of the radiation force in the transducer focal plane produced on the silicone oil droplet in the resonant regime $ka = 1$. The vector field is plot on top of the axial radiation force.

5

Acoustic radiation force and torque exerted on a collection of objects

Noncontact particle manipulation by means of the acoustic radiation force has recently attracted much attention in biotechnology [74, 75]. In most cases, applications include the interaction of an ultrasound wave with several suspended objects such as micro-particles or biological cells. Thus, understanding how the acoustic radiation force is generated on many objects is a crucial step on the development and improvement of methods for acoustic manipulation of particles. The aim of this chapter is to present a theoretical method to compute the acoustic radiation force and torque to a collection of objects interacting with an acoustic beam of arbitrary wavefront. To illustrate the method we compute the radiation force and torque in a system formed by three olive oil droplets suspended in water.

5.1 Acoustic radiation force on a many-body system

So far, we have obtained the acoustic radiation force exerted on a single object suspended in a fluid. Let us now consider the problem of having more than one object in the medium. An external incident wave of arbitrary wavefront are imposed on a set of N suspended object. In Fig. 5.1, we depict this situation for three suspended objects of arbitrary geometry in a fluid. The surface of each object is denoted by S_n with $n = 1, 2, \dots, N$.

The farfield method used to obtain the acoustic radiation force as given in Eq. (3.33) cannot be used straightforwardly to the many-body problem described here. Using the divergent theorem given in Eq. (3.27) for the many-body problem, we obtain

$$\int_{V_c} \nabla \cdot \overline{\mathbf{S}^{(2)}} d^3\mathbf{r} = \int_{S_c} \overline{\mathbf{S}^{(2)}} \cdot \mathbf{n} d^2\mathbf{r} + \sum_{n=1}^N \int_{S_n} \overline{\mathbf{S}^{(2)}} \cdot \mathbf{n} d^2\mathbf{r} = 0. \quad (5.1)$$

Hence,

$$\sum_{n=1}^N \int_{S_n} \overline{\mathbf{S}^{(2)}} \cdot \mathbf{n} d^2\mathbf{r} = \sum_{n=1}^N \mathbf{F}_n^{\text{rad}} = - \int_{S_c} \overline{\mathbf{S}^{(2)}} \cdot \mathbf{n} d^2\mathbf{r}, \quad (5.2)$$

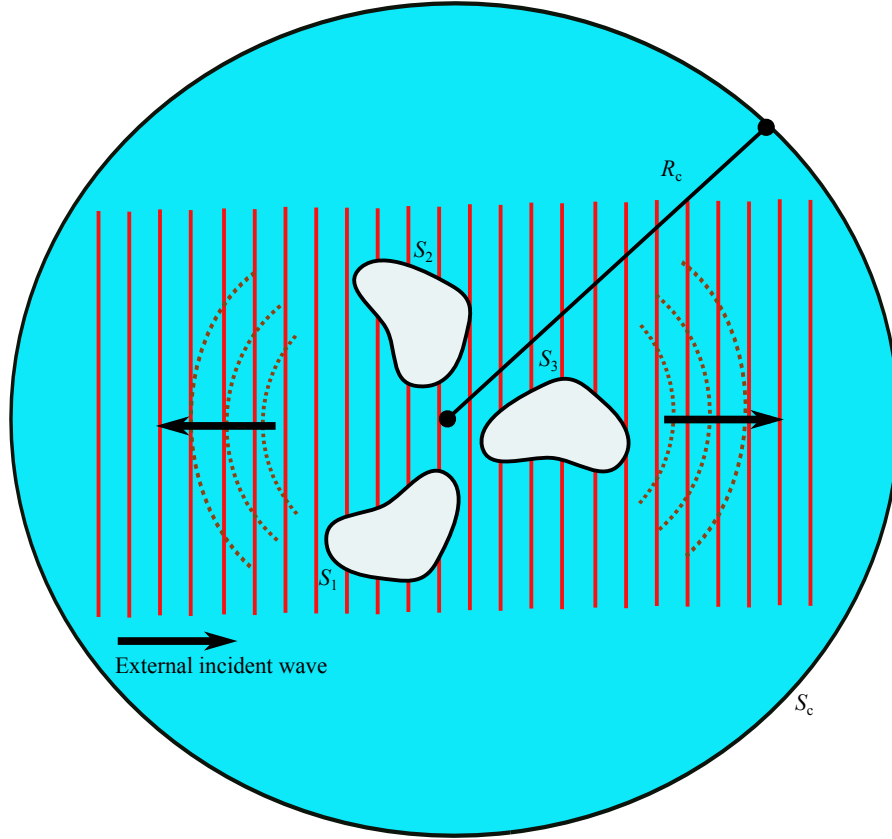


Figure 5.1: A sketch of the interaction between an external incident wave of arbitrary wavefront (vertical bars) and three suspended objects of any geometrical shape. The total scattered wave is denoted by dotted arches. The surfaces of the objects are S_1 , S_2 , and S_3 , while a control surface is drawn with radius R_c and surface S_c .

where $\mathbf{F}_n^{\text{rad}}$ is the acoustic radiation force on each individual object. It is clear that the integral of the radiation stress tensor $\overline{\mathbf{S}}^{(2)}$ on the control surface is not the radiation force on each individual object. If we want to benefit from the farfield radiation force method based on Eq. (3.36), a new approach to the many-body radiation force problem is on demand.

To devise a new approach to the farfield radiation force method applicable to a system of many objects, assume that a probe object is placed at \mathbf{r}'_p with respect to the system O . The probe can be any object in the N -object system, i.e. $p = 1, 2, \dots, N$. The position denoted by \mathbf{r}'_p defines the system O_p in which the position vector is \mathbf{r}_p . Now we describe the scattering problem by the probe sphere as seen from its own reference O_p . The effective incident velocity potential to the probe object will be given from the contributions of the external incident wave and all rescattered waves by the other objects in the medium. If we consider rescattering events to the M th-order, the approximate effective incident potential is

$$\phi_{\text{in}}^{\text{eff}, M}(\mathbf{r}_p) = \phi_{\text{ex}}(\mathbf{r}_p) + \phi_{\text{sc}}^M(\mathbf{r}_p), \quad (5.3)$$

where ϕ_{ex} is the velocity potential of the external incident wave. The M th-order scattered

potential incident to the probe object is

$$\phi_{\text{sc}}^M(\mathbf{r}_p) = \sum'_s \sum_{m=0}^M \phi_{\text{sc}}^m(\mathbf{r}_p | \mathbf{r}_{sp}), \quad (5.4)$$

where the primed sum means that $s \neq p$ in \mathbf{r}_{sp} , and $\phi_{\text{sc}}^m(\mathbf{r}_p | \mathbf{r}_{sp})$ is the m th-order rescattered potential by the object placed at $\mathbf{r}_{sp} = \mathbf{r}'_s - \mathbf{r}'_p$. The M th-order effective incident potential is then scattered by the probe sphere giving rise to $(M + 1)$ th-order scattering events. The corresponding scattered potential is then

$$\phi_{\text{sc}}^{\text{eff},M+1}(\mathbf{r}_p) = \phi_{\text{sc}}^{\text{ex}}(\mathbf{r}_p) + \phi_{\text{sc}}^{\text{sc},M+1}(\mathbf{r}_p), \quad (5.5)$$

where $\phi_{\text{sc}}^{\text{ex}}$ and $\phi_{\text{sc}}^{\text{sc},M+1}(\mathbf{r}_p)$ are related to the scattered external $\phi_{\text{ex}}(\mathbf{r}_p)$ and M th-order scattered wave by the other objects $\phi_{\text{sc}}^M(\mathbf{r}_p)$.

Now, substituting the approximate effective incident and the corresponding scattered potential into Eq. (3.36), we obtain the approximate radiation force on the probe object as

$$\mathbf{F}_p^{\text{rad},M} = -\frac{1}{k^2} \lim_{kR \rightarrow \infty} (kR)^2 \int_{4\pi} \text{Re} \left[\left(\phi_{\text{in}}^{\text{eff},M} - \frac{i}{k} \partial_{r_p} \phi_{\text{in}}^{\text{eff},M} \right) \phi_{\text{sc}}^{\text{eff},M+1*} + |\phi_{\text{sc}}^{\text{eff},M+1}|^2 \right] \mathbf{e}_{r_p} d\Omega. \quad (5.6)$$

We can now expand the effective incident and scattered fields in partial-wave series as follows

$$\phi_{\text{in}}^{\text{eff},M}(k\mathbf{r}_p) = \sum_{n,m} a_{p,nm}^M J_n^m(k\mathbf{r}_p), \quad (5.7)$$

$$\phi_{\text{sc}}^{\text{eff},M+1}(k\mathbf{r}_p) = \sum_{n,m} s_{p,n} a_{p,nm}^M H_n^m(k\mathbf{r}_p). \quad (5.8)$$

where a_{nm}^M is the effective beam-shape coefficient and $s_{p,n}$ is the scaled scattering coefficient of the probe object. A description on how to obtain the coefficients a_{nm}^{eff} and $s_{p,n}$ was given in Sec. 2.5. The farfield asymptotic expansions of Eqs. (5.7) and (5.8) are similar to those in Eqs. (2.62) and (2.67). Therefore, using the farfield expressions of $\phi_{\text{in}}^{\text{eff},M}$ and $\phi_{\text{sc}}^{\text{eff},M+1}$, the acoustic radiation force to the M th scattering order on the probe object is found to be

$$\mathbf{F}_p^{\text{rad},M} = A_p E_0 \mathbf{Y}_p^M, \quad (5.9)$$

where A_p is a cross-section area of the probe object and \mathbf{Y}_p^M is the dimensionless radiation force vector, whose components in Cartesian coordinates are given by Eqs. (3.39) and

(3.40) by setting $a_{nm} \rightarrow a_{nm}^{\text{eff}}$ and $s_n \rightarrow s_{p,n}$. In other words, we have

$$Y_{p,x}^M + iY_{p,y}^M = \frac{i}{2k^2 A_p} \sum_{n,m} \sqrt{\frac{(n+m+1)(n+m+2)}{(2n+1)(2n+3)}} \times (S_{p,n} a_{p,nm}^M a_{p,n+1,m+1}^M + S_{p,n}^* a_{p,n,-m}^{M*} a_{p,n+1,-m-1}^M), \quad (5.10)$$

$$Y_{p,z}^M = \frac{1}{k^2 A_p} \sum_{n,m} \sqrt{\frac{(n-m+1)(n+m+1)}{(2n+1)(2n+3)}} \text{Im} [S_{p,n} a_{p,nm}^M a_{p,n+1,m}^{M*}], \quad (5.11)$$

Referring to Eq. (5.6), we see that the radiation force on the probe particle has two contributions, namely the external $\mathbf{F}_{\text{ext},p}^{\text{rad}}$ and the interaction acoustic forces $\mathbf{F}_{\text{int},p}^{\text{rad},M}$. Hence,

$$\mathbf{F}_p^{\text{rad},M} = \mathbf{F}_{\text{ext},p}^{\text{rad}} + \mathbf{F}_{\text{int},p}^{\text{rad},M}. \quad (5.12)$$

The external acoustic force is due to the external incident wave only. Therefore, the external acoustic force can be written as

$$\mathbf{F}_{\text{ext},p}^{\text{rad}} = A_p E_0 \mathbf{Y}_{\text{ext},p}, \quad (5.13)$$

where A_p is a cross-section area of the probe object and $\mathbf{Y}_{\text{ext},p}$ is the dimensionless radiation force vector, whose components in Cartesian coordinates are given by Eqs. (3.39) and (3.40). Finally, the interaction acoustic force is given by

$$\mathbf{F}_{\text{int},p}^{\text{rad},M} = \mathbf{F}_p^{\text{rad},M} - \mathbf{F}_{\text{ext},p}^{\text{rad}} = A_p E_0 (\mathbf{Y}_p^M - \mathbf{Y}_{\text{ext},p}). \quad (5.14)$$

The interaction acoustic force given by this equation is an approximate result. It depends on a chosen scattering order M . In the limit $M \rightarrow \infty$, we obtain an exact solution. However, the associated multiple scattering problem requires a truncation to be solved numerically as discussed in Sec. 2.5. This truncation corresponds to the scattering order M adopted here for the interaction acoustic force.

The choice of M to yield better accuracy in the interaction acoustic force in Eq. (5.14) depends on the inter-object distance and objects' size, both relative to the incident wavelength. However, computational time rapidly increases with M . It is mostly related to the computation of Gaunt coefficients [48].

5.2 Acoustic radiation torque on a many-body system

The problem of generating acoustic radiation torque in a collection of objects is very similar to the radiation force problem discussed in Sec. 5.1. The effective incident wave to the probe object and its corresponding scattered wave given, respectively, by Eqs. (5.7) and (5.7), can be used to determine the produced radiation torque. Hence, the acoustic radiation torque exerted by an M th-order effective incident wave to the probe object is given by

$$\mathbf{N}_p^{\text{rad},M} = V E_0 \boldsymbol{\tau}_p^M, \quad (5.15)$$

with the Cartesian coordinates of the dimensionless radiation torque being

$$\begin{aligned} \tau_{p,x}^M + i\tau_{p,y}^M &= -\frac{1}{2k^3V} \sum_{n,m} \sqrt{(n-m)(n+m+1)} \\ &\times \left[(1 + s_{p,n}) s_{p,n}^* a_{p,nm}^M a_{p,n,m+1}^{M*} + (1 + s_{p,n}^*) s_{p,n} a_{p,n,-m}^{M*} a_{p,n,-m-1}^M \right], \end{aligned} \quad (5.16)$$

$$\tau_{p,z}^M = -\frac{1}{k^3V} \sum_{n,m} m \operatorname{Re} \left[(1 + s_{p,n}^M) s_{p,n}^{M*} |a_{p,n,m}^M|^2 \right]. \quad (5.17)$$

The radiation torque on the probe object have contributions of the radiation torque $\mathbf{N}_{\text{ext},p}^{\text{rad}}$ caused by the external wave and the acoustic interaction torque $\mathbf{N}_{\text{int},p}^{\text{rad},M}$ due to the re-scattering events by other objects. Therefore the acoustic radiation torque can be expressed as

$$\mathbf{N}_p^{\text{rad},M} = \mathbf{N}_{\text{ext},p}^{\text{rad}} + \mathbf{N}_{\text{int},p}^{\text{rad},M}. \quad (5.18)$$

The radiation torque due to the external wave is given by Eq. (3.51).

5.3 Numerical results

We compute the radiation force and torque on each constituent of a system formed by three droplets suspended in water at room temperature. The acoustic parameters of water are ($\rho_0 = 1000 \text{ kg/m}^3$ and $c_0 = 1480 \text{ m/s}$). The droplets are made of olive oil whose physical parameters are $\rho_q = 915.8 \text{ kg/m}^3$, $c_q = 1464 \text{ m/s}$, and $\alpha_{0,q} = 4.10 \times 10^{-14} \text{ Np/(MHz}^2 \text{ m)}$. Note that the droplets are immiscible in water. Two types of external waves are considered, namely plane progressive and plane standing waves at 1 MHz frequency. The droplets have equal radius of $a = 0.24 \text{ mm}$, thus the corresponding size parameter is $ka = 1$. This size parameter corresponds to the Mie scattering regime $ka \gtrsim 1$.

A MATLAB (MathWorks Inc.) code was developed to numerically solve the linear system in (2.89). Using this code, the form-function results for the scattering of a tilted plane progressive wave (i.e. forming an angle of 45° with the z -axis) by two spheres, given in Ref. [43], were recovered with excellent agreement.

The truncation order used to compute the effective beam-shape coefficient $n = M$ was determined from the following condition

$$\left| \frac{b_{00,q}^{(M)}}{b_{Mm,q}^{(M)}} \right| < 10^{-6}, \quad q = p, 1, 2, \dots, N-1. \quad (5.19)$$

This criterion was achieved for spheres with size parameter $ka = 1$ by setting $M = 12$.

The results will be presented in terms of the dimensionless radiation force $\mathbf{Y}_p^{(M)} = \mathbf{F}_p^{(M)}/(E_0 a_p^2)$ and the dimensionless radiation torque $\boldsymbol{\tau}_p^{(M)} = \mathbf{N}_p^{(M)}/(E_0 a_p^3)$.

5.3.1 Traveling plane wave

Consider that an external plane wave propagates along the $+z$ -direction and interacts with spheres placed at \mathbf{r}'_q ($q = 1, 2, \dots, N$). The normalized velocity potential of the external wave with respect to O_q (the system determined by the droplet at \mathbf{r}'_q) is given by

$$\phi_{\text{ex}}(z) = e^{ik(z-z'_q)}. \quad (5.20)$$

The corresponding beam-shape coefficient is [55]

$$a_{nm,q} = i^n \sqrt{4\pi(2n+1)} e^{-ikz'_q} \delta_{m,0}, \quad (5.21)$$

where $\delta_{m,m'}$ is the Kronecker delta symbol.

The first example presented here is the case of the plane wave interaction with two rigid particles in the Rayleigh scattering limit, $ka_q = 0.1$ ($q = 1, 2$). The particles are placed in the y -axis at $\mathbf{r}'_1 = -(d/2)\mathbf{e}_y$ and $\mathbf{r}'_2 = (d/2)\mathbf{e}_y$, where d is the inter-particle distance. We want to compare the numerical result obtained with our method with that derived by Zhuk [?], which gives the acoustic interaction force as

$$\mathbf{F}_{\text{int},1} = -\mathbf{F}_{\text{int},2} = \frac{2\pi E_0 k^3 a_1^3 a_2^3 \sin kd}{9 kd} \mathbf{e}_y, \quad kd \gg 1. \quad (5.22)$$

The acoustic interaction force exerted on the sphere placed at \mathbf{r}'_1 is shown in Fig. 5.2. Excellent agreement is found between our method and the analytical result in (5.22). The observed spatial oscillations in the interaction force is due to the stationary interference pattern of the re-scattered waves by each sphere.

In Fig. 5.3, we show the acoustic interaction force and torque between two olive oil droplets with size parameter $ka_1 = ka_2 = 1$. The droplets are located at $\mathbf{r}'_1 = -(d/2)\mathbf{e}_y$ and $\mathbf{r}'_2 = (d/2)\mathbf{e}_y$, where d is the inter-droplet distance. Due to the symmetry between the droplets and the external wave, the interaction force along the x -axis is zero. Likewise, using this symmetry argument, there is acoustic interaction torque only in the x -direction. The interaction force in the y -direction is a pair antisymmetric force, i.e. $F_{\text{int},y,1}^{(M)} = -F_{\text{int},y,2}^{(M)}$. Here the spheres interact directly to each other through the re-scattered waves. In other words, the spatial amplitude variation of the external wave remains constant in the xy -plane at which the spheres are positioned. In contrast, the z -component of the interaction force is the same for each droplet with spatial oscillations around the value of the radiation force due to the external wave (see the dashed line in Fig. 5.3.b). This happens because the effective incident wave to both droplets, formed by the external and the re-scattered waves, has the same interference pattern due to the symmetric position of the droplets. Moreover, the y -component of the interaction force asymptotically approaches zero as $d \rightarrow \infty$, whereas the z -component asymptotically approaches $Y_{z,1}^{(M)} = Y_{z,2}^{(M)} \rightarrow 1.04$, which corresponds to the radiation force on non-interacting droplets. The acoustic interaction torque depends only on the direct interaction of the droplets through the re-scattered waves. Therefore, this interaction leads to a pair antisymmetric torque. Moreover, the interaction torque also fades out as the

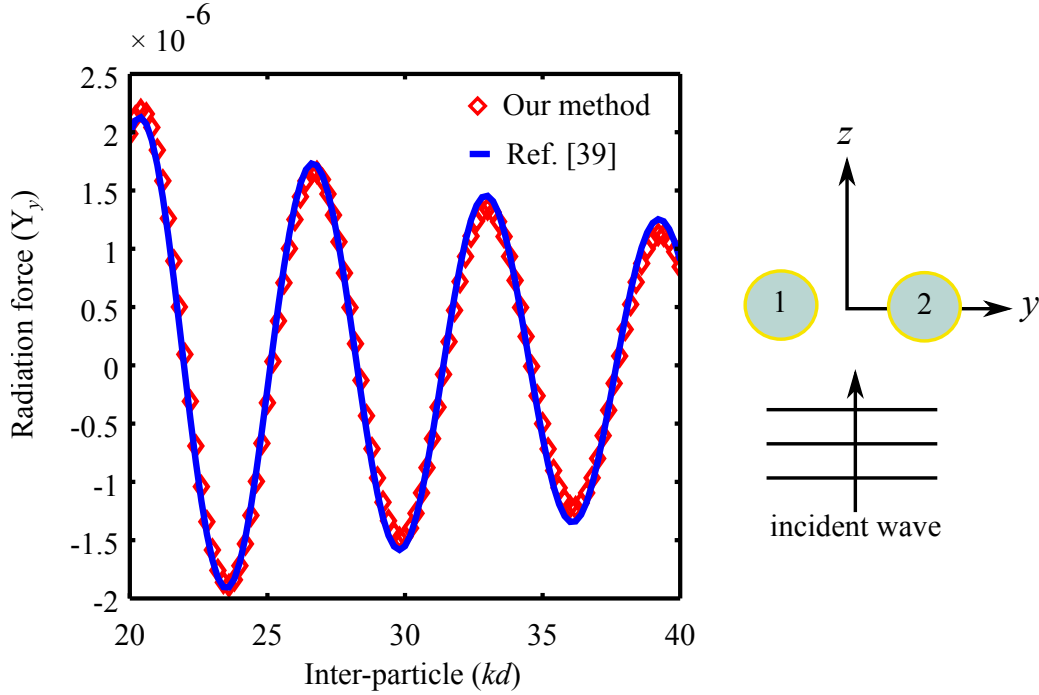


Figure 5.2: (Color online) Acoustic interaction force between two rigid Rayleigh particles ($ka_1 = ka_2 = 0.1$) induced by a plane wave propagating along $+z$ direction. The circles labeled as ‘1’ and ‘2’ denote, respectively, the particles located at $\mathbf{r}'_1 = -(d/2)\mathbf{e}_y$ and $\mathbf{r}'_2 = (d/2)\mathbf{e}_y$, where d is the inter-droplet distance.

droplets are set apart.

The acoustic interaction force and torque caused by the traveling plane wave on two olive oil droplets with size parameters $ka_1 = ka_2 = 1$ are shown Fig. 5.4 The droplets are positioned at $\mathbf{r}'_1 = -(d\sqrt{2}/2)(\mathbf{e}_x + \mathbf{e}_y)$ and $\mathbf{r}'_2 = (d\sqrt{2}/2)(\mathbf{e}_x + \mathbf{e}_y)$. The axis that connects the droplets is tilted 45° with respect to the plane wave propagation direction. No acoustic interaction force is present in the x -direction due to the symmetry of the droplets and the external wave. Furthermore, the only component of the acoustic interaction torque is along the x -direction, because the asymmetric shape of the effective incident wave to the droplets lies on the yz -plane only. The droplet located at \mathbf{r}'_1 interacts with an effective asymmetric stationary wave formed by the external and re-scattered waves. This explains the oscillatory pattern seen on the acoustic interaction force and torque. For the droplet at \mathbf{r}'_2 the external and re-scattered waves propagate almost along the same direction. This leads to a mild correction on the radiation force due to the traveling plane wave. We remark that a traveling plane wave does not produce torque on a single particle. Note also that both interaction force and torque asymptotically approach to zero as the droplets are set apart.

In Fig. 5.5, we present the acoustic interaction force and torque exerted on three olive oil droplets with size parameters $ka_1 = ka_2 = ka_3 = 1$. The droplets are placed at $\mathbf{r}'_1 = -(d/2)\mathbf{e}_y$, $\mathbf{r}'_2 = -(d\sqrt{3}/2)\mathbf{e}_z$, and $\mathbf{r}'_3 = (d/2)\mathbf{e}_y$, where d is the inter-droplet distance. The effective incident wave to droplets at \mathbf{r}'_1 and \mathbf{r}'_3 is a stationary wave formed by the external plane wave and the backscattered waves from the droplet at \mathbf{r}'_2 . Thus,

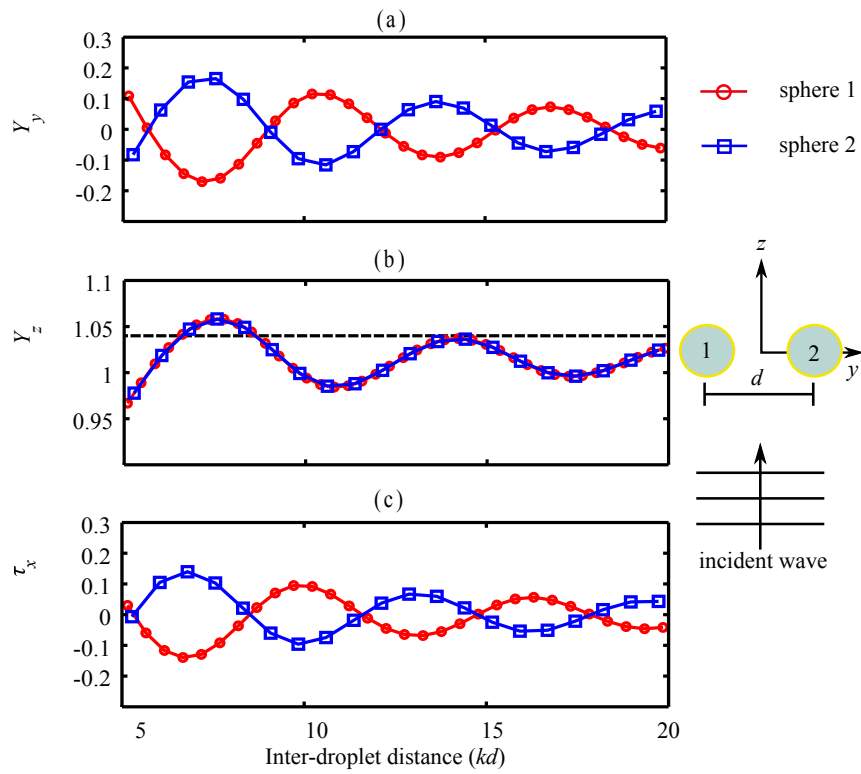


Figure 5.3: (Color online) Cartesian components of the acoustic interaction force and torque between two olive oil droplets with size parameter $ka_1 = ka_2 = 1$ induced by a plane wave propagating along the $+z$ -direction. The circles labeled as ‘1’ and ‘2’ denote, respectively, the droplets located at $\mathbf{r}'_1 = -(d/2)\mathbf{e}_y$ and $\mathbf{r}'_2 = (d/2)\mathbf{e}_y$, where d is the inter-droplet distance. The dashed line in (b) denotes the acoustic radiation force caused by the external traveling plane wave.

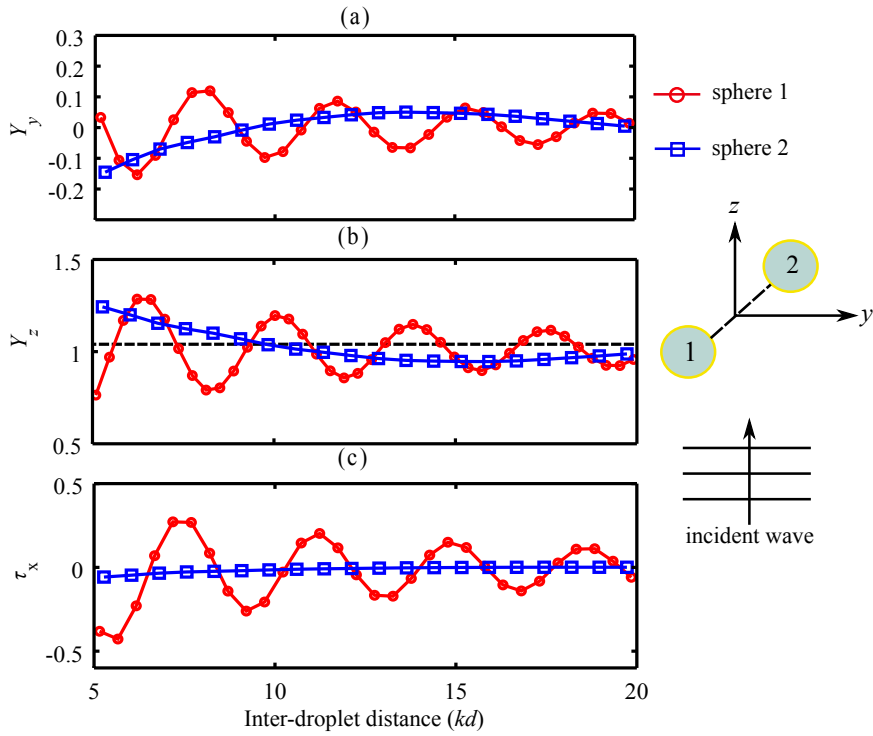


Figure 5.4: (Color online) Cartesian components of the acoustic interaction force and torque between two olive oil droplets with size parameter $ka_1 = ka_2 = 1$ (Mie scatterers) induced by a plane wave propagating along the $+z$ -direction. The circles labeled as ‘1’ and ‘2’ denote, respectively, the droplets located at $\mathbf{r}'_1 = -(d\sqrt{2}/2)(\mathbf{e}_x + \mathbf{e}_y)$ and $\mathbf{r}'_2 = (d\sqrt{2}/2)(\mathbf{e}_x + \mathbf{e}_y)$, where d is the inter-droplet distance. The dashed line in (b) denotes the acoustic radiation force caused by the external traveling plane wave.

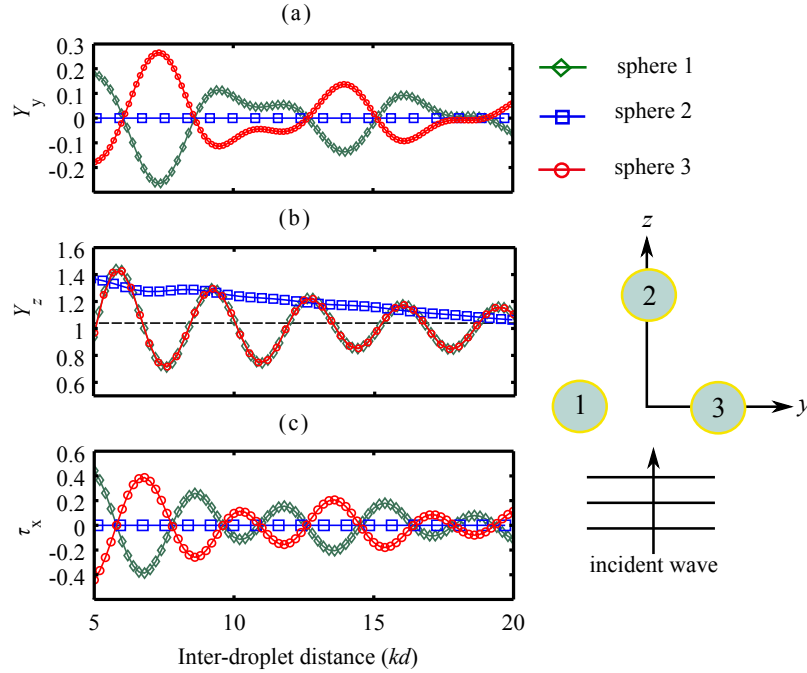


Figure 5.5: (Color online) Cartesian components of the acoustic interaction force and torque between three olive oil droplets with size parameter $ka_1 = ka_2 = ka_3 = 1$ induced by a plane wave propagating along the $+z$ -direction. The circles labeled as ‘1’, ‘2’, and ‘3’ denote, respectively, the droplets located at $\mathbf{r}'_1 = -(d/2)\mathbf{e}_y$, $\mathbf{r}'_2 = -(d\sqrt{3}/2)\mathbf{e}_z$, and $\mathbf{r}'_3 = (d/2)\mathbf{e}_y$, where d is the inter-droplet distance. The dashed line in (b) denotes the acoustic radiation force caused by the external traveling plane wave.

the z -component of the interaction force are the same on the droplets at \mathbf{r}'_1 and \mathbf{r}'_3 due to their symmetrical position. Moreover, the effective incident stationary wave causes the oscillatory pattern of interaction force. The droplet located at \mathbf{r}'_2 experiences an effective incident wave composed by the external plane wave and the forward scattered waves by the droplets at \mathbf{r}'_1 and \mathbf{r}'_3 . Hence, the z -component of the interaction force on the droplet at \mathbf{r}'_2 is larger than the radiation force magnitude due to the external wave only, which values 1.04. The y -component of the interaction forces on the droplets at \mathbf{r}'_1 and \mathbf{r}'_3 form an antisymmetric force-pair because these droplets interact directly through the re-scattered waves from each other. Likewise the interaction torques on these droplets also form an antisymmetric torque-pair. No interaction torque appears on the droplet at \mathbf{r}'_2 because of its symmetrical position with respect to the other droplets.

In Fig. 5.6, we show the interaction of an external traveling plane wave with three olive oil droplets with size parameters $ka_1 = ka_2 = ka_3 = 1$. The background shows the amplitude of the external plus scattered waves. The droplets are placed at $\mathbf{r}'_1 = -(d/2)\mathbf{e}_y$, $\mathbf{r}'_2 = -(d\sqrt{3}/2)\mathbf{e}_z$, and $\mathbf{r}'_3 = (d/2)\mathbf{e}_y$, with the inter-droplet distance being $d = 2$ mm. The values of the dimensionless acoustic interaction force which arise on each droplet is $\mathbf{Y}_1^{(M)} = -0.06\mathbf{e}_y + 1.01\mathbf{e}_z$, $\mathbf{Y}_2^{(M)} = 1.28\mathbf{e}_z$, and $\mathbf{Y}_3^{(M)} = 0.06\mathbf{e}_y + 1.01\mathbf{e}_z$. The dimensionless interaction torque on the droplets at \mathbf{r}'_1 and \mathbf{r}'_3 is $\tau_{1,x}^{(M)} = -\tau_{3,x}^{(M)} = 0.24$.

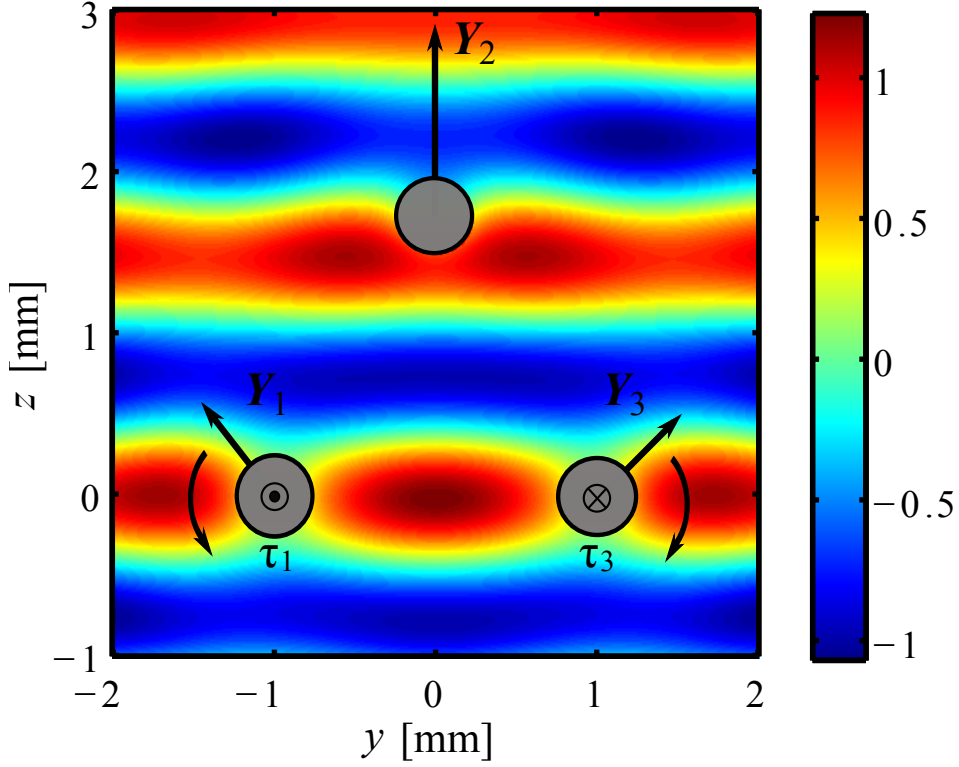


Figure 5.6: (Color online) Acoustic interaction forces and torques exerted on three olive oil droplets with size parameter $ka_1 = ka_2 = ka_3 = 1$ by a traveling plane wave along the $+z$ -direction. The droplets are located at $\mathbf{r}'_1 = -(d/2)\mathbf{e}_y$, $\mathbf{r}'_2 = -(d\sqrt{3}/2)\mathbf{e}_z$, and $\mathbf{r}'_3 = (d/2)\mathbf{e}_y$, with the inter-droplet distance being $d = 2$ mm. The dimensionless acoustic forces, which are depicted by the straight arrows, are $\mathbf{Y}_1^{(M)} = -0.06\mathbf{e}_y + 1.01\mathbf{e}_z$, $\mathbf{Y}_2^{(M)} = 1.28\mathbf{e}_z$, and $\mathbf{Y}_3^{(M)} = 0.06\mathbf{e}_y + 1.01\mathbf{e}_z$. The dimensionless interaction torques are represented by \odot (outward vector to the yz -plane) and \otimes (inward vector to the yz -plane) and they value $\tau_{1,x}^{(M)} = -\tau_{3,x}^{(M)} = 0.24$. The background is the amplitude of the external plus the scattered waves.

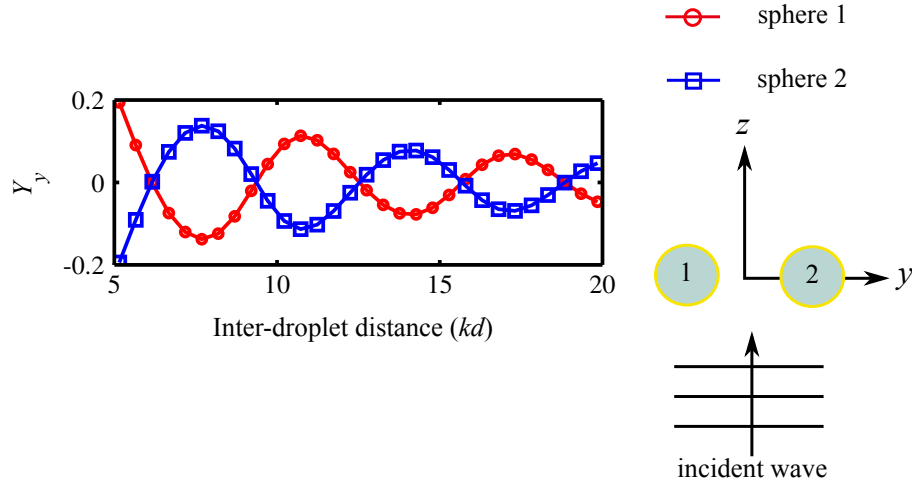


Figure 5.7: (Color online) The y -component of the acoustic interaction force exerted on two olive oil droplets with size parameter $ka_1 = ka_2 = 1$ induced by a standing plane wave along z -direction. The circles labeled as ‘1’ and ‘2’ denote, respectively, the droplets are located at $\mathbf{r}'_1 = -(d/2)\mathbf{e}_y$ and $\mathbf{r}'_2 = (d/2)\mathbf{e}_y$, where d is the inter-droplet distance.

5.3.2 Standing plane wave

The case of acoustic interaction forces and torques exerted on multiple spheres in a standing plane wave field is of great importance in acoustophoresis applications. Assume that a standing plane wave is formed along the z -axis and interacts with a system of spheres placed at \mathbf{r}'_q ($q = 1, 2, \dots, N$). The amplitude of the velocity potential of the standing wave with respect to the system O_q is given by

$$\phi_{\text{ex}}(z) = \cos[k(z - z'_q)]. \quad (5.23)$$

Using (5.21), we find that the corresponding beam-shape coefficient of the standing wave is

$$a_{nm,q} = \sqrt{4\pi(2n+1)} \cos\left(kz'_q - \frac{n\pi}{2}\right) \delta_{m,0}. \quad (5.24)$$

The acoustic interaction force exerted on two olive oil droplets with size parameter $ka_1 = ka_2 = 1$ by the standing wave is illustrated in Fig. 5.7. The droplets are located at $\mathbf{r}'_1 = -(d/2)\mathbf{e}_y$ and $\mathbf{r}'_2 = (d/2)\mathbf{e}_y$, where d is the inter-droplet distance. The droplets are in a node of the external standing wave $z = 0$. Thus, the z -component of the radiation force on both droplets is zero [12]. Furthermore, no interaction torque is produced on the droplets because the effective incident wave is symmetric with respect to the droplets.

In Fig. 5.8, we show the acoustic interaction force and torque caused by the standing plane wave on two olive oil droplets with size parameters $ka_1 = ka_2 = ka_3 = 1$. The droplets are placed at $\mathbf{r}'_1 = -(d\sqrt{2}/2)(\mathbf{e}_x + \mathbf{e}_y)$ and $\mathbf{r}'_2 = (d\sqrt{2}/2)(\mathbf{e}_x + \mathbf{e}_y)$. Due to the symmetrical position of the droplets with respect to the external wave, no acoustic interaction force appears in the x -direction. Moreover, the amplitude of the effective incident wave is the same on both droplets. Thus, the acoustic interaction forces along the y -direction form an antisymmetric force-pair $F_{y,1}^{(M)} = -F_{y,2}^{(M)}$, because the effective incident

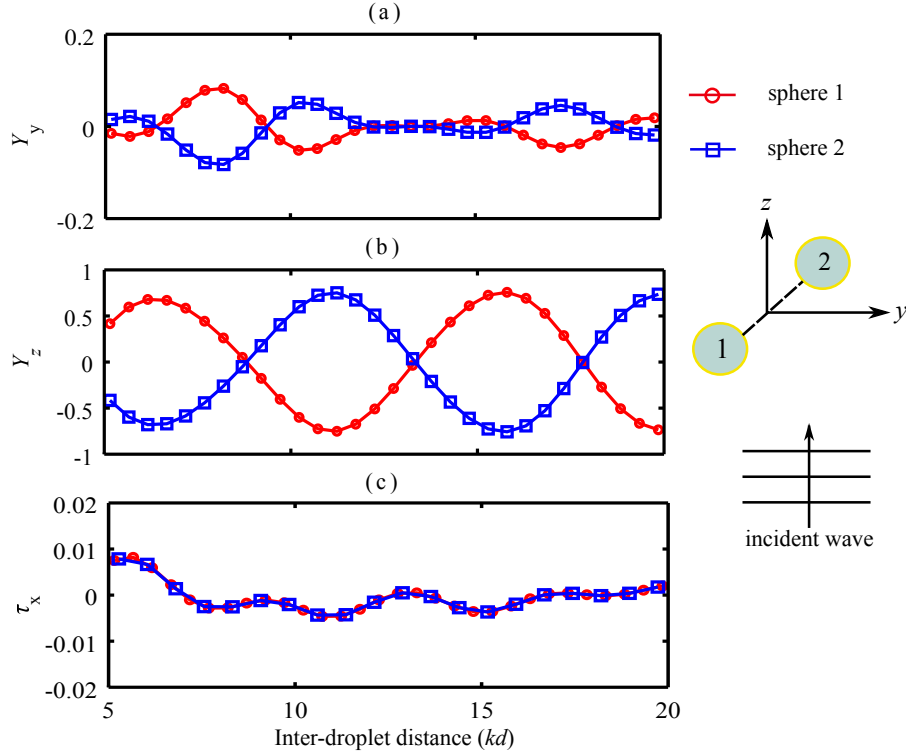


Figure 5.8: (Color online) Cartesian components of the acoustic interaction force and torque exerted on two olive oil droplets with size parameter $ka_1 = ka_2 = 1$ induced by a standing plane wave along z -direction. The circles labeled as ‘1’ and ‘2’ denote, respectively, the droplets located at $\mathbf{r}'_1 = \mathbf{0}$ and $\mathbf{r}'_2 = (d\sqrt{2}/2)(\mathbf{e}_x + \mathbf{e}_y)$, where d is the inter-droplet distance.

wave on one droplet is related to the backscattered wave of the opposite droplet. The y -component of the interaction force and the interaction torque asymptotically approach to zero as the droplets are set apart. It is further noticed that the z -component of the force exerted on the droplets is mostly caused by the external standing wave. According to Gorkov’s result [12], the radiation force varies spatially as $\sin(2kz)$. Thus, this force is an odd function of z , which explains the antisymmetric pattern of the radiation force in the z -direction. This and fact that the droplets interact through each others backscattered wave explains why the interaction torques on both spheres are equal.

In Fig. 5.9, we show the acoustic interaction forces and torques exerted on three olive oil droplets ($ka_1 = ka_2 = ka_3 = 1$) by the external standing plane wave. The droplets are placed at $\mathbf{r}'_1 = -(d/2)\mathbf{e}_y$, $\mathbf{r}'_2 = -(d\sqrt{3}/2)\mathbf{e}_z$, and $\mathbf{r}'_3 = (d/2)\mathbf{e}_y$, where d is the inter-droplet distance. The pair antisymmetric interaction force along the y -direction and torque on the x -direction on the droplets at \mathbf{r}'_1 and \mathbf{r}'_3 are formed because the re-scattered of these droplets are equal but propagate in opposite directions. On the other hand, the z -component of the radiation force is mostly due to the external standing wave. For the droplets located at \mathbf{r}'_1 and \mathbf{r}'_3 , we have $z = 0$; thus, the radiation force along z -direction is nearly zero. Whereas, this force varies as $\sin(2kz)$ on the droplet at \mathbf{r}'_2 .

In Fig. 5.6, we show the interaction of an external standing plane wave with three olive oil droplets with size parameters $ka_1 = ka_2 = ka_3 = 1$. The background is the

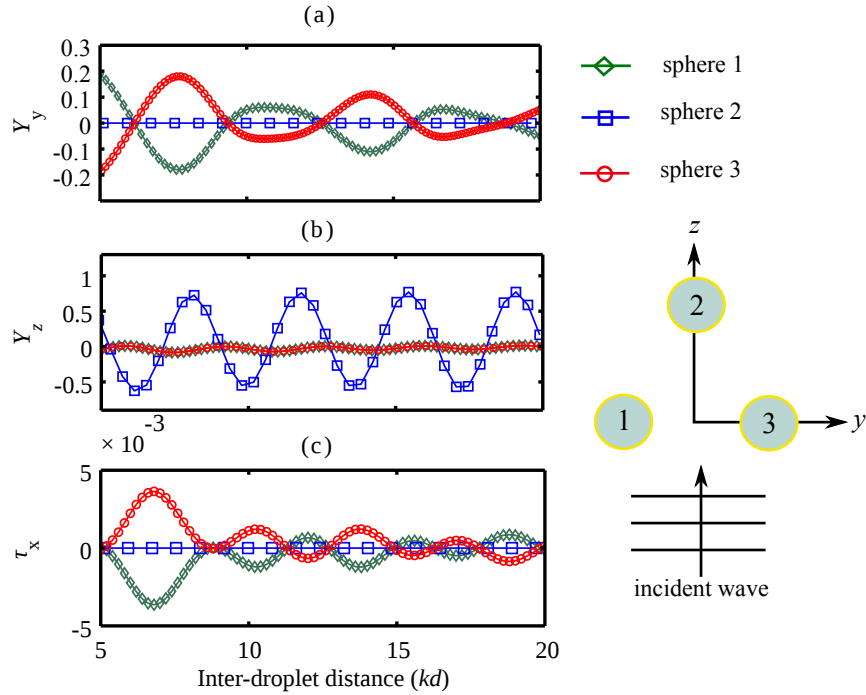


Figure 5.9: (Color online) Cartesian components of the acoustic interaction force and torque between three olive oil droplets with size parameter $ka_1 = ka_2 = ka_3 = 1$ induced by a standing plane wave along z -direction. The circles labeled as ‘1’, ‘2’, and ‘3’ denote, respectively, the droplets located at $\mathbf{r}'_1 = -(d/2)\mathbf{e}_y$, $\mathbf{r}'_2 = -(d\sqrt{3}/2)\mathbf{e}_z$, and $\mathbf{r}'_3 = (d/2)\mathbf{e}_y$, where d is the inter-droplet distance.

amplitude of the external plus scattered waves. The droplets are placed at $\mathbf{r}'_1 = -(d/2)\mathbf{e}_y$, $\mathbf{r}'_2 = -(d\sqrt{3}/2)\mathbf{e}_z$, and $\mathbf{r}'_3 = (d/2)\mathbf{e}_y$, with the inter-droplet distance being $d = 2$ mm. The values of the dimensionless acoustic interaction force on each droplet is $\mathbf{Y}_1^{(M)} = -0.13\mathbf{e}_y - 0.3\mathbf{e}_z$, $\mathbf{Y}_2^{(M)} = 0.63\mathbf{e}_z$, and $\mathbf{Y}_3^{(M)} = 0.13\mathbf{e}_y - 0.3\mathbf{e}_z$. The dimensionless interaction torque on the droplets at \mathbf{r}'_1 and \mathbf{r}'_3 is $\tau_{1,x}^{(M)} = -\tau_{3,x}^{(M)} = 0.003$.

We have presented a method to compute the acoustic radiation force and torque of a cluster N spheres suspended in an inviscid fluid. The proposed method relies on the solution of multiple scattering problem using spherical partial-wave expansions and on the farfield radiation force and torque formulas in (5.13) and (5.15). Results were provided for three olive oil droplets with size factor $ka = 1$, which corresponds to the so-called Mie sized particles. The method can be readily applied to solid elastic and viscoelastic materials, and spherical shells, provided the appropriate scaled scattering coefficients of these materials. In particular, we studied the interaction radiation force caused by a traveling and a standing plane wave. Additionally, we showed for the first time that an interaction radiation torque may arise on the suspended spheres depending on the geometric arrangement of the spheres.

The proposed method can be useful to understand the dynamics of many particle system in experiments performed in acoustofluidics and acoustical tweezer devices. It can also be helpful to predict geometrical aspects of particles clustering under an ultrasound field.

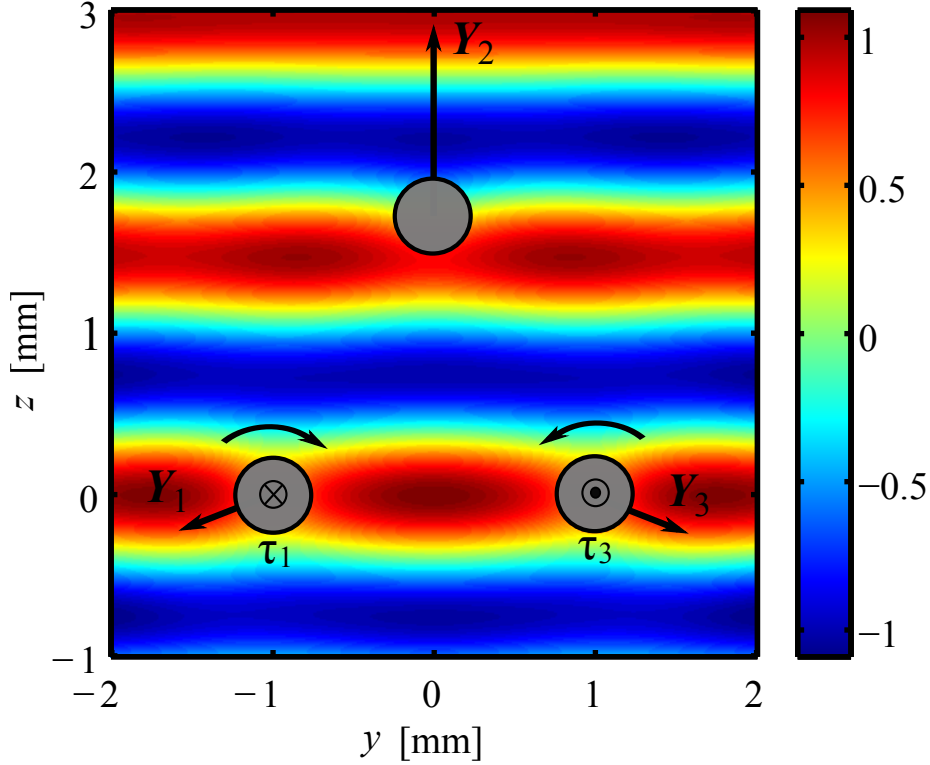


Figure 5.10: (Color online) Acoustic interaction forces and torques exerted on three olive oil droplets with size parameter $ka_1 = ka_2 = ka_3 = 1$ by a standing plane wave along z -direction. The droplets are located at $\mathbf{r}'_1 = -(d/2)\mathbf{e}_y$, $\mathbf{r}'_2 = -(d\sqrt{3}/2)\mathbf{e}_z$, and $\mathbf{r}'_3 = (d/2)\mathbf{e}_y$, with the inter-droplet distance being $d = 2$ mm. The dimensionless acoustic forces, which are depicted by the straight arrows, are $\mathbf{Y}_1^{(M)} = -0.13\mathbf{e}_y - 0.3\mathbf{e}_z$, $\mathbf{Y}_2^{(M)} = 0.63\mathbf{e}_z$, and $\mathbf{Y}_3^{(M)} = 0.13\mathbf{e}_y - 0.3\mathbf{e}_z$. The dimensionless interaction torques are represented by \odot (outward vector to the yz -plane) and \otimes (inward vector to the yz -plane) and they value $\tau_{1,x}^{(M)} = -\tau_{3,x}^{(M)} = 0.003$. The background is the amplitude of the external plus the scattered waves.

6

Conclusions

6.1 Summary

We have proposed a theoretical model to compute the acoustic radiation force and torque exerted by a beam with arbitrary wavefront on an object or a collection of suspended objects of any geometrical shape in an ideal fluid.

Stemming from the fluid conservation equations for ideal fluids, we derived the linear wave equation and the Helmholtz equation for the amplitude of time-harmonic waves. The Helmholtz equation is the cornerstone to obtain the acoustic fields necessary to solve the radiation force and torque problems considering either a single-body or a many-body system. This is because these phenomena depend directly on the corresponding scattering problem involving the suspended objects in the medium. Formulas for the acoustic radiation force and torque were obtained from first principles based on the fluid conservation equations as well. In particular, we obtain the farfield formulas for both the radiation force and torque, which depend only on the beam-shape coefficient a_{nm} of the incident wave, and the scaled scattering coefficient s_n of the object. The farfield formulas are simpler to obtain and implement than their nearfield counterpart.

We have studied the acoustic radiation force generated by an ultrasound focused and Bessel beams on a single sphere. For the focused beam the addition theorem was used to determine the beam-shape coefficients with respect to an off-focused sphere. Whilst the discrete spherical harmonics transform was employed to obtain the beam-shape coefficients of the Bessel beams with respect to an off-axis sphere. The addition theorem method yields exact values for unknown beam-shape coefficients with respect to an arbitrary coordinate system stemming from a set of given a set of known beam-shape coefficients. Nevertheless, the addition theorem demands much more computational resources (time and memory) than the discrete spherical harmonics transform.

Using the farfield radiation force expressions derived in Chap. 3, both the axial and transverse components of the radiation force exerted on a silicone-oil droplet. The radiation force generated by the focused beam was considered in the paraxial approximation. Both axial and transverse radiation forces were computed in the Rayleigh $ka \ll 1$ and resonant (Mie) scattering $ka \sim 1$ regimes. In the Rayleigh regime, some deviation of our

results and the Gorkov's radiation force [12] was found due to the fact that we considered particle absorption. On the other hand, a tractor behavior of the Bessel beam was noticed. This means that the droplet was pulled instead of being pushed away along the beam propagation direction. However, as the droplet is set apart from the beam axis, the negative radiation force becomes weaker. The negative radiation force also depends on the half-cone angle β and the sphere's size factor ka .

In Chap. 5, the acoustic radiation forces and torques of N -body system were investigated. We proposed a method to obtain the force and torque based on the farfield formulas derived in Chap. 3 and in a truncated numerical solution of the corresponding multiple scattering problem discussed in Chap. 2. Specifically, the method is based on the partial-wave expansion series and the addition theorem for spherical functions. It can be applied to objects made of rigid, void, compressible fluid, solid elastic, viscoelastic, and layered materials; since appropriate boundary conditions across the surface of the object are provided. In particular, the radiation forces and torques were computed to an configuration of three olive oil droplets for an external traveling and standing plane wave. The analysis was carried out for the Mie and the Rayleigh scattering regimes. The obtained results show that an acoustic interaction torque arises on the droplets due to break of symmetry of the effective incident waves over them. The interaction torque may induce either a clockwise or a counterclockwise rotation on the droplets, depending on the interdroplet distance. Moreover, an acoustic interaction force can significantly deviate the noninteracting radiation force exerted directly by the external incident wave. Both attractive and repulsive acoustic interaction forces were observed on the oil droplets, depending on their relative distance.

6.2 Conclusion

The success of a scientific theoretical prediction lies on its experimental confirmation. Nowadays, problems involving the acoustic radiation force and torque exerted on a collection of objects is customary on acoustofluidics and acoustical tweezer experimental systems. Hence, an experimental setup for the problems discussed in this work can be devised, in principle. Should the theoretical predictions of this work agree with experimental results, the proposed method may become a valuable tool on the study of systems involving the interaction between many objects through acoustic waves and also on the enhancement of acoustofluidics and acoustical tweezer devices.

Bibliography

- [1] Hultstrom, J., Manneberg, O., Dopf, K., Hertz, H. M., Brismar, H., and Wiklund, M. *Ultrasound Med. Biol.* **33**, 145–151 (2007).
- [2] Svennebring, J., Manneberg, O., Skafte-Pedersen, P., and H. Bruus, M. W. *Biotechnol. Bioeng.* **103**, 323–328 (2009).
- [3] Evander, M., Johansson, L., Lilliehorn, T., Piskur, J., Lindvall, M., Johansson, S., Almqvist, M., Laurell, T., and Nilsson, J. *Anal. Chem.* **79(7)**, 2984–2991 (2007).
- [4] Grenvall, C., Augustsson, P., Folkenberg, J. R., and Laurell, T. *Anal. Chem.* **81**, 6195–6200 (2009).
- [5] Franke, T., Braunmueller, S., Schmid, L., Wixforth, A., and Weitz, D. A. *Lab. Chip.* **10**, 789–794 (2010).
- [6] Rayleigh, L. *Philos. Magazine* **3**, 338–346 (1905).
- [7] King, L. V. *Proc. R. Soc. A* **147(861)**, 212–240 (1934).
- [8] Embleton, T. F. W. *J. Acoust. Soc. Am.* **26**, 40–45 (1954).
- [9] Embleton, T. F. W. *J. Acoust. Soc. Am.* **26**, 46–50 (1954).
- [10] Yosioka, K. and Kawasima, Y. *Acustica* **5**, 167–173 (1955).
- [11] Westervelt, P. J. *J. Acoust. Soc. Am.* **29**, 26–29 (1957).
- [12] Gorkov, L. P. *Sov. Phys. Dokl.* **6**, 773–775, (1962).
- [13] Nyborg, W. L. *J. Acoust. Soc. Am.* **42**, 947–952 (1967).
- [14] Hasegawa, T. and Yosioka, K. *J. Acoust. Soc. Am.* **46**, 1139–1143 (1969).
- [15] Hasegawa, T., Ochi, M., and Matsuzawa, K. *J. Acoust. Soc. Am.* **69**, 937–942 (1981).
- [16] Wu, J. and Du, G. *J. Acoust. Soc. Am.* **87**, 997–1003 (1990).
- [17] Silva, G. T. *J. Acoust. Soc. Am.* **130**, 3541–3545 (2011).

- [18] Marston, P. L. *J. Acoust. Soc. Am.* **120**, 3518–3524 (2006).
- [19] Mitri, F. G. *J. Phys. A* **42**(245202) (2009).
- [20] Silva, G. T., Lopes, J. H., and Mitri, F. G. *IEEE Trans. Ultras. Ferroel. Freq. Control* **60**, 1207–1212 (2013).
- [21] Rayleigh, L. *Phyl. Magazine series 5* **14**, 186–187 (1882).
- [22] Kotani, M. *Proc. Phys. and Math. Soc. Japan* , 15–30 (1933).
- [23] King, L. *Proc. Royal Soc. A: Math., Phys. and Engineering* **153**, 17–40 (1936).
- [24] Keller, J. B. *J. Acoust. Soc. Am.* **30**(3), 1085–1090 (1957).
- [25] Maidanik, G. *J. Acoust. Soc. Am.* **30**, 620 (1958).
- [26] Fan, Z., Yang, D. M. K., and Chen, Z. *J. Acoust. Soc. Am.* **124**, 2727 (2008).
- [27] Hefner, B. T. and Marston, P. L. *J. Acoust. Soc. Am.* **106**, 3313–3316 (1999).
- [28] Zhang, L. and Marston, P. *J. Acoust. Soc. Am.* **129**, 1679–1680 (2011).
- [29] F. G. Mitri, T. P. L. and Silva, G. T. *Phys. Rev. E* **85**(026602) (2012).
- [30] G. T. Silva, T. P. L. and Mitri, F. G. *Europhys. Phys. Lett.* **97**(54003) (2012).
- [31] Bjerknes, V. F. K. (*Columbia University*) (1906).
- [32] Konig, W. *Ann. Phys.* **42**, 549 (1891). in German.
- [33] Embleton, T. F. W. *J. Acoust. Soc. Am.* **34**, 1714–1720 (1962).
- [34] Nyborg, W. L. *Ultras. Med. Biol.* **15**, 93 (1989).
- [35] Doinikov, A. A. and Zavtrak, S. T. *Phys Fluides* **7**, 1923 (1995).
- [36] Crum, L. A. *J. Acoust. Soc. Am.* **57**, 1363–1370 (1975).
- [37] Doinikov, A. A. and Zavtrak, S. T. *Ultrasonics* **34**, 807 (1996).
- [38] Doinikov, A. A. and Zavtrak, S. T. *J. Acoust. Soc. Am.* **99**, 3373 (1996).
- [39] Zhuk, A. P. *Sov. Appl. Mech.* **21**, 110 (1985).
- [40] Doinikov, A. A. *J. Acoust. Soc. Am.* **106**, 3305 (1999).
- [41] Doinikov, A. A. *J. Acoust. Soc. Am.* **111**, 1602 (2002).
- [42] Zheng, X. and Apfel, R. E. *J. Acoust. Soc. Am.* **97**, 2218 (1995).
- [43] Gaunaurd, G. C., Huang, H., and Strifors, H. C. *J. Acoust. Soc. Am.* **98**, 495–507 (1995).

- [44] Doinikov, A. A. *J. Fluid Mech.* **444**, 1–21 (2001).
- [45] Mase, G. E. *Theory and problems of continuum mechanics*, volume 1. McGraw-Hill book company, (1970).
- [46] Pierce, A. D. *Acoustics: An Introduction to Its Physical Principles and Applications*. Number p. 215. Melville, NY: Acoustical Society of America, (1989).
- [47] Williams, E. G. *Fourier Acoustics: Sound Radiation and Nearfield Acoustical Holography*. Number ch. 6. San Diego, CA: Academic Press, (1999).
- [48] Ivanov, Y. A. *National Aeronautics and Space Administration, Washington, DC, NASA technical translation F-597*, 125–130 (1970).
- [49] Szabo, T. L. *J. Acoust. Soc. Am.* **96**, 491–500 (1994).
- [50] Hasheminejad, S. M. and Azarpeyvand, M. *Acust. Acta. Acust.* **89**, 998–1007 (2003).
- [51] Hasheminejad, S. M. and Azarpeyvand, M. *Shock and Vibration* **11**(5), 625–635 (2004).
- [52] Hasheminejad, S. M. and Azarpeyvand, M. *IEEE Trans. Ultrason. Ferroelectr. Freq. Control* **50**, 1444–1454 (2003).
- [53] Hasheminejad, S. M. and M. Azarpeyvand. *Acoustical Physics* **31**(8), 1129–1146 (2008).
- [54] Hasheminejad, S. M. and M. Azarpeyvand. *Acust. Acta. Acust.* **96**, 491–500 (2003).
- [55] Colton, D. and Kress, R. *Inverse Acoustic and Electromagnetic Scattering Theory*. Number ch. 3. Springer-Verlag, Berlin, Germany, 2nd ed. edition, (1998).
- [56] Annamalai, S., Balachandar, S., and Parmar, M. K. *Phys. Rev. E* **89**, 053008 (2014).
- [57] Jackson, J. D. *Classical Electrodynamics*. Number ch. 9. Wiley, New York, 3rd ed. edition, (1998).
- [58] Faran, J. J. *J. Acoust. Soc. Am.* **23**, 405–418 (1951).
- [59] Gaunaurd, G. C. and Uberall, H. *J. Acoust. Soc. Am.* **63**, 5–16 (1978).
- [60] Silva, G. T. *Phys. Rev. E* **74**, 026609 (2006).
- [61] Wang, S. *J. Acoust. Soc. Am.* **99**, 1924–1931 (1996).
- [62] Bayliss, A. *J. Comput. Phys.* **59**, 396–404 (1985).
- [63] Morse, P. M. and Ingard, K. U. *Theoretical Acoustics*. Number ch. 7. Princeton University Press, Princeton, New Jersey, (1968).
- [64] Silva, G. T. *IEEE Trans. Ultrason. Ferroelec. Freq. Contr.* **58**, 298–304 (2011).

- [65] Edwards, P. L. and Jarzynski, J. *J. Acoust. Soc. Am.* **74**, 1006–1012 (1983).
- [66] Lucas, B. G. and Muir, T. G. *J. Acoust. Soc. Am.* **72**, 1289–1289 (1982).
- [67] Durbin, J., Jr., J. J. M., and Eberly, J. H. *Phys. Rev. Lett.* **56**(13), 1499–1501 (1987).
- [68] Straton, J. *Electromagnetic Theory*. Number Ch. 6 and 7. (2010).
- [69] Schroder, A. and Raphael, E. *Europhys. Lett.* **17**, 565–570 (1992).
- [70] K. V. Sepulveda, S. C. C. V. G. C. and Dholakia, K. *J. Opt. Soc. Am. B* **21**, 1749–1757 (2004).
- [71] Lofstedt, R. and Putterman, S. *J. Acoust. Soc. Am.* **90**(4), 2027–2033 (1991).
- [72] Silva, G. T. *J. Acoust. Soc. Am.* (2014). arXiv:1307.4705v2, [physics.class-ph].
- [73] Lee, J., Teh, S., Lee, A., Kim, H., Lee, C., and Shung, K. *Appl. Phys. Lett.* **95**, 073701 (2009).
- [74] Chu, S. *Rev. Mod. Phys.* **70**, 685–706 (1998).
- [75] Ding, X., Lin, S. C. S., Kiraly, B., Yue, H., Li, S., Chiang, I. K., Shi, J., Benkovic, S. J., and Huang, T. J. *Proc. Natl. Acad. Sci. U.S.A.* **109**(11105) (2012).